Electronics Research Laboratory
University of California
Berkeley 4, California

EXPERIMENTAL INVESTIGATION OF MICROWAVE PROPAGATION IN A PLASMA WAVEGUIDE

by

R. N. Carlile

The research reported herein is made possible through support received from the Departments of Army, Navy, and Air Force Office of Scientific Research under Grant AF-AFOSR-139-63.

August 12, 1963

TABLE OF CONTENTS

LIST OF ILLUSTRATIONS

ACKNOWLEDGMENT

The author wishes to thank Professors T. E. Everhart, A. W. Trivelpiece, and C. A. Desoer of this University and Professor G. S. Kino of Stanford University for helpful discussions. Thanks are also extended to Mr. G. Becker, who constructed the experimental tubes; to Mr. J. Meade, who constructed the magnet; and to Mrs. Lynn Schell, who prepared the manuscript; and, finally, to my wife, Marybeth, for proofreading some of the material and for her interest and encouragement throughout this project.

The author would also like to acknowledge the loan of equipment by the Department of Electrical Engineering of the University of Arizona.

The text of this report is similar to that of a thesis which has been submitted to the Graduate Division of the University of California at Berkeley, in partial fulfillment of the requirements for the degree of Doctor of Philosophy.

SUMMARY

The phase characteristics of a backward-wave pass-band mode have been measured in a circular waveguide which is coaxial with a circular isotropic plasma column. This mode has been identified as an n = 1 surface wave similar to that described by Trivelpiece.

Zero temperature plasma waveguide theory, which predicts this mode quite accurately, shows that a simple relation exists between the lower cut-off frequency and the electron plasma frequency. It is demonstrated that the plasma frequency obtained from this relation, where the cut-off frequency is determined from a measurement of the phase characteristics, agrees well with an independent measurement of the plasma frequency using the well known cavity perturbation method.

Noise measurements on the n = 1 and the symmetric n = 0 modes indicate that the signal-to-noise ratio is independent of input signal power and is about 7 db for the n = 1 mode and varies from about 7 to greater than 30 db for the n = 0 mode. A simple model of the plasma is proposed which explains all the noise observations reported here. It is pointed out that Crawford and Lawson independently propose a similar model.

A strong dc axial magnetic field was applied to the plasma and the phase characteristics of the perturbed TE_{11} empty waveguide mode were measured and are presented. In this case, the two degenerate circularly polarized modes which constitute the TE_{11} mode in an empty waveguide become non-degenerate and thus will have different phase characteristics. The results are in qualitative agreement with the theoretical work of Bevc and Everhart. It is demonstrated experimentally that as the magnetic field is reduced, at a given frequency, the propagation constants of the two modes approach each other and finally coincide at zero magnetic field.

I. INTRODUCTION

A plasma waveguide is any longitudinally uniform transmission system which has as one of its constituents a plasma. From a structural point of view, one of the simplest plasma waveguides is shown in Fig. 1. In this figure, the surface whose radius is c is metallic and of high conductivity, i.e., a copper surface. The region bounded by radii c and b contains vacuum or air so that the dielectric constant ϵ_3 in Fig. 1 is unity. The region bounded by radii b and a is a dielectric tube with a scalar permittivity ϵ_2, i.e., a glass tube, and the region bounded by radius a is filled with plasma. Finally, this system is immersed in a finite, longitudinal, constant magnetic field.

We see that this is a closed system with all fields contained within the metallic boundary. If c is of the order of an inch, we will not be surprised to find that the frequencies of wave propagation occur in the microwave range.

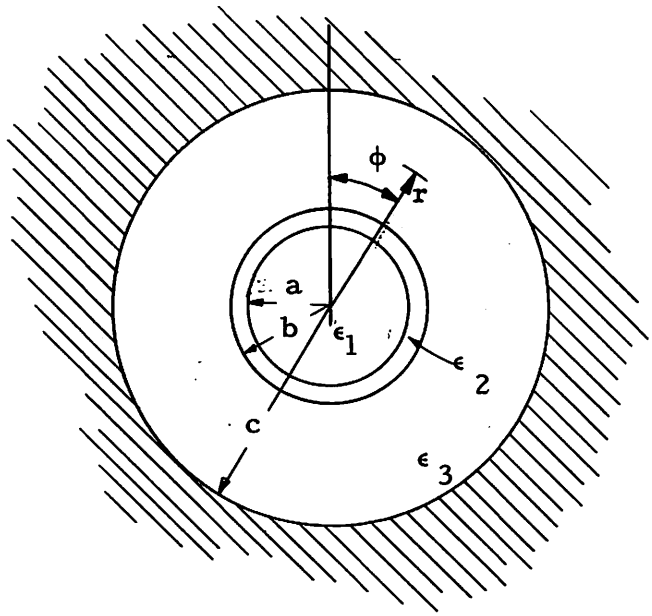

Fig. 1 Cross-Section of the Plasma Waveguide: Positive z-Axis Extends into Page.

The dielectric tube may in some cases be omitted so that instead of the three-region system shown in Fig. 1, we would have a two-region system of plasma and air. From a practical point of view, the function of the dielectric tube is to contain the plasma and would be necessary if the plasma, for example, was the positive column of a gaseous discharge. On the other hand, it could and would be omitted if the plasma were a cesium thermal plasma[1-3] which is contained by a magnetic field.

Due to its simplicity, this structure lends itself well to analysis. In 1939 the two-region system was investigated by Hahn[4] and Ramo[5] in which the plasma was a drifting electron beam confined by a magnetic field. In 1958, a thorough analysis of this system was made by Trivelpiece[6] in which a quasi-statis analysis was used throughout and the resulting modes were slow modes and transverse magnetic (TM). This work was extended by Bevc and Everhart[7] in which they carried the solutions into the fast-wave regime. Various other workers have analyzed this system from specialized points of view.[8,-11]

The results of the analyses show that in the presence of a plasma the empty waveguide modes become perturbed so that their propagation constants and field distributions are modified. Let us cause a non-symmetric waveguide mode to propagate alternately as a left-hand and then as a right-hand circularly polarized mode. If we introduce an isotropic plasma, we would find that the oppositely rotating modes are degenerate in the sense that both their propagation constants will be perturbed equally. If the plasma is made anisotropic by the application of the magnetic field, then this degeneracy is removed and the two modes will have different propagation constants--and therefore different--field distributions.

In addition to the perturbed waveguide modes, space charge waves are found.[6, 7, 9-11] If the plasma is isotropic, an infinite set of space charge modes will exist, the azimuthally symmetric mode being a low-pass

mode while the rest are passband modes.[6] These modes are called "surface waves" because their energy is concentrated at the plasma-glass interface and also because there is no charge accumulation inside the plasma, only on the plasma cylinder surface.

With the application of a magnetic field, additional low-pass modes are introduced[6] and a class of pass-band modes known as cyclotron modes[6,9,11] appear. These latter modes are backward-wave modes. All non-symmetric modes are non-degenerate.

Although the theory shows that an abundance of modes should exist in this system, their experimental investigation has been somewhat limited, and, particularly, there has been little good quantitative agreement between theory and experiment. This project was started in order to see what modes could be measured which had not been measured previously, to develop new techniques, and to determine how well the zero-temperature plasma waveguide theory will predict the modes that are measured.

The symmetric low-pass space-charge mode with and without magnetic field has been measured by Trivelpiece[6] and also by Reidel and Thelan.[12] They also were able to detect the presence of a backward-wave cyclotron mode. Their work has been extended here to a measurement of the non-symmetric mode whose field components vary as exp (i ϕ). ϕ is the azimuthal coordinate shown in Fig. 1. The magnetic field for these measurements is zero. This has been found to be a backward-wave pass-band mode, and it is shown that zero-temperature plasma waveguide theory predicts it and the accompanying symmetric mode quite precisely.

Historically, measurement of the perturbed waveguide modes has preceded space=charge mode measurements by at least a decade.[13] While a number of workers concerned themselves with perturbation by an

isotropic plasma,[13-17] Goldstein and his co-workers at the University of Illinois[18-20] and Pringle and Bradley[21] have observed Faraday rotation of the TE_{11} waveguide mode perturbed by an anisotropic plasma. In the work reported here, the propagation constants of the two oppositely rotating circularly polarized TE_{11} modes have been measured for the case of a perturbing anisotropic plasma. In these measurements, a resonant cavity technique was used.

II. THEORETICAL BACKGROUND

We present here a plasma waveguide theory which is pertinent to the experimental results that have been obtained. In particular, we consider surface waves for no magnetic field and perturbation of the TE_{11} waveguide mode. In both cases, loss is neglected. Finally, we consider loss and its consequences.

The theoretical investigation of wave propagation in plasma waveguides depends upon the solution of Maxwell's equations

$$\nabla \times \bar{E} = - i \omega \mu_j \bar{H}$$
$$\nabla \times \bar{H} = i \omega \epsilon_j \bar{E} \qquad (2.1)$$

subject to appropriate boundary conditions. $\bar{E}$ and $\bar{H}$ are the vector electric and magnetic fields and a time dependence of $e^{i\omega t}$ for these quantities is assumed. μ_j and ϵ_j are the permeability and permittivity, respectively, of the j-th region of the waveguide. In all cases considered here, $\mu_j = \mu_o$, the scalar permeability of free space.

If the j-th region is filled with plasma, then ϵ_j will in general be a tensor. An expression for ϵ_j which is in wide use today is[22]

$$\epsilon_j = \epsilon_o \begin{pmatrix} \epsilon_{rr} & \epsilon_{r\phi} & 0 \\ \epsilon_{\phi r} & \epsilon_{\phi\phi} & 0 \\ 0 & 0 & \epsilon_{zz} \end{pmatrix} , \qquad (2.2)$$

where

$$\epsilon_{rr} = \epsilon_{\phi\phi} = 1 - \frac{\omega_p^2 (1 - i\nu/\omega)}{\omega^2 (1 - i\nu/\omega)^2 - \omega_c^2} , \qquad (2.3a)$$

$$\epsilon_{r\phi} = -\epsilon_{\phi r} = i \frac{\omega_p^2 \omega_c/\omega}{\omega^2(1 - i\nu/\omega)^2 - \omega_c^2} \qquad (2.3b)$$

and

$$\epsilon_{zz} = 1 - \frac{\omega_p^2}{\omega^2} \frac{1}{(1 - i\nu/\omega)} \qquad (2.3c)$$

with

ϵ_o = permittivity of free space,

ω_p = plasma angular frequency $= \sqrt{\frac{e^2}{m_e} \frac{n_e}{\epsilon_o}}$,

n_e = electron number density,

ω_c = cyclotron angular frequency $= \frac{e}{m_e} B_o$,

ν = collision frequency,

m_e = electron mass,

e = electron charge (absolute value).

Here, we have assumed the use of cylindrical coordinates r, ϕ, and z shown in Fig. 1. Then $\bar{E}$ will have components E_r, E_ϕ and E_z with similar components for $\bar{H}$.

A. THE PERMITTIVITY TENSOR

At this point, it will be worthwhile to consider the assumptions that have been made in the expression for the plasma permittivity tensor (Eq. 2.2), where the plasma is the positive column of a mercury-vapor discharge. This is the plasma which has been used in the experiments described below. We may do this most easily by considering the Boltzmann

distribution function $f(\bar{r}, \bar{w}, t)$ for electrons of the plasma. Each electron of the plasma at a given time t may be specified by six numbers, the three components of its spatial position vector $\bar{r}$, and the three components of its vector velocity $\bar{w}$ and so may be represented by a point in a six-dimensional space called phase space which has as its six coordinates the three coordinates of $\bar{r}$ and the three coordinates of $\bar{w}$. Let us call the three-dimensional space in which $\bar{r}$ is the position vector, configuration space, and that in which $\bar{w}$ is the position vector, velocity space. When all the electrons of the plasma have been represented by points in phase space, f is the density of these points in that space.

If no perturbing forces act on the electrons, an equilibrium distribution will be reached which is invariant with time and may be represented by $f_o(\bar{r}, |\bar{w}|)$ where we indicate that f_o depends on the magnitude of $\bar{w}$ and so is isotropic in $\bar{w}$. If we now apply a small electric field to the plasma, the electrons tend to move in the direction of the field so that f is no longer isotropic in $\bar{w}$, and may be represented by an isotropic part $f_o(\bar{r}, |\bar{w}|)$ plus a small anisotropic part $f_1(\bar{r}, \bar{w}, t)$. If the electric field is suddenly removed, f_1 at every point in phase space will decline to zero. We assume that we can represent this by

$$f_1(\bar{r}, \bar{w}, t) \propto e^{-\nu t} \qquad (2.4)$$

where we assume for the moment that ν is a constant and has the physical significance of being the relaxation frequency of the anisotropic part of f. The mechanism by which the anisotropy in f is removed is through encounters between the electrons and the other components of the system, i.e., neutral atoms, ions, the container wall, and other electrons. ν is commonly called the collision frequency and a rigorous analysis[23] shows that for the case of a billiard ball system which is the only case for which the idea of collision frequency has a precise meaning, the expression for ν is just the classical collision frequency for that system.

From Eq. (2.4),

$$\frac{\partial f_1}{\partial t} = - \nu f_1 \ . \tag{2.5}$$

Now $f = f_o + f_1$ must obey Boltzmann's equation which in its most general non-relativistic form is

$$\frac{\partial f}{\partial t} + \bar{w} \ . \ \nabla f + \frac{\bar{F}(\bar{r}, t)}{m_e} \ . \nabla_w f = \left(\frac{\partial f}{\partial t}\right)_{coll} \tag{2.6}$$

where ∇ is the gradient in configuration space and ∇_w is the gradient in velocity space. $\bar{F}(\bar{r}, t)$ is the force on an electron at $\bar{r}$ and t. $\left(\frac{\partial f}{\partial t}\right)_{coll}$ is the collision term. For a force free region and one in which there is no diffusion so that $\bar{w} . \nabla f$ is zero, we have, using Eq. (2.5),

$$\left(\frac{\partial f}{\partial t}\right)_{coll} = - \nu f_1 \ . \tag{2.7}$$

We shall assume that Eq. (2.7) is valid when external forces are present and when the electrons experience diffusion, so that Boltzmann's equation becomes

$$\frac{\partial f}{\partial t} + \bar{w} \ . \ \nabla f + \frac{\bar{F}(\bar{r}, t)}{m_e} \ . \ \nabla_w f = - \nu f_1 \ . \tag{2.8}$$

The average vector speed $\bar{v}$ of electrons at the point $\bar{r}$ in configuration space is just the average of $\bar{w}$ at $\bar{r}$ over all possible velocities and weighted by $f(\bar{r}, \bar{w}, t)$,

$$\bar{v}(\bar{r}, t) = \frac{\int \bar{w} f(\bar{r}, \bar{w}, t) \, d\bar{w}}{\int f(\bar{r}, \bar{w}, t) \, d\bar{w}} \tag{2.9}$$

where $d\bar{w}$ is an element of volume in velocity space. Only f_1 contributes to the integral in the numerator. We recognize that $\int f(\bar{r}, \bar{w}, t) d\bar{w}$ is just $n_e(\bar{r}, t)$, the electron number density.

We now allow an rf electric field $\bar{E}$ to perturb the plasma and allow a dc magnetic field $\bar{B}_o$ to exist. If we then multiply Eq. (2.8) through by $m_e \bar{w}$ and integrate over all velocity space, it can be shown[23] that the following equation results:

$$m_e \left(\frac{\partial}{\partial t} + \bar{v} \cdot \nabla\right) \bar{v} = -e(\bar{E} + \bar{v} \times \bar{B}_o) - n_e^{-1} \nabla p - n_e^{-1} \int m_e \bar{w} \nu f_1 d\bar{w} \tag{2.10}$$

where we assume that the pressure tensor $\int m_e \bar{w} \bar{w} \, d\bar{w}$ can be represented by pI, where I is the identity tensor and p is the scalar pressure, given by an equation of state,

$$p \propto n_e^{\xi}$$

where ξ = constant.[10]

Equation (2.10) is rather like the mathematical statement of Newton's second law in which the left side is $m \, d\bar{v}/dt$ while the right side consists of the applied forces. It is known as the equation of <u>momentum transfer</u>.[23]

If the electric field is an rf field so that $\bar{E} = \bar{E}(\bar{r}) e^{i\omega t}$, then we may expect f_1 to vary as $e^{i\omega t}$ as will $\bar{v}$, which is derived from f_1. Neglecting $\bar{v} \cdot \nabla \bar{v}$ and $n_e^{-1} \nabla p$ and assuming that ν is a constant, Eq. (2.10) becomes

$$(i\omega + \nu) \bar{v} = -\frac{e}{m_e} (\bar{E} + \bar{v} \times \bar{B}_o) . \tag{2.11}$$

Using Eq. (2.11) and the relation for the rf current density

$$\bar{J} = e n_e \bar{v} ,$$

it is a matter of simple algebra to obtain the expression for the permittivity tensor, Eqs. (2.2) and (2.3).

Although Eq. (2.8) was derived in a rather non-rigorous fashion, it can be shown [23-25] that the same result is obtained from a rigorous approach. Equations (2.10) and (2.11) then result if ν is independent of $\bar{w}$. It must also be independent of $\bar{r}$ or else the elements of the permittivity tensor will be a function of spatial position. Referring to Eq. (2.4), this means that the relaxation frequency must be the same at all points in phase space. It can be shown [22-24] that for encounters between electrons and atoms this will indeed be the case as long as the electron doesn't approach the atom too closely. If encounters between electrons and the wall are predominant, then we might expect the relaxation frequency to be large at those values of $\bar{w}$ which cause electrons to move to a wall quickly, i.e., radially directed $\bar{w}$, and small for those values of $\bar{w}$ which tend to inhibit movement to the wall, i.e., axially directed $\bar{w}$. Also, ν may be a function of $\bar{r}$.

We will point out in Table III.1 that for the mercury-vapor discharge that has been used in the experiments to be reported in this work, encounters between electrons and the wall are more than twice as great as encounters between electrons and neutral atoms. Thus, conclusions drawn from the assumption of constant ν should be viewed with caution. This is especially true when the magnetic field is zero. For a finite magnetic field, wall encounters are reduced so that here, ν may indeed be a constant.

It should be clear that the effect of collisions on wave propagation is to introduce loss. We have established that wave propagation depends on an anisotropy in velocity being created by the electric field. Since collisions tend to destroy this anisotropy, they will consequently tend to damp the wave.

Inclusion of the diffusion term $n_e^{-1} \nabla p$ into the equation of momentum transfer leads to a small rf term in Eqs. (2.10) and (2.11) which varies as $e^{i\omega t}$, but which has been calculated using the parameters of our system to be of the order of 10^{-5} smaller than the term $\frac{e}{m_e} \bar{E}$, and so can be neglected. The smallness of this term is due to the relatively low temperature of the electrons, and shows that temperature effects for our system are negligible.

Finally, we may summarize this Section by noting that the expression for the permittivity tensor, Eqs. (2.2) and (2.3), should give an accurate mathematical description of the plasma used in the experiments to be reported here, except that it may not be possible to represent collisional effects by a scalar constant ν.

B. LOSSLESS PLASMA WAVEGUIDES

Consider a plasma which is collisionless and therefore loseless. We shall see how these results may be modified due to collisions in the latter part of this section. For a collisionless plasma, $\nu = 0$ and the elements of the permittivity tensor become simply,

$$\epsilon_{rr} = \epsilon_{\phi\phi} = 1 - \frac{\omega_p^2}{\omega^2 - \omega_c^2} \quad ,$$

$$\epsilon_{r\phi} = -\epsilon_{\phi r} = i \frac{\omega_p^2 (\omega_c/\omega)}{\omega^2 - \omega_c^2} \quad , \tag{2.12}$$

$$\epsilon_{zz} = 1 - \omega_p^2/\omega^2 \quad .$$

We shall be interested in the solution of Eq. (2.1) for the case of zero magnetic field ($\omega_c = 0$) which leads to surface waves, or waves whose energy is concentrated at the plasma-glass wall interface. Also, we

shall be interested in the perturbed TE_{11} waveguide mode.

1. Surface Modes ($\omega_c = 0$). This case has been treated in considerable detail by Trivelpiece,[6] although he has not found all the results that we shall need. Here, the permittivity of the plasma is a simple scalar,

$$\epsilon_1/\epsilon_o = 1 - (\omega_p/\omega)^2 . \tag{2.13}$$

Trivelpiece finds that this case may be adequately treated by using a quasi-static analysis in which only TM modes exist which are slow modes, i.e. $\beta^2 >> (\omega/c)^2$, where we assume that the z (axial) dependence of all field components is $e^{-i\beta z}$.

Because a quasi-static analysis is used,

$$\overline{E} = -\nabla\Phi$$

where

$$\Phi = R_n(r)\, e^{in\phi}\, e^{-i\beta z} \tag{2.14}$$

Then,

$$R_n(r) = \begin{cases} A\, I_n(\beta r) & \text{inside the plasma} \\ B[I_n(\beta r)\ K_n(\beta b) - I_n(\beta b)\, K_n(\beta r)] & \text{outside the plasma,} \end{cases} \tag{2.15}$$

where I_n and K_n are the modified Bessel functions of order n, an integer, and $\underline{b}$ is shown in Fig. 1. It is seen that we obtain an infinite set of modes, one for each value of the integer n. Since the fields vary as the modified Bessel functions, inside the plasma they will be largest at the plasma edge, i.e., at $r = \underline{a}$. Outside the plasma, E_ϕ and E_z will decrease and become zero at the metal waveguide wall. Thus, the energy stored in the electric field is concentrated in the region of the plasma-glass interface. This fact becomes especially true when β is large.

We may obtain a determinantal equation for β by taking the solutions given by Eqs. (2.14) and (2.15) in the various regions and applying the appropriate boundary conditions at the edges of a region. In particular, we require that E_z and ϵE_r be continuous across a boundary. The resulting determinantal equation is[6]

$$\left[1 - \left(\frac{\omega_p}{\omega}\right)^2\right]\frac{I_n'(\beta a)}{I_n(\beta a)} =$$

$$\epsilon_2 \frac{\epsilon_2[I_n'(\beta a)K_n'(\beta b) - I_n'(\beta b)K_n'(\beta a)] + Q[I_n(\beta b)K_n'(\beta a) - I_n'(\beta a)K_n(\beta b)]}{\epsilon_2[I_n(\beta a)K_n'(\beta b) - I_n'(\beta b)K_n(\beta a)] + Q[I_n(\beta b)K_n(\beta a) - I_n(\beta a)K_n(\beta b)]}, \tag{2.16}$$

where

$$Q = \frac{I_n(\beta c)K_n'(\beta b) - I_n'(\beta b)K_n(\beta c)}{I_n(\beta c)K_n(\beta b) - I_n(\beta b)K_n(\beta c)}$$

for the three-region system shown in Fig. 1.

In Fig. 2, βa has been plotted versus ω/ω_{co} for n = 0, 1, 2 where

$$\omega_{co} = \omega_p / \sqrt{1 + \epsilon_2} \tag{2.17}$$

It is seen that the symmetric mode (n = 0) is a low-pass mode, as has been amply demonstrated theoretically and experimentally by Trivelpiece.[6] The higher-order modes, however, are seen to be backward-waves, each occupying a narrow pass-band. By using the large argument approximations for the various Bessel functions in Eq. (2-16), it is possible to determine that all modes approach the common cut-off frequency ω_{co} given by Eq. (2.17) at large values of β.

If we consider a two-region system in which the plasma column of radius $\underline{a}$ is bounded by a material of permittivity ϵ_2 which fills the space

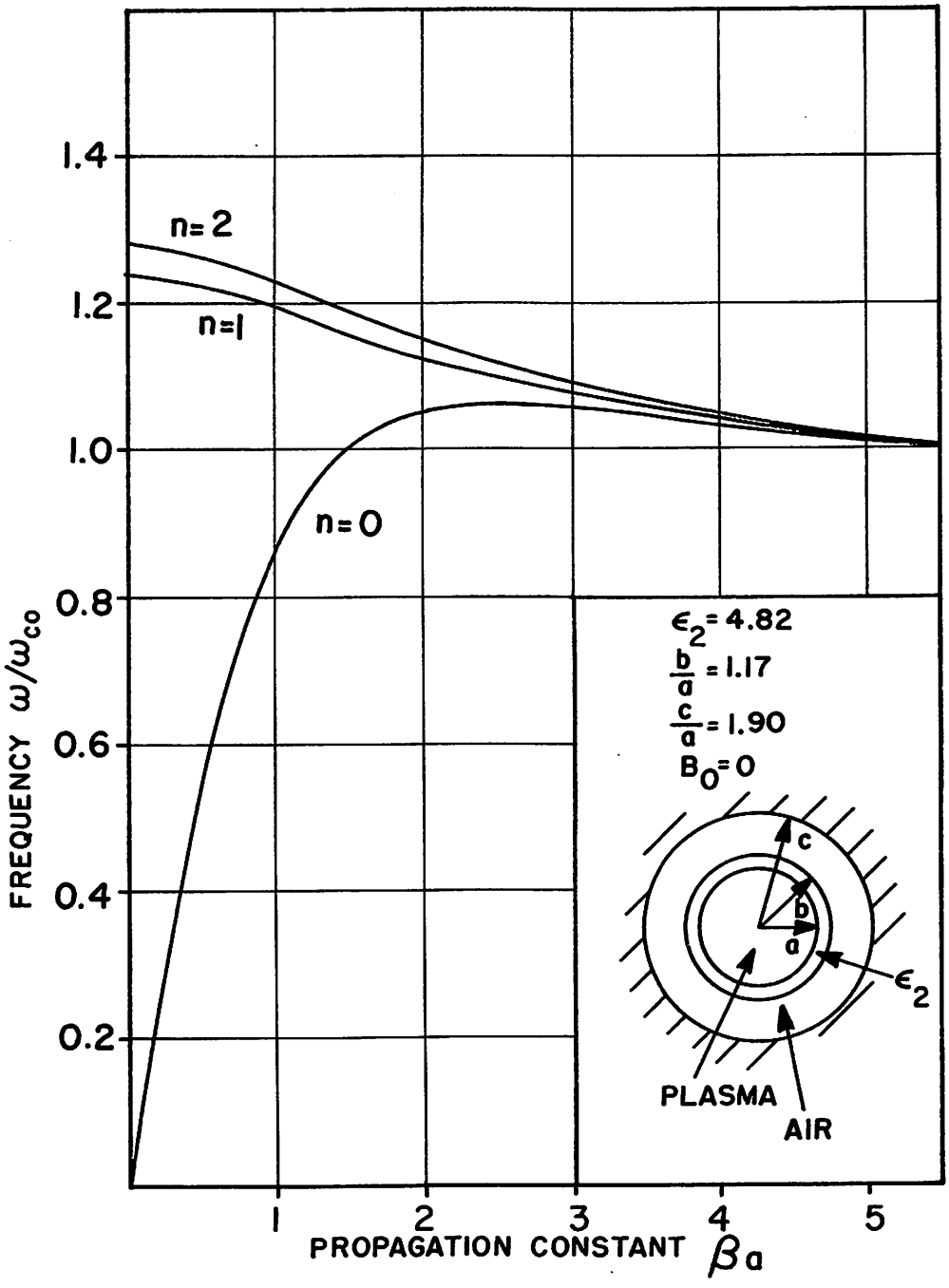

Fig. 2 Phase Characteristics of the n = 0, 1, 2 Surface Modes on a Plasma Column Surrounded by a Thin Dielectric Tube.

between the plasma and the metal wall of radius b, then it has been shown[6] that the n = 1 mode is a forward mode (except at values of βa lower than about 1/2) again occupying a narrow pass-band. The cut-off frequency at β = 0 is

$$\omega_u = \omega_p / \sqrt{1 + p\epsilon_2} \tag{2.18}$$

where

$$p = \frac{b^2 + a^2}{b^2 - a^2} > 1 ,$$

while the cut-off frequency at infinite β is again given by Eq. (2.17). We can now discern that in the three-region system, the glass tube causes the n = 1 mode (and probably the higher order modes) to be a backward mode. Referring to Fig. 3, at β = 0, the cut-off frequency ω_u is determined by permittivity ϵ'_2 which is an average of the permittivity of the glass tube and the air space weighted approximately according to the volume occupied by each. This is because at β = 0, the energy in the electric field is not concentrated near r = a, and a large portion of it will be found in the air space.

As β increases, the energy in the electric field becomes increasingly concentrated near r = a or in the glass. Thus, the effective permittivity of the glass and air space approaches that of the glass so that ω_{co} is continually decreasing. In the limit of infinite β, the effective permittivity is just that of the glass, ϵ_2. This can cause ω_{co} to be less than ω_u with the result that we will have a backward-wave mode. This is illustrated in Fig. 3.

2. Perturbed TE_{11} Waveguide Mode. If we consider a TE_{11} mode in an empty circular waveguide, it is well known that this mode is linearly polarized in the plane transverse to the waveguide axis. This linearly

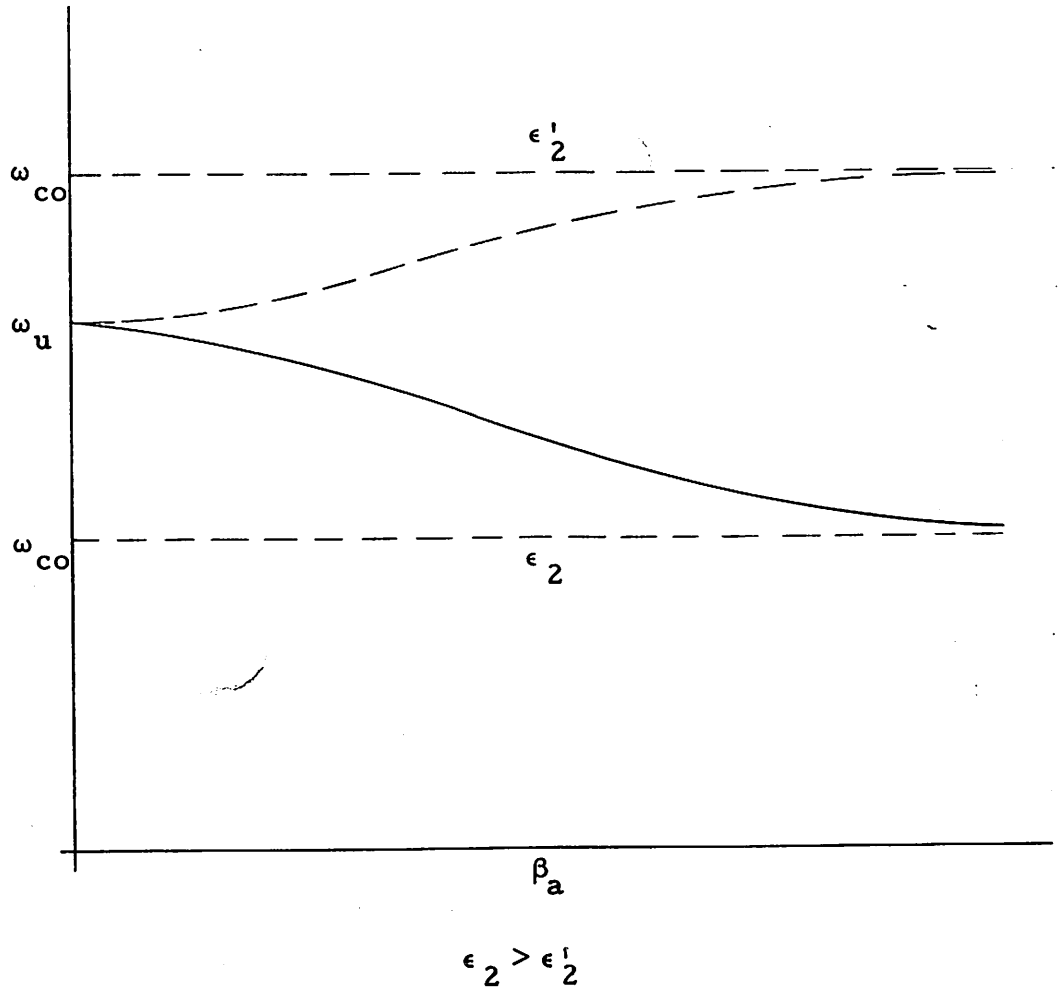

Fig. 3 Effect of the Permittivity of the Dielectric Tube on the Cut-off Frequencies of the n=1 Mode.

polarized mode can be resolved into two circularly polarized modes rotating in opposite directions but with the same propagation constant. If we now introduce a plasma column on the waveguide axis and introduce an axial constant magnetic field B_o, we may expect that the resulting anisotropic plasma will have an unequal perturbing effect on the two circularly polarized modes. This is because the electrons of the plasma have a preferred sense of rotation and so will interact

with the mode which rotates in the same sense as they, in a different manner from the mode which rotates in the opposite sense. We designate the circularly polarized mode rotating in the same sense as the electrons by TE_{11}^{+} and the mode rotating in the opposite sense by TE_{11}^{-}. Specifically, at a given frequency, we may expect β-- and therefore the fields of the two modes--to be different.

We might expect that if the radius of the plasma column was small compared to that of the metal waveguide and if the plasma frequency were small compared to the signal frequency, the perturbations of β could be found by the perturbation techniques developed by Slater.[26] Indeed, this has been done by Buchsbaum, et al.,[22] in which they considered the perturbation of the resonant frequency of a cavity resonant in the TE_{lmn} mode. They found that the TE_{lmn}^{+} resonance shifts up in frequency from the TE_{lmn} resonance at $\omega_c = 0$, while the TE_{lmn}^{-} resonance shifts down. The shift in frequency of the TE_{lmn}^{+} resonance is larger than the TE_{lmn}^{-} frequency. Thus, we would expect the plot of ω vs. β for the TE_{11}^{+} mode to lie above the plot for the TE_{11}^{-} mode on the Brillouin diagram.

These results are in accord with those of a formal field analysis of this case made by Bevc and Everhart.[7] Like Trivelpiece, they assumed that all field components have a variation proportional to

$$e^{i(\omega t - \beta z + n\phi)} \qquad (2.19)$$

but now we may expect that β for $+|n|$ will be different from β for $-|n|$. The variation of Eq. (2.19) indicates a field pattern which at constant z rotates with an angular velocity of

$$\dot{\phi} = -\frac{\omega}{n}, \quad n \neq 0 \quad , \qquad (2.20)$$

so that a mode characterized by a certain signed n is a circularly polarized mode.

We shall not attempt to find the precise quantitative dependence of ω on β for the three-region system used in the experiments as was done in part a above. The Slater perturbation technique is not useful because of large ω_p/ω and because the plasma radius is not small compared to waveguide radius. Referring to the results of Bevc and Everhart, for a two-region system in which the plasma diameter is half the waveguide diameter of 1.20 in. (the same as in our experimental system), for $f_p = 1.98$ Gc., they find that the cut-off frequency of the TE_{11}^{+} mode increases by 130 Mc. in going from $f_c = 0$ to $f_c = 2.73$ Gc. For the case of a filled waveguide they show that the cut-off frequency of the TE_{11}^{-} mode changes much less than that of the TE_{11}^{+} mode. At large values of β, the two modes coincide. Thus, in a measurement of the TE_{11}^{+} and TE_{11}^{-} modes, we would expect to find on the Brillouin diagram the plot of the TE_{11}^{+} mode located approximately 130 Mc above that for the TE_{11}^{-} mode at small values of β, with the two merging at large β.

C. RELATION BETWEEN THE COLLISION FREQUENCY AND THE ATTENUATION CONSTANT

In II. B it was assumed that $\nu = 0$ so that a mode propagates without loss. Thus all field components propagate as $e^{-i\beta z}$ where β is real. In the real world, ν is not zero, losses are always present, and we would expect a field component to propagate as $e^{-i\gamma z}$ where $\gamma = \beta - i\alpha$ is complex. We call β the propagation constant and α the attenuation constant.

We would like to now show in a non-rigorous way the relation between ν and α. In the next section, we will show that approximately the same expression can be obtained by using a rigorous approach.

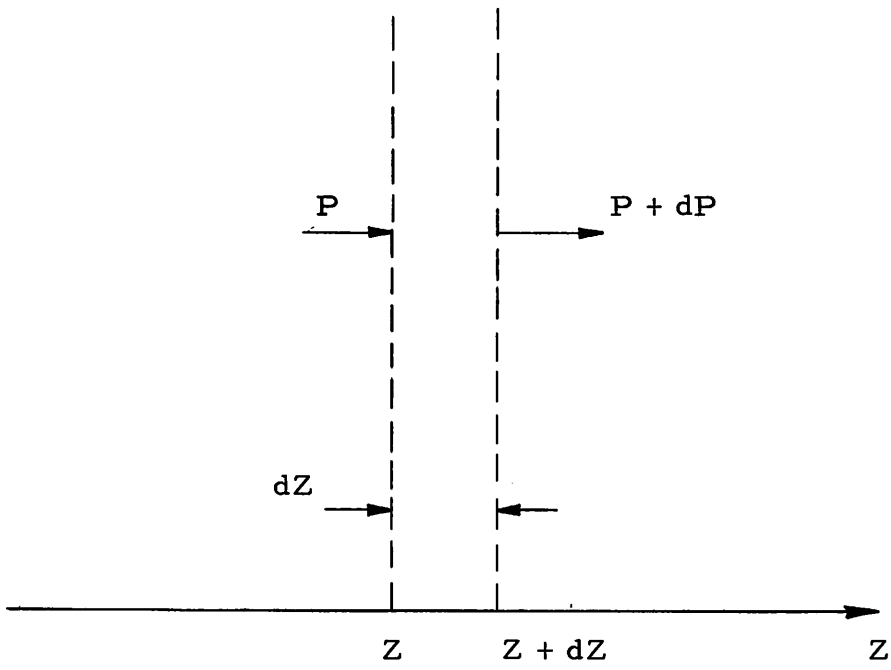

Fig. 4 Power Flow in a One-Dimensional System.

We consider a one-dimensional system in which a single mode propagates in the + z direction as shown in Fig. 4. It is now convenient to think of collisions between electrons and the other components of the system as occurring in the billiard ball sense, i. e., a collision takes place in a time interval very much shorter than the time between collisions, before and after this collision time-interval there is no interaction between an electron and the component of the system with which it collides, and the collision is purely elastic. Thus, a collision is well defined and so the collision frequency has a precise meaning. We call this frequency ν and assume it is a constant, independent of $\bar{r}$ and $\bar{w}$.

In Fig. 4 we represent the power per unit area of the mode at a point z by P. If the plasma is lossy, the power per unit area will be less at z + dz, namely, P + dP where dP is negative. The energy

stored in the mode will be partly stored in the electromagnetic fields of the mode (in the electric field almost entirely if the wave is a slow mode)and partly in the form of kinetic energy of the electrons.

There is a continual exchange of energy from the electromagnetic form to the kinetic form. The electric field acts upon an electron, and transfers mode energy to it. In doing this it gives it an rf velocity which that electron must maintain in order to be able to give its mode energy back to the electric field again. If the electron suffers a collision, the direction of its rf velocity becomes changed and the electron cannot give its mode energy back to the electric field. This energy eventually becomes distributed among the other degrees of freedom of the system and is lost to the mode.

In Fig. 4, let the number of electrons per unit volume be N and call the velocity with which the energy of the mode travels, v_g, the group velocity. Since the energy per unit volume is P/v_g, we have that the energy per unit area stored between z and z + dz is $(P/v_g)dz$, and that the energy carried per electron in dz is

$$\frac{1}{2} \left(\frac{P}{v_g}\right) dz \left(\frac{1}{Ndz}\right) = \frac{1}{2} \frac{P}{v_g N} ,$$

where we introduce the factor $\frac{1}{2}$ since on the average only $\frac{1}{2}$ the total stored energy is in the form of kinetic energy of the electrons.

Since an electron suffers ν collisions per second, in one second one electron will cause $\frac{1}{2} \frac{P}{v_g N} \nu$ units of energy to be lost and since there are Ndz electrons per unit area in dz, the total energy per unit area lost per second in dz is

$$dP = - \frac{P \nu}{2 v_g} dz . \qquad (2.21)$$

where the minus sign indicates power lost. Integrating Eq. (2. 21) yields

$$P = P_o e^{-\frac{\nu}{2v_g} z} \tag{2. 22}$$

But it is well known[27] that power decays as

$$P = P_o e^{-2\alpha z} \tag{2. 23}$$

so that

$$\alpha = \frac{\nu}{4v_g} \tag{2. 24}$$

Thus we see that when a mode has its stored energy traveling slowly the mode will propagate with greater loss than when the energy velocity is high.

In the above, it would have been more correct to use energy velocity than group velocity since in a medium which is dispersive, such as a plasma, the two are not always the same.[28] Nevertheless, we have assumed their equivalence in this development.

D. PLASMA WAVEGUIDE WITH LOSS

We now present an introduction to the subject of plasma waveguides with loss. We shall consider a specific case, namely the propagation of the n = 0 surface wave ($\omega_c = 0$) considered in II. B. We will use only a two-region system (no glass tube) and will call the radius of the plasma a as before but will call the radius of the metal waveguide b. ϵ_1 is the permittivity of the plasma and ϵ_2 is the permittivity of the material filling the space between the plasma and the metal wall, the latter being a scalar constant.

For ϵ_1 we use Eqs. (2. 2) and (2. 3) where we will let $\omega_c = 0$. Then,

$$\epsilon_1 = \epsilon_1' + i\epsilon_1'' ,$$

$$\epsilon_1' = 1 - \left(\frac{\omega_p}{\omega}\right)^2 \cdot \frac{1}{1 + \frac{\nu^2}{\omega^2}} , \qquad (2.25)$$

$$\epsilon_1'' = - \frac{\omega_p^2}{\omega^2} \frac{\nu}{\omega} \cdot \frac{1}{1 + \frac{\nu^2}{\omega^2}} .$$

We assume ν is a constant of the system, and not a function of $\bar{r}$ or $\bar{w}$.

A non-zero ϵ_1'' will result in energy being absorbed from a wave propagating in the system. We therefore assume an axial variation of any field component of

$$e^{-i\gamma z}$$

where $\gamma = \beta - i\alpha$.

The calculation of the determinantal equation for γ proceeds exactly as shown by Trivelpiece[6] and is identical to his Eq. (IV. 9) except that his β has been replaced by our γ and the term in ϵ_1'' now appears. This equation is

$$\frac{\epsilon_1'}{\epsilon_2} + i \frac{\epsilon_1''}{\epsilon_2} = \frac{I_o(\gamma a)}{I_o'(\gamma a)} \frac{I_o'(\gamma a) K_o(\gamma b) - I_o(\gamma b) K_o'(\gamma a)}{I_o(\gamma a) K_o(\gamma b) - I_o(\gamma b) K_o(\gamma a)} , \qquad (2.26)$$

The assumption by which this equation was derived is that

$$|\mathrm{Re}\ \gamma^2| = |\beta^2 - \alpha^2| >> \left(\frac{\omega}{c}\right)^2 |\epsilon_i|$$

$$|\mathrm{Im}\ \gamma^2| = |2\alpha\beta| >> \left(\frac{\omega}{c}\right)^2 |\epsilon_1''| \,. \qquad (2.27)$$

This and the assumption of a TM mode allows the quasi-static approximation to be used where

$$\vec{E} = -\nabla\Phi \,.$$

The form of Φ which will satisfy the differential equations is

$$\Phi = A_n(r)\, e^{-i\gamma z} \,.$$

We shall be interested in the dependence of γ on ω, obtained from Eq. (2.26), in the vicinity of the large β cut-off frequency ω_{co}. We may expect α to be fairly large here so that conditions stated in Eq. (2.27) should easily be met.

For large β, the Bessel functions in Eq. (2.26) can be replaced by the simple algebraic functions

$$I_n(v) \longrightarrow \sqrt{\frac{1}{2\pi v}}\, e^{v} \,,$$

$$|v| \longrightarrow \infty \,, \quad \frac{\pi}{2} > \arg v > -\frac{\pi}{2} \,, \qquad (2.28)$$

$$K_n(v) \rightarrow \sqrt{\frac{\pi}{2v}}\, e^{-v} \,,$$

$$|v| \longrightarrow \infty, \quad \frac{\pi}{2} > \arg v > -\frac{\pi}{2} \,.$$

Using Eqs. (2.28), Eq. (2.26) becomes*

$$\frac{\epsilon_1'}{\epsilon_2} + i\,\frac{\epsilon_1''}{\epsilon_2} = \frac{e^{-\gamma s} + e^{\gamma s}}{e^{-\gamma s} - e^{\gamma s}} \qquad (2.29)$$

where $s = b - a$.

Note that for $\nu = 0$, $\gamma = \beta \longrightarrow \infty$,

$$\frac{\epsilon_1'}{\epsilon_2} = \frac{1}{\epsilon_2}\left(1 - \frac{\omega_p^2}{\omega^2}\right) = -1$$

and $\omega = \omega_{co} = \dfrac{\omega_p}{\sqrt{1 + \epsilon_2}}$, in agreement with Trivelpiece.[6]

Substituting $\beta - i\alpha$ for γ in Eq. (2.29) we find

$$\frac{\epsilon_1'}{\epsilon_2} + i\,\frac{\epsilon_1''}{\epsilon_2} = -\frac{1 - e^{-4\beta a} + 2i\,e^{-2\beta s}\sin 2\alpha s}{1 - 2e^{-2\beta s}\cos 2\alpha s + e^{-4\beta s}}\,. \qquad (2.30)$$

We now define

$$x = e^{-2\beta s}\,,\ 1 \geq x \geq 0 \text{ for } \beta \geq 0, \qquad (2.31a)$$

$$y = 2\alpha s,\ y \geq 0, \qquad (2.31b)$$

$$A = -\frac{1}{\epsilon_2}\left[1 - \frac{\omega_p^2}{\omega^2}\,\frac{1}{1 + \frac{\nu^2}{\omega^2}}\right]\,,\ A > 0 \text{ for } \omega < \omega_p \Big/ \sqrt{1 + \frac{\nu^2}{\omega^2}}\,, \qquad (2.31c)$$

---

* This asymptotic form of the determinantal equation for γ would be found for a surface wave of any order n using the asymptotic expressions in Eqs. (2.28). However the error in γ, where γ is obtained from it, is least for the n = 0 mode and increases rapidly with n, especially at low values of $|\gamma|$.

$$B = \frac{1}{2\epsilon_2}\left(\frac{\omega_p^2}{\omega^2}\right)\left(\frac{\nu}{\omega}\right)\frac{1}{1+\frac{\nu^2}{\omega^2}} \quad \text{(loss parameter)}, \quad B \geq 0. \tag{2.31d}$$

Then

$$A = \frac{1 - x^2}{1 - 2x\cos y + x^2}, \tag{2.32}$$

$$B = \frac{x \sin y}{1 - 2x\cos y + x^2}.$$

The expression for A is divided into the expression for B to give a quotient dependent on x and sin y. This may be solved for sin y. The expression for A is solved for cos y. By using

$$\sin^2 y + \cos^2 y = 1$$

an equation for x alone will result. This is a bi-quadratic in x, and it can be easily solved for x^2:

$$x^2 = \pm\frac{(2B)^2 + (A \mp 1)^2}{(2B)^2 + (A+1)^2}. \tag{2.33}$$

The negative solution must be discarded since x is positive or zero. The solution with (A + 1) must be discarded since this would give a trivial solution of $x^2 = 1$. We have, finally,

$$x^2 = \frac{(2B)^2 + (A-1)^2}{(2B)^2 + (A+1)^2}. \tag{2.34}$$

The expression for y may now be found:

$$\sin y = \frac{4B}{\sqrt{(2B)^4 + 2(2B)^2(1 + A^2) + (A^2 - 1)^2}} \qquad (2.35)$$

When $A = 1$, $\omega = \omega_{co}$. At this value of ω,

$$\left.\begin{aligned} x = e^{-2\beta s} &= \frac{B}{\sqrt{B^2 + 1}} \\ \sin y = \sin 2\alpha s &= \frac{1}{\sqrt{B^2 + 1}} \end{aligned}\right\} \quad \omega \doteq \omega_{co} \qquad (2.36)$$

This value of x corresponds to approximately a maximum value of β. Reference to Eq. (2.34) shows that β will increase to this maximum at $\omega = \omega_{co}$ and then will decrease for $\omega > \omega_{co}$. This behavior is shown in Fig. 5 for a set of typical parameters. Thus, β does not approach infinity as in the lossless case, but has a maximum value determined by ν.

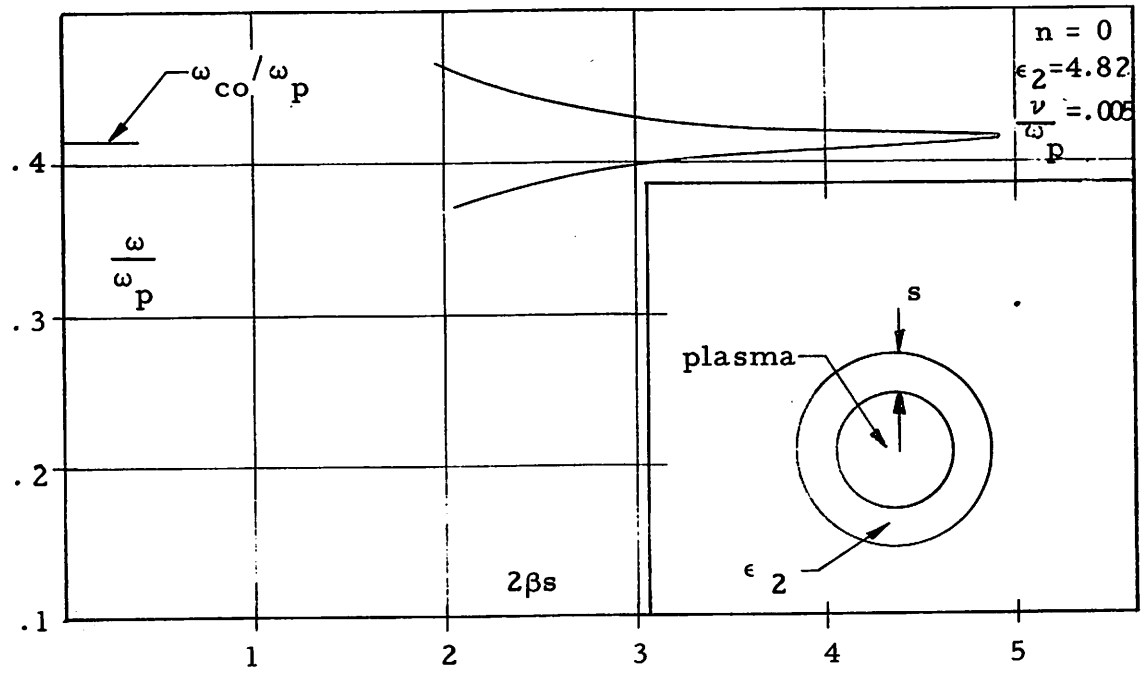

Fig. 5 The Phase Characteristics of the n = 0 Mode at Large Values of $2|\gamma|s$.

Also we note from Eq. (2.34) that β is unaffected by loss except near its maximum, i.e., very near $\omega = \omega_{co}$ where $\sin 2\alpha s = 1/\sqrt{B^2+1} \approx 1$. Thus, if

$$2\alpha s < \frac{\pi}{2}, \tag{2.37}$$

the parameter controlling β is ω_p and not ν. From the discussion in II.A we may then conclude that for the n = 0 mode, if Eq. (2.37) is satisfied, the permittivity ϵ_1/ϵ'_0 given in Eq. (2.13) should allow an accurate calculation of β.

y, on the other hand, is small at $\omega < \omega_{co}$, increases to about $\pi/2$ at $\omega = \omega_{co}$, and then continues to increase to a maximum of

$$\sin y = \frac{4B}{(2B)^2+1}, \quad \pi \geq y > \frac{\pi}{2}$$

for $\omega > \omega_{co}$. This behavior is shown in Fig. 6.

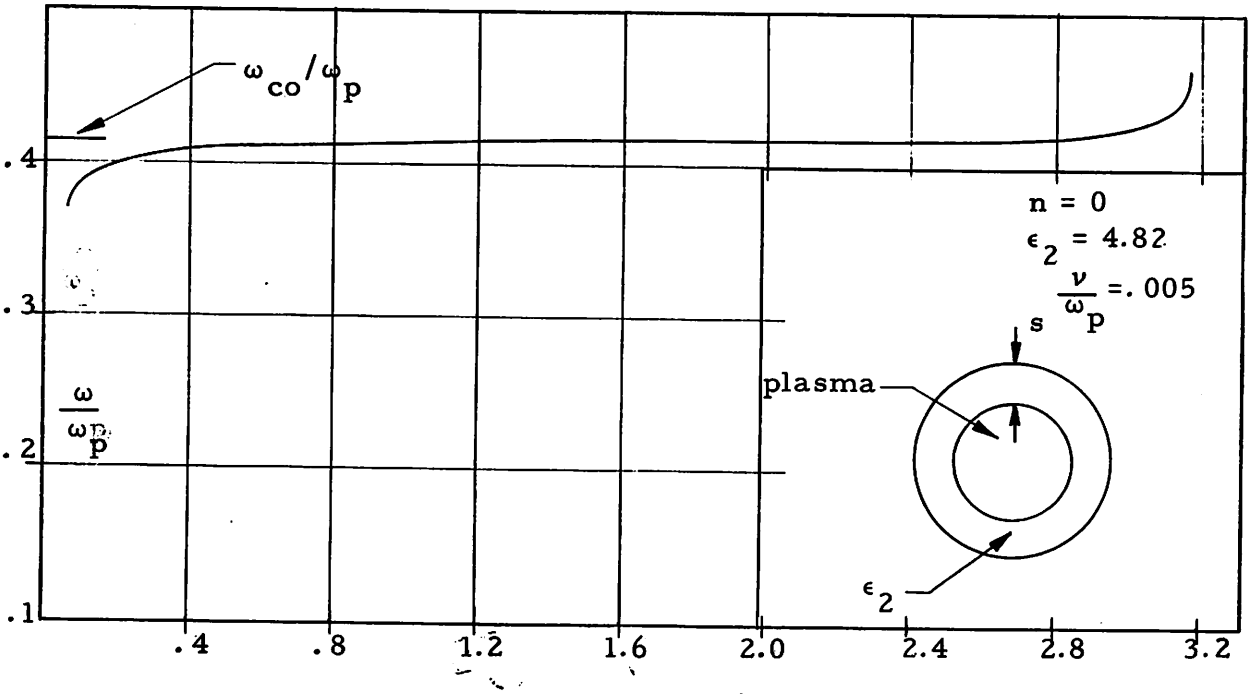

Fig. 6 The Attenuation Characteristics of the n = 0 Mode at Large Values of $2|\gamma|s$.

It is now possible to obtain an expression for α in terms of the group velocity subject to the limitations expressed in Eqs.(2. 27) and (2.28). We further assume that A is enough different from unity so that the term $(2B)^2$ in Eqs.(2. 34) and (2. 35) is negligible compared to $(A - 1)^2$ or $(A + 1)^2$. This further limits the analysis to regions removed from where β has its maximum. Then Eqs. (2. 34) and (2. 35) reduce to

$$x = \frac{A - 1}{A + 1} , \tag{2. 38}$$

$$\sin 2\alpha s = \frac{4B}{A^2 - 1} . \tag{2. 39}$$

Now $x = e^{-2\beta s}$ so that

$$\frac{dx}{d\omega} = - 2 \frac{d\beta}{d\omega} s e^{-2\beta s} = \frac{-2sx}{v_g} \tag{2. 40}$$

where we recognize $d\omega/d\beta$ as the group velocity, v_g. Differentiating Eq. (2. 38) with respect to ω, we have

$$\frac{dx}{d\omega} = 2 \frac{dA}{d\omega} \frac{1}{(1 + A)^2} . \tag{2. 41}$$

The derivative of A with respect to ω may be obtained from Eq. (2. 31c),

$$\frac{dA}{d\omega} = - \frac{4}{v} B . \tag{2. 42}$$

Equating Eqs. (2. 41) and (2. 40) and making use of Eq. (2. 42), Eq. (2. 39) becomes,

$$\frac{\sin 2 \alpha s}{2 s} = \frac{1}{2} \frac{v}{v_g} \tag{2. 43}$$

For $2\alpha s << 1$, $(\omega < \omega_{co})$ we have

$$\alpha = \frac{1}{2} \frac{\nu}{v_g} \tag{2.44}$$

Comparing this with Eq. (2.24), we see that the simple derivation of II. C yields a result which is qualitatively correct in that it shows the correct dependence of α on the parameter of the system. It is quantitatively correct to within a factor of 1/2.

III. THE EXPERIMENTAL SYSTEMS

The experimental systems used in this work were a traveling wave system and a resonant system. The former was used to measure the characteristics of the surface modes because their attenuation was expected to be high over a large range of propagation constant; the latter was used with the perturbed TE_{11} mode where attenuation was expected to be low. The pertinent structural details of these systems are described below.

A. THE PLASMA WAVEGUIDE

The basic unit in both systems is the plasma waveguide. This consists of a copper circular waveguide 1.2 in. in diameter coaxial with a mercury-vapor discharge tube. The properties of this discharge are described in III. D of this section and in the Appendix. In all measurements reported here, the glass tube containing the discharge is pyrex with an inner diameter of .63 in. and an outer diameter of .74 in. The wall thickness of the glass was found to vary by $\pm$ .022 in. The discharge tube is shown in Fig. 7.

In all measurements, the radial component of the electric field, E_r, in the air space between the glass tube and the copper waveguide was sampled by means of a small probe inserted through the copper wall. In order to move the probe longitudinally, the copper waveguide was slotted along its entire length. A sliding carriage through which the probe protruded was made such that it filled the slot at all positions. This can be seen in Fig. 8. It was necessary to fill the slot in anticipation of exciting modes with circumferentially directed wall currents. Mechanically, the system was nearly optimum. There was no play between the carriage and the waveguide.

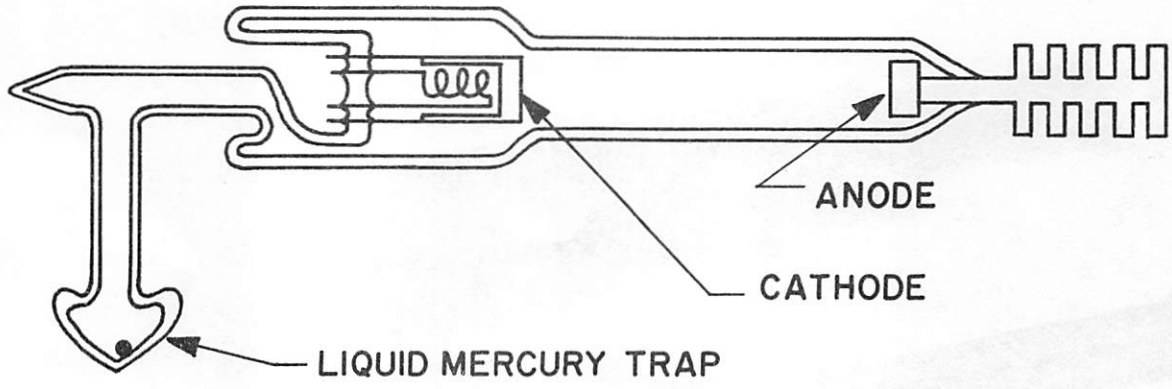

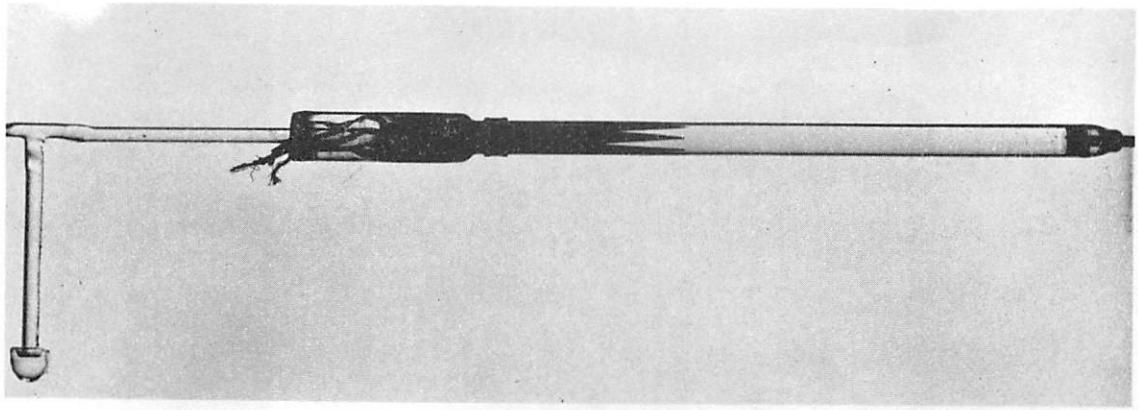

Fig. 7 Mercury-Vapor Discharge Tube. Photograph Shows Tapered Aqua-Dag Attenuator.

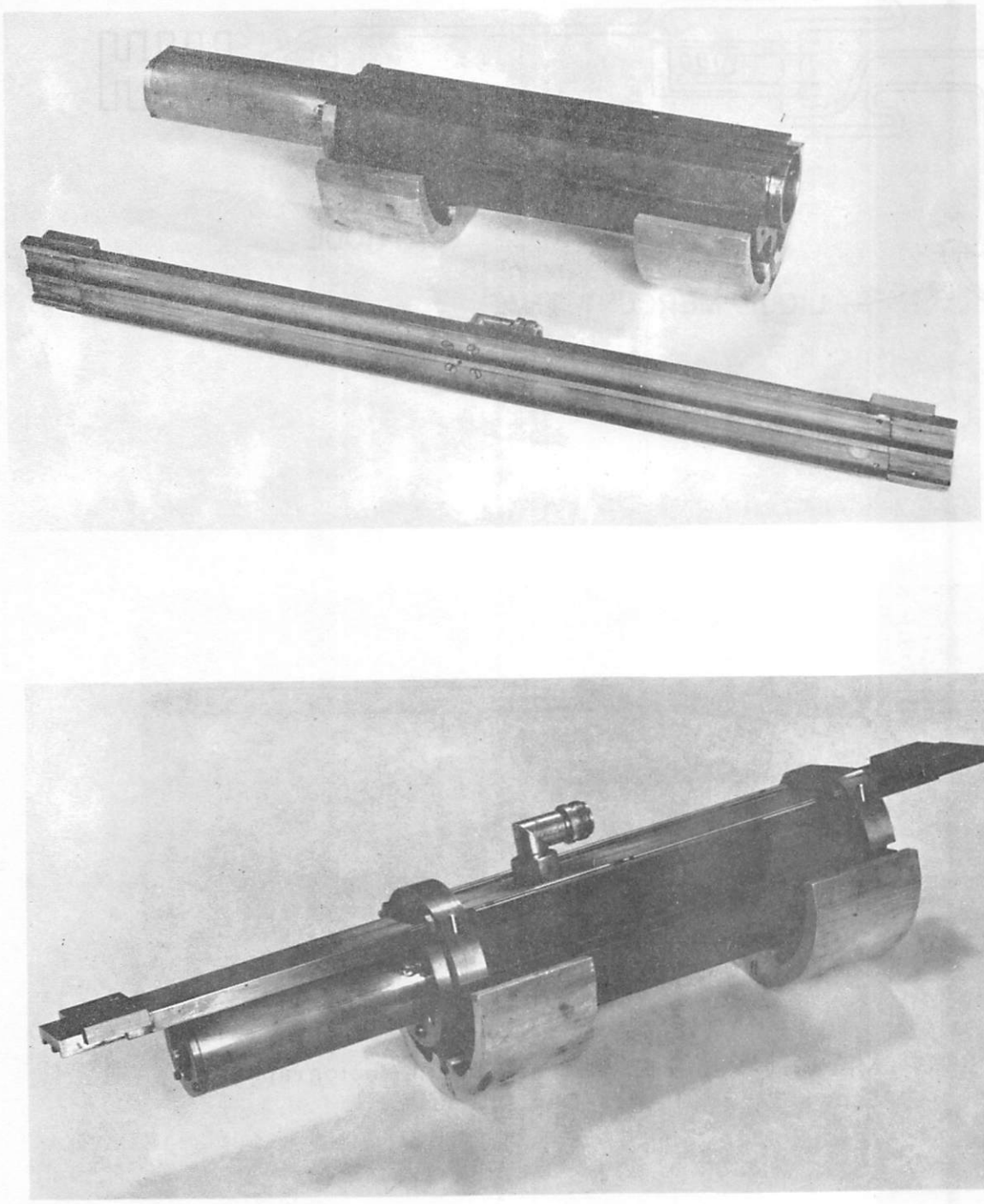

Fig. 8 Copper Waveguide and Probe Carriage.

The magnet used to provide the magnetic field in these measurements was 26 in. long with a 4 in. bore. The magnet current was time-regulated to approximately one part in one-thousand. The magnetic axis of symmetry (assumed to be a straight line) did not coincide with the geometric axis of symmetry so that extraordinary measures had to be taken to insure that the plasma waveguide was coaxial with the magnetic axis. At large magnetic fields, it was found that on the magnet axis and at the center of the magnet a region 7.5 in. long existed at the extreme ends of which the magnetic field had dropped off by 1 percent of its value at the magnet center. For a region 13.5 in. long, the field at each end had dropped by 3 percent. The active region of the plasma waveguide was always located within this 13.5 in. region, so that the maximum variation of the magnetic field over it was 3 percent. At low magnetic fields, such as those used in the surface mode measurements, this is no longer true. Fig. 9 shows the field variation on the axis as a function of distance along the magnet at low fields. Here we see that the variation of field over the active length of the plasma waveguide never exceeds one gauss.

B. TRAVELING WAVE SYSTEM

This system, used in measuring the characteristics of the surface mode , makes use of an input coupler and a waveguide termination. It is shown in Fig. 10.

1. Double-ring coupler. It has been shown in Section II that the surface mode which propagate in the absence of a magnetic field have a z-component of electric field, E_z, which varies radially as the modified Bessel functions. For example, inside the plasma, for a mode whose azimuthal phase varies by $2n\pi$ around the circumference,

$$E_{zn} = A\, I_n(\beta r)\, e^{in\phi}\, e^{-i\beta z} \qquad (3.1)$$

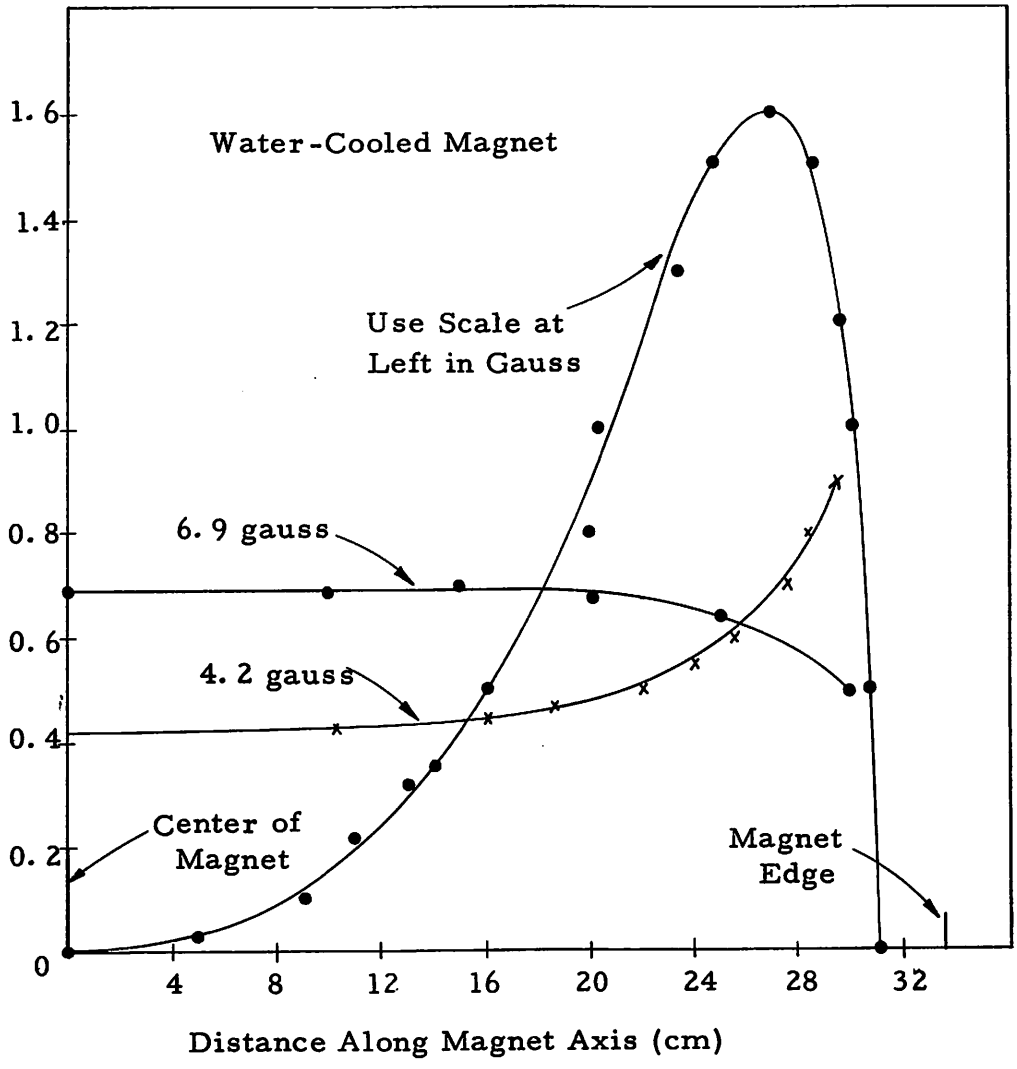

Fig. 9 Axial Variation of Magnetic Field in Water-Cooled Magnet.

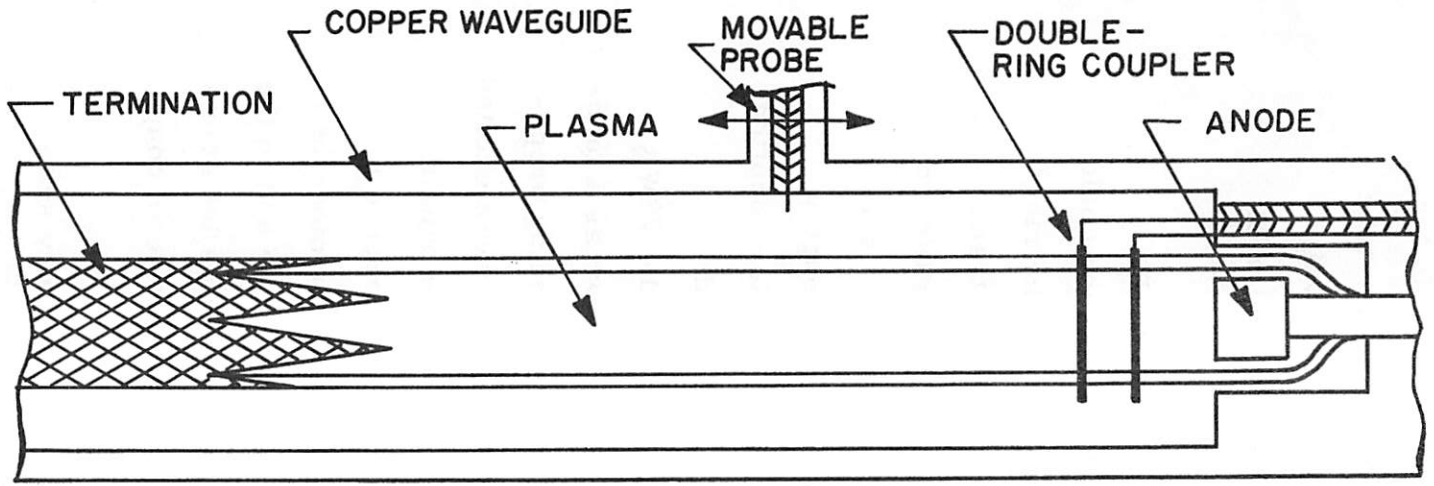

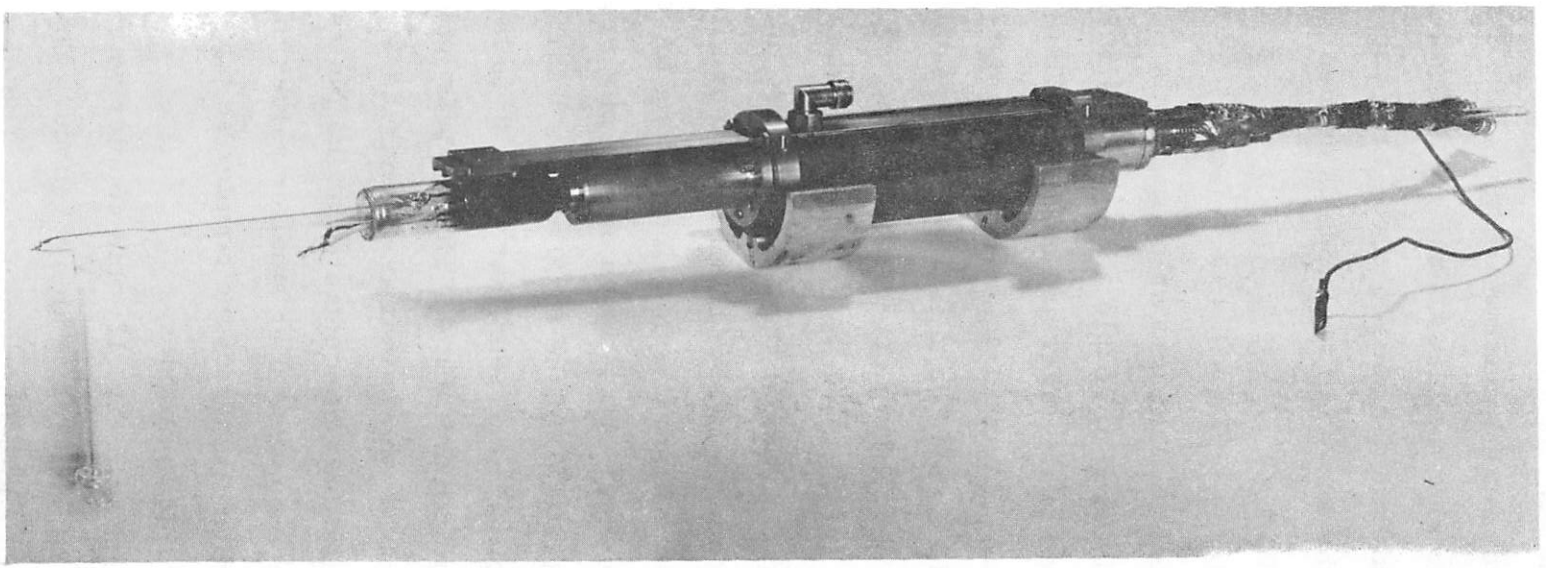

Fig. 10 Traveling Wave System.

In the plasma, E_z is a maximum at the plasma edge, i.e., at the interface between the plasma and the glass discharge tube. In the air region outside the glass tube, E_z is a maximum at the air-tube interface and then declines to zero at the copper waveguide wall. Evidently, the energy of the mode is concentrated in the region of the glass tube.

This fact suggests that two metal rings whose planes are parallel to one another and which fit tightly over the glass tube could be effectively used to couple energy into a surface mode. The rings are connected to the inner and outer conductors of a coaxial transmission line. The electric field between the two rings is parallel to E_z of a surface mode, and is applied at a position where E_z is a maximum. Since the electric field on the coupler must be roughly matched to E_z of the surface mode, we have a mechanism for coupling energy from the coaxial transmission line into a surface mode.

This coupler is shown in Figs. 10 and 11. In Fig. 12, the VSWR looking into the transmission line feeding the coupler is shown as a function of frequency. Also shown on this plot are the corresponding propagation constants (β) of the n = 0 and n = 1 surface modes that were excited by this coupler. It is seen that when β is large the VSWR is small, reaching a minimum of 1.4. This may be understood by reference to Eq. (3.1), which shows that as β increases the energy of the mode becomes increasingly concentrated at the plasma-glass interface and in the region of the coupler. For smaller values of β, the energy is less concentrated in the region of the coupler so that it is less effective in coupling energy into the modes.

According to Fig. 12, this coupler which is geometrically symmetric was able to excite an n = 1 mode. This is probably due to the electric field <u>not</u> being symmetric. The electric field between the two rings is probably greatest at the point at which the rings are fed from the

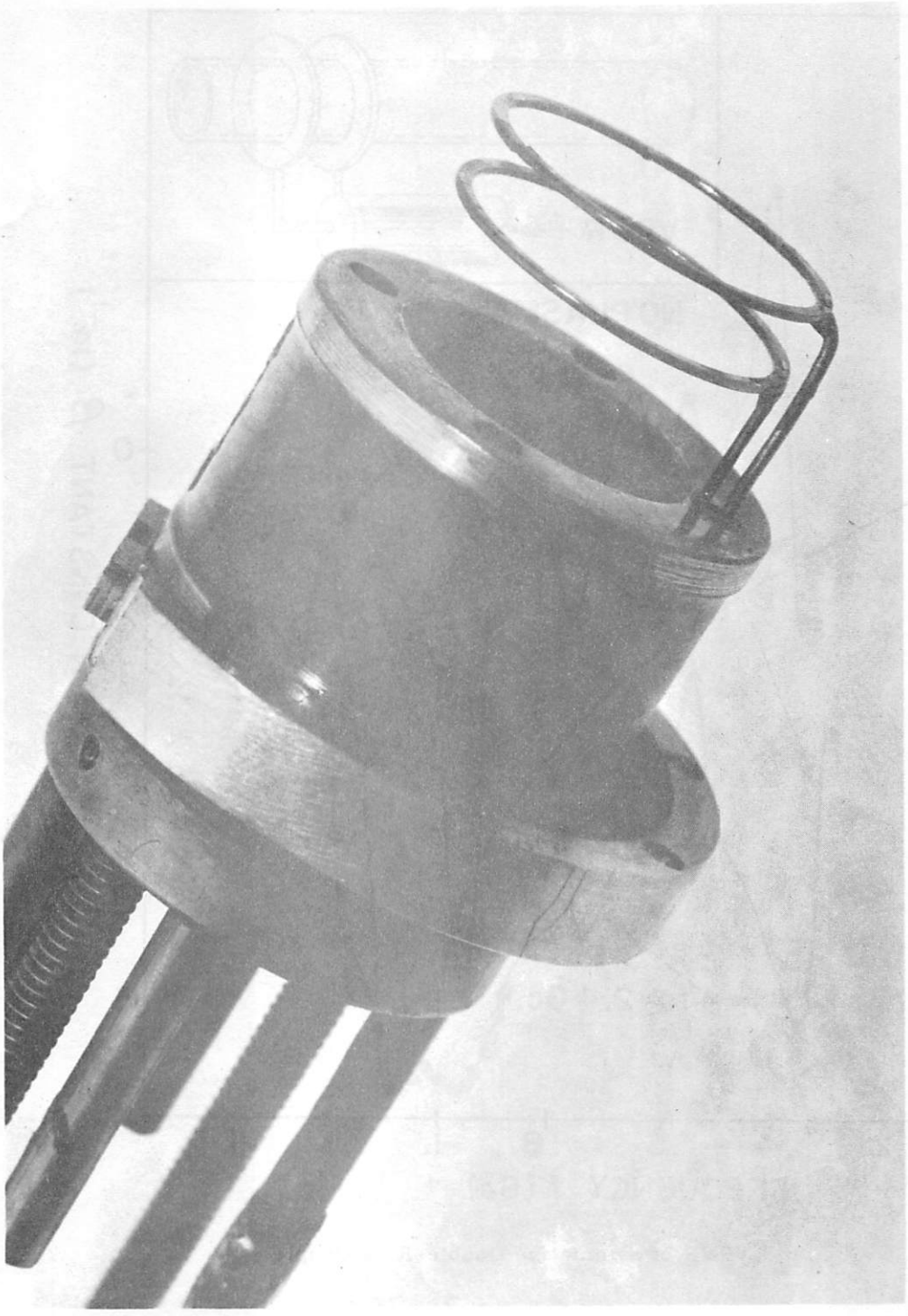

Fig. 11 The Symmetric Double-Ring Coupler.

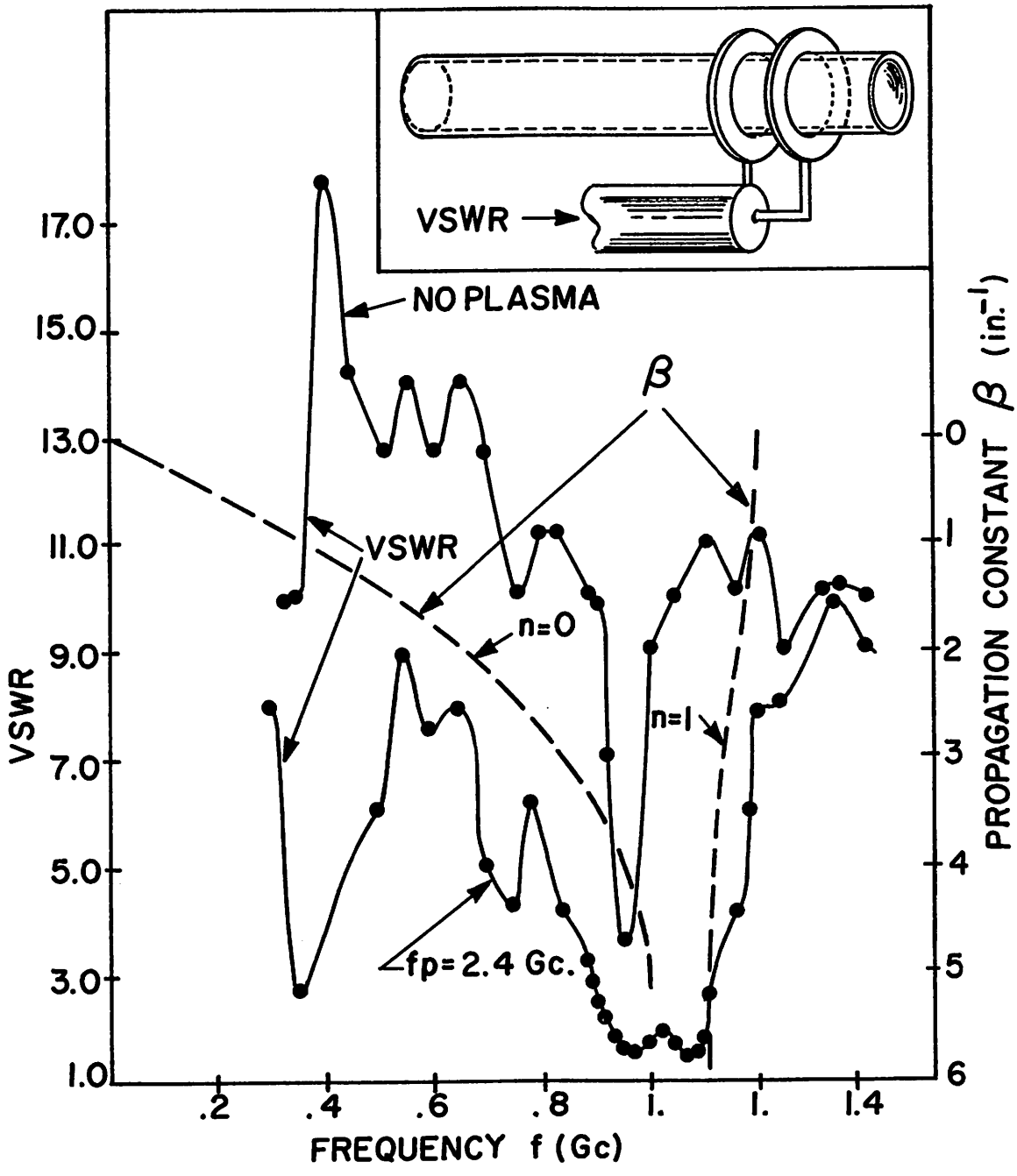

Fig. 12 VSWR of Symmetric Double-Ring Coupler.

coaxial transmission line and declines to a minimum on the opposite side of the rings. No measurements have been made to determine the maximum and minimum values of the field. If ϕ is the azimuthal coordinate, with $\phi = 0$ occurring at the point at which the rings are fed, according to the above reasoning, the exciting electric field between the rings would vary as

$$1 + a \cos \phi, \; a < 1.$$

The first term, unity, will cause the n = 0 mode to be excited. Because the magnetic field is nearly zero and the plasma is isotropic, the coupler will excite both the n = 1 and the n = -1 modes equally. These two modes combined will have an azimuthal variation of E_z of cos ϕ. The second term, a cos ϕ, then, will cause the n = 1, -1 modes* to be excited. In addition to the n = 0 and n = 1 modes, this coupler under certain conditions was observed to excite modes with higher n.

Besides the geometrically symmetric coupler, a nonsymmetric coupler was used in some measurements. Here, a complete ring was replaced by a 60° arc of a ring. This coupler is shown in Fig. 13. It had stronger coupling to the n = 1 mode than the symmetric coupler. Also, it would excite modes of higher n.

2. Attenuator. This consisted of a tapered, aqua-dag coating on the glass approximately 4 in. long and located at the end of the transmission region. It may be seen in Figs. 7 and 10. Like the double-ring coupler, it depends for success on the mode energy being concentrated in the glass. A typical VSWR for this termination for the n = 0 mode was 1.2.

3. Rotating coupler. In order to determine the azimuthal variation of a mode, a coupler mount was made so that discharge tube and double-ring coupler would rotate as a unit. The coupler was glued to the glass tube so that there could be no relative motion between the coupler

*Hereafter called the n = 1 mode.

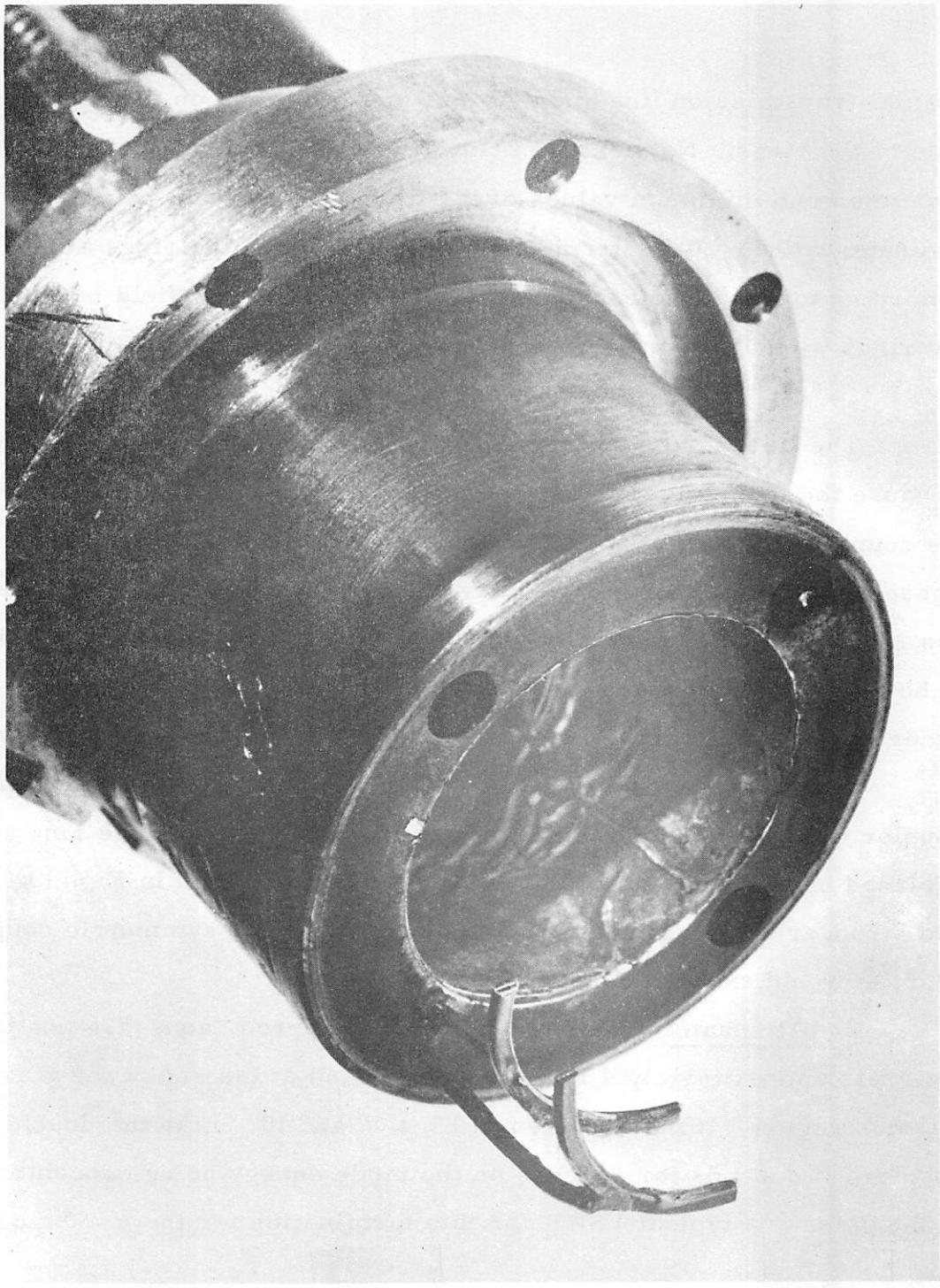

Fig. 13 The 60° Non-Symmetric Double-Ring Coupler.

and the glass tube. This arrangement allowed the field pattern of the mode to be rotated and by means of the detection probe of III. A, the azimuthal properties of the mode could be determined.

4. Microwave bridge. A schematic drawing of the microwave bridge used with this system is shown in Fig. 14. The usual precautions of isolating the two arms of the bridge from one another were observed.

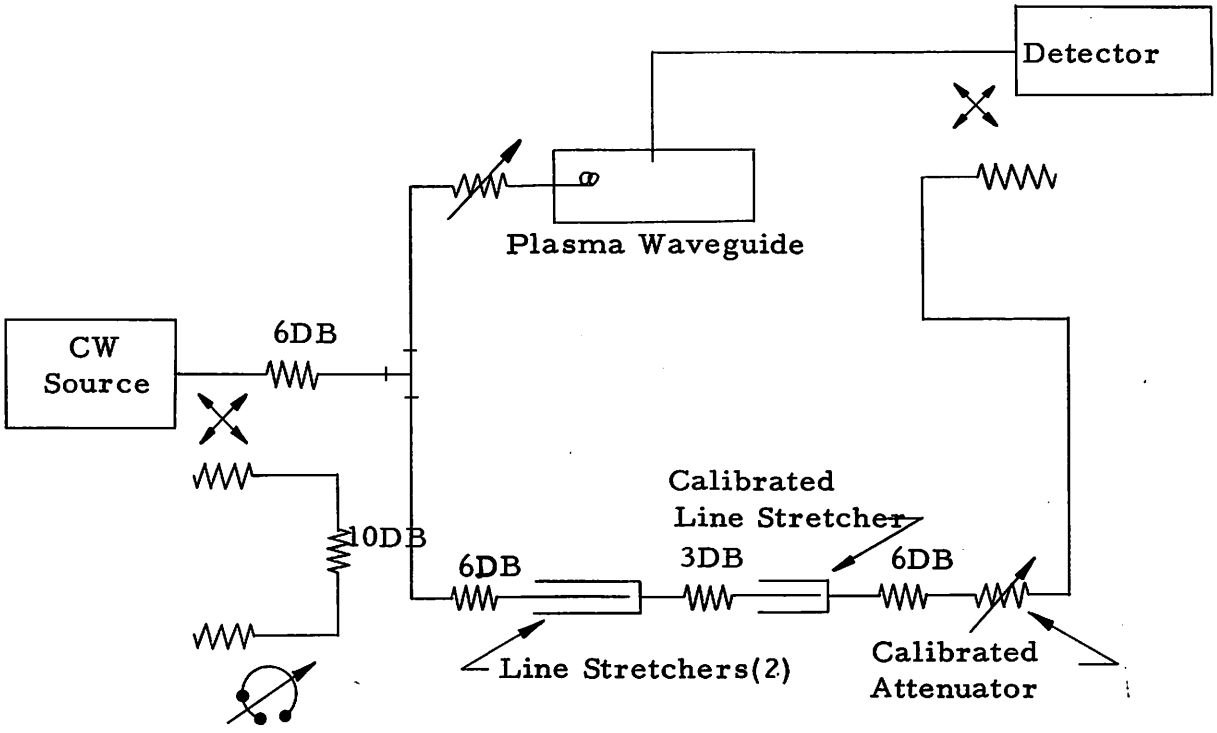

Fig. 14 Microwave Bridge

The calibrated phase shifter was a calibrated line stretcher with an extremely low VSWR; the calibrated attenuator was a calibrated coaxial attenuator whose attenuation was derived from a waveguide below cut-off and whose length was made variable. Thus the propagation constant across the waveguide is zero and ideally the phase shift across the attenuator is constant, independent of the attenuation setting. This

behavior was confirmed experimentally. The detector that was used with the bridge was either a receiver with high sensitivity or a spectrum analyzer which allowed visual inspection of noise components present.

C. THE RESONANT SYSTEM.

This system was used to measure the characteristics of the perturbed TE_{11} waveguide mode. It has the advantage of being much simpler than the traveling wave system but may only be used when the mode to be investigated is relatively lossless. It is shown in Fig. 15.

1. Theory of operation. By placing shorting planes across the plasma waveguide a distance L apart, a resonant system is created which will resonate whenever the β of the corresponding waveguide mode equals $m\pi/L$, where $m = 1, 2, 3, \ldots$. Alternately, at resonance, if ℓ is the distance between two adjacent nodes of any field component, then

$$\beta = \pi/\ell \,. \qquad (3.2)$$

Thus, it becomes possible to find β as a function of frequency for the waveguide mode by constructing a resonant system, causing it to resonate at a sufficiently large number of frequencies by varying L and m, and at each resonance, finding β from Eq. (3.2). For the TE_{11} waveguide mode, the standard notation for a resonant mode for which $\beta = m\pi/L$ is TE_{11m}.

We have pointed out in Section II that in the presence of an anisotropic plasma, the plasma waveguide will support both the $TE_{11}+$ and $TE_{11}-$ circularly polarized modes which have different propagation constants and therefore different field distributions. Now, it can be shown that if either of these circularly polarized modes encounters a conducting wall across the plasma waveguide, a single reflected wave will result which has the same propagation constant, rotates in the same absolute

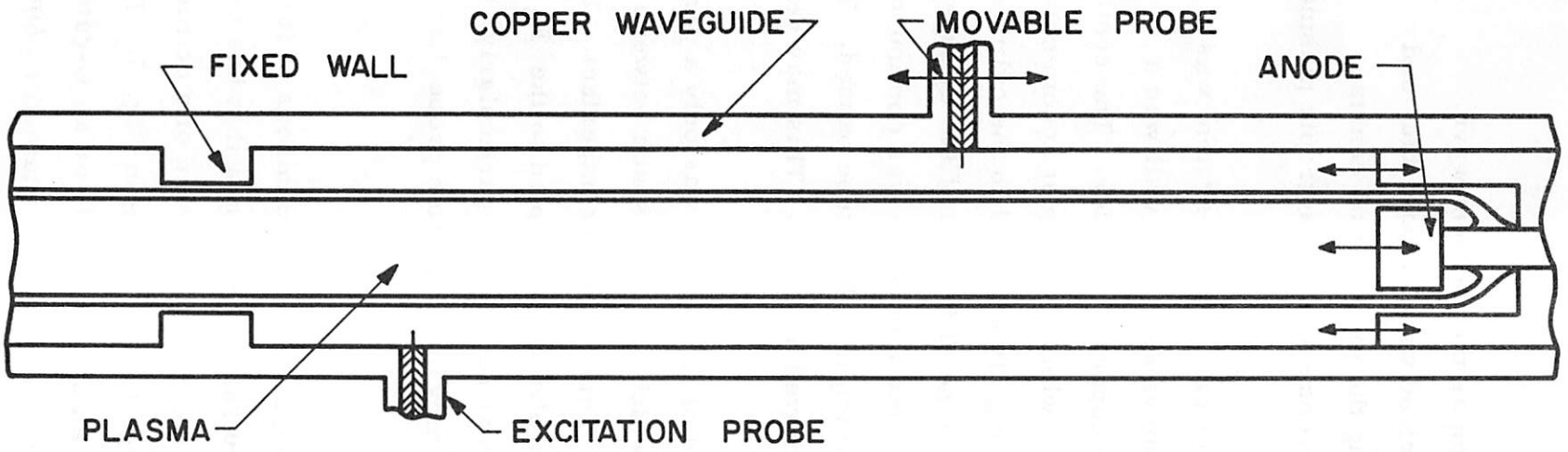

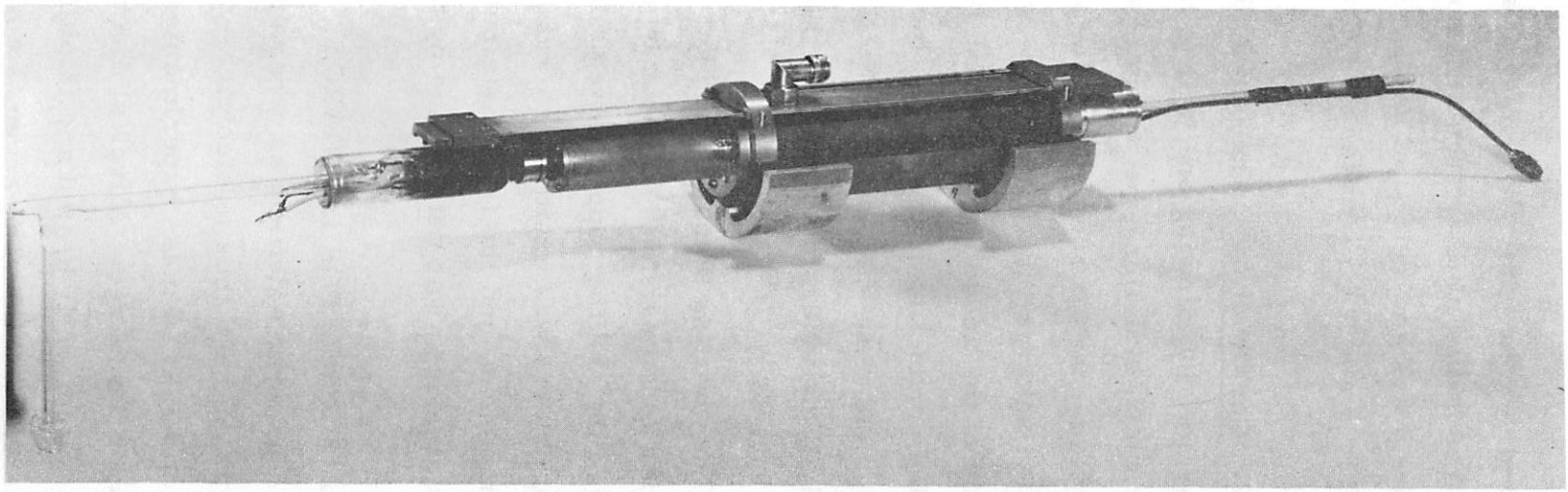

Fig. 15. The Resonant System.

sense, and has the same field configuration as the incident wave. Thus, a resonance of this circularly polarized wave is possible, and the resonant system method of determining the propagation constant for the $TE_{11}+$ and $TE_{11}-$ modes in the presence of an anisotropic plasma is useful.

2. Construction. The length L of the resonant system was made variable by allowing one wall to be movable. This wall was a cylinder which slid along the inside of the copper waveguide. The center of the cylinder was bored out to a diameter which would just accommodate the glass discharge tube and the tube was rigidly attached to the cylinder. The plane of the anode coincided with the plane of the end of the cylinder so that the conducting plane across the plasma waveguide was continuous except for the ring-shaped area through which the glass tube passed. The assembly of cylinder and discharge tube moved as a unit. This may be seen in Fig. 15.

The shorting plane at the other end of the system was only a partial plane, and consisted of a metal ring which filled the space between the glass tube and the copper waveguide. This is clearly imperfect. The resonant system was excited by a small probe which coupled to the E_r field component, and the field distribution at resonance, particularly, the location of nodes, was determined by the movable detection probe discussed in III. A.

D. MERCURY-VAPOR DISCHARGE

A plasma is defined as a region containing equal numbers of ions and electrons, and thus is electrically neutral. The plasma that has been used exclusively in these experiments is the positive column of a dc mercury-vapor discharge. A typical discharge tube is shown in Fig. 7. The cathode is indirectly heated and is either an oxide-cathode or an L-cathode* of diameter .600 in. The anode is a molybdenum disk of diameter .600 in.

* Manufactured by Semi-con Associates of California, Inc., Watsonville, California, (trade name is Semicon Type S).

so that both anode and cathode have diameters that are nearly the inner diameter of the glass tube. The separation between the anode and the cathode is 13.5 in. Typical values of parameters for this discharge tube are given in Table 3.1. The characteristics of the discharge for zero magnetic field are discussed in the Appendix.

1. Electrical characteristics in the presence of a magnetic field. In the presence of a magnetic field, the motion of the charge particles of the mercury-vapor discharge can be helical about the direction of the magnetic field if the gyration radius is less than the diameter of the confining dielectric tube. For 20,000° K electrons, the critical magnetic field at which the gyration radius is the same as the discharge tube radius used in these experiments is 2.8 gauss. For 500°K mercury ions, it is 245 gauss. In the presence of a strong magnetic field of 1000 gauss or more, we may expect a charged particle to follow a magnetic field line with a velocity equal to its thermal plus drift velocities in the axial direction, while its position transverse to the field line is confined to the gyration radius which will be small compared to the tube radius.

An observation which bears out this restricted type of motion was made on an early tube which had a spiral oxide cathode. By accident, the spiral turns became distorted so that there were two spots which had very high emission. In the presence of a magnetic field of 1000 gauss with the cathode inside the magnet far enough so that it did not experience the fringing field, two bright lines (brighter than the surrounding glow) parallel to the tube axis and the magnetic field were observed to originate on these two spots. The intensity and sharpness of definition of these two lines was quite well maintained along the entire length from cathode to anode. We interpret this to mean that an electron leaving the cathode does indeed follow a field line from its origin at the cathode to the anode. Further, because the lines did not lose definition, the electron suffers few collisions.

Further evidence that the electrons follow field lines was available when it was observed that if the cathode is located well outside the magnet

TABLE 3.1 - TYPICAL VALUES OF DISCHARGE TUBE PARAMETERS

QUANTITY	SYMBOL	VALUE	COMMENT
radius of discharge tube	a	. 36 in.	
mercury vapor pressure	p	1.7×10^{-3} mmHg	At room temperature T of 75°F (24°C)
discharge current	I_o	. 5 amp	
cathode-anode voltage	V_o	26 volts	cathode-anode separation, 13.5 in.
plasma frequency (electrons)	f_p	2.4 Gc.	Tube No. 2. Determined by cavity perturbation technique.
plasma frequency (ions)	f_{pi}	4.1 Mc.	$f_{pi}/f_p = \sqrt{m_e/m_i}$
number density (electrons)	n_e	$7.4 \times 10^{10}/cm^3$	$n_e = 1.24 \times 10^{10} f_p^2$
number density (ions)	n_i	$7.4 \times 10^{10}/cm^3$	$n_i \approx n_e$
number density (neutrals)	n	$5540 \times 10^{10}/cm^3$	$n = 9.68 \times 10^{18} p/T$
percent ionization		~ . 1 percent	
temperature (electrons)	T_e	26,000°K	Ref. 29, p. 158 and Ref. 30, p. 223.
rms thermal speed (electrons)	v_t	1.1×10^8 cm/s	$v_t = 6.74 \times 10^5 \sqrt{T_e}$
axial current density (electrons)	j_e	. 27 amp/cm^2	$j_e \approx I_o$/anode area
drift velocity (electrons)	v_d	2.3×10^7 cm/s	$v_d = j_e/e\, n_e$
mean free path (electrons)	λ_e	4 cm.	Ref. 30, p. 30
electron-neutral collision frequency (elastic)	ν_n	27 Mc.	$\nu = v_t/\lambda_e$
electron-wall collision frequency (elastic)	ν_w	68 Mc.	$\nu_w = v_t/2a$

so that the fringing field exists in the positive column, then the tube glow contracts over the region of the fringing field to a cylinder of small diameter on the tube axis. It retains this character over the remaining length of the tube. Here it is hypothesized that the electrons are converged by the fringing field to the axis where they then follow the field lines to the anode.

It should be pointed out here that the "glow" of the discharge tube is intimately associated with the electrons. It is the result of direct excitation of normal atoms by electrons or of the collision of an electron and an atom in an excited state.[29]

Assuming that electrons do follow field lines from the cathode to the anode, subsequent tubes were constructed with a planar cathode whose diameter was only slightly less than the inner diameter of the discharge tube. If this cathode was placed inside the magnet far enough so that it does not experience the fringing field, and if it is uniformly heated so that its emission is uniform over its surface, then we may expect in the presence of a magnetic field that the electron density in the positive column will be relatively uniform across the cross-section of the tube except near the dielectric wall where a sheath with a negative potential must exist.

The alteration of the discharge characteristics discussed in the Appendix due to the magnetic field is far from clear. Certainly, the magnetic field reduces wall currents of both electrons and ions. This reduces electron-wall collisions and recombination. The latter results in a reduction in ionization in the body of the positive column which in turn causes the potential across the length of the positive column (or electric field) to decrease. It was observed that, indeed, the potential did drop across the tube by as much as 6 percent. The electron temperature also decreases.[30]

2. Tube construction. Seven tubes (in some cases old tubes were rebuilt) have been constructed for this project, although only three were usable. All but the last had oxide cathodes and all of these eventually suffered from deterioration of cathode emission. The resulting temperature-limited cathode emission caused the voltage drop across the tube to increase and to be increasingly sensitive to discharge current. This condition could be temporarily cured by increasing the filament voltage. Several of the tubes had such short lives that no data could be obtained from them.

It was found that the emission life of the cathode could be increased by taking extra precautions to remove all residual gases from the tube before it was finally sealed off. With the last oxide coated cathode tube that was built, the tube was sealed off from the diffusion pump with an ion-pump still attached. This pump was connected to the tube via a cold-trap which excluded the mercury vapor from the ion-pump. This pump was then allowed to continue to remove gases for about 24 hours before it was sealed off. The result was a tube which lasted for approximately 200 hours of use (Tube No. 2).

The final tube contained an L-cathode (Tube No. 3). It was processed in the same way as the tube described above. It has lasted for at least 300 hours of operation with no indication of cathode emission deterioration.

The anode consists of a disc of molybdenum which has a highly polished planar surface, with a diameter only slightly less than that of the inner diameter of the discharge tube. It was observed that under conditions of poor cathode emission, the anode would glow red at moderate discharge currents. By attaching a finned structure onto the anode lead and blowing air onto it, the anode was kept below the "red hot" condition.

Under certain conditions, brightly glowing spherical regions appeared in front of the anode and which moved about the anode surface in a random manner. These are probably the anode spots described by Armstrong, Emeleus, and Neill.[31] It is not clear how to insure that these spots will not be present, but from the experience here and the work of others it appears that they will not appear if the anode fills the discharge tube, it is highly polished, and is not too hot.

The vapor pressure in the tube was controlled by causing all the mercury in liquid form to be located in a "trap" distant enough from the active part of the tube to be at room temperature. The trap is shown in Fig. 7. The condensation of the mercury in the trap was accomplished by immersing the trap in liquid nitrogen for a period of several hours. Since the mercury vapor tends to diffuse toward the coolest part of the tube, in this case the trap, one would expect that the temperature of the trap would control the vapor pressure. In truth, good quality pressure control was not achieved, probably due to a very slow pumping speed of the trap.

IV. SPECIAL TECHNIQUES

A. MEASUREMENTS ON SIMULTANEOUSLY PROPAGATING MODES

In Fig. 2, we have seen that there is a frequency range which is common to both the n = 0 and n = 1 modes. Referring to that figure, this frequency range extends from $\omega_{co}/2\pi$ to the maximum frequency of propagation of the n = 0 mode. In Section V, we will find that the double-ring coupler will indeed excite both modes in this frequency range. Thus, we need a method for measuring the propagation characteristics of the two modes while they are propagating simultaneously.

If the complex propagation constants of the two modes are $\gamma_{1,2} = \beta_{1,2} - i\,\alpha_{1,2}$, then the real parts of the propagation constants, β_1 and β_2, can easily be found from the interference pattern of the two modes. Let A(z) be the complex voltage induced in the detection probe, which can move in the z direction, by the radial component of the electric field of the composite wave. Then,

$$A(z) = k \left[E_1 e^{-\alpha_1 z} e^{-i\beta_1 z} + E_2 e^{-\alpha_2 z} e^{-i\beta_2 z} \right] \quad (4.1)$$

where E_1 and E_2 are the radial components of the electric field of the two modes which excite the probe at $z = 0$, and may be assumed real and positive without loss of generality. k is a proportionality constant.

The magnitude of A(z) will be characterized by a series of maxima and minima (the interference pattern). We note that $z = 0$ occurs at a maximum. The next maximum will occur a distance 2ℓ away where 2ℓ is determined by the relation

$$e^{-i2\beta_1 \ell} = e^{-i2\beta_2 \ell} \quad (4.2)$$

so that if θ is the shift in phase of A(z) in going from one maximum to

the next,

$$\theta = 2\beta_1 \ell = 2\beta_2 \ell + 2\pi \tag{4.3}$$

where we assume $\beta_1 > \beta_2$. Since, from Eq. (4.3),

$$e^{-i\beta_1 \ell} = -e^{i\beta_2 \ell},$$

at $z = \ell$ there will be a minimum. Thus, ℓ is the separation of a maximum and the adjacent minimum.

If we measure θ by using the microwave bridge described in Section III, and if ℓ is known, then β_1 can be found from Eq. (4.3), and β_2 from

$$\beta_2 = \beta_1 - \pi/\ell . \tag{4.4}$$

We note that the accuracy with which β_1 and β_2 can be determined depends on how precisely θ and ℓ can be measured. α_1 and α_2 cannot be related by such simple relations to measureable quantities, and in general can be found only after four measurements on A(z) have been made.[32] In Fig. 28 in Section V, the method described above was used to determine the values of β for the n = 0 and n = 1 modes at those frequencies where these two modes propagated simultaneously.

B. MEASUREMENT OF PLASMA FREQUENCY

1. Slater Perturbation Theory. As an independent method of determining the plasma frequency of the electrons in the positive column of the mercury-vapor discharge, a cavity perturbation technique was used. Following Slater,[26] if a cavity resonant in one of its normal modes is perturbed by partially filling its volume with a dielectric material of tensor permittivity ϵ, then the quality factor Q_a and resonant frequency ω_a of the empty cavity will be shifted to new values ω and Q given by

$$\frac{1}{2Q} - \frac{1}{2Q_a} - i\left(\frac{\omega - \omega_a}{\omega_a}\right) = \Delta\left(\frac{1}{2Q}\right) - i\,\frac{\Delta\omega}{\omega_a} = \frac{i\omega}{2\omega_a}\,\frac{\int_\tau (\epsilon - I)\bar{E}\cdot\bar{E}_a dv}{\int_v \bar{E}\cdot\bar{E}_a dv}. \tag{4.5}$$

Here, $\bar{E}_a$ and $\bar{E}$ are the vector electric fields in the unperturbed and perturbed cavity, respectively, τ and v are the volumes of the dielectric and cavity, respectively, and I is the identity operator. If the perturbing dielectric does not perturb the electric field appreciably, so that the expansion of $\bar{E}$ in terms of the electric fields of the normal modes consists of a predominant term, $\bar{E}_a$, then

$$\Delta\left(\frac{1}{2Q}\right) = \frac{-\omega}{2\omega_a}\,\frac{\int_\tau \epsilon''\,\bar{E}_a\cdot\bar{E}_a\,dv}{\int_v E_a^2\,dv} \tag{4.6a}$$

$$\frac{\Delta\omega}{\omega_a} = -\frac{\omega}{2\omega_a}\,\frac{\int_\tau (\epsilon' - I)E_a\cdot E_a\,dv}{\int_v E_a^2\,dv} \tag{4.6b}$$

where $\epsilon = \epsilon' + i\epsilon''$. If the dielectric is a plasma region, then ϵ is given by Eqs. (2.2) and (2.3).

The TM_{010} mode in a cylindrical cavity is particularly advantageous because it has only one component of electric field, E_z, the component parallel to the cavity axis. Thus, if the discharge tube is placed coaxial with the cavity, with a magnetic field also parallel to the axis, inside the plasma

$$\bar{E}_a = \bar{a}_z\,\epsilon_{zz}\,E_z$$

where $\bar{a}_z$ is a unit vector in the axial direction. Finally, from Eq. (2.2) and (2.3),

$$\Delta\left(\frac{1}{2Q}\right) = \frac{\nu}{\omega_a}\left(\frac{\omega_p}{\omega}\right)^2 \frac{1}{1+\frac{\nu^2}{\omega^2}} M \,, \qquad (4.7a)$$

$$\frac{\Delta\omega}{\omega} = \left(\frac{\omega_p}{\omega}\right)^2 \frac{1}{1+\frac{\nu^2}{\omega^2}} M \,, \qquad (4.7b)$$

where

$$M = \frac{1}{2} \frac{\int_\tau E_z^2 \, dv}{\int_v E_z^2 \, dv} \qquad (4.7c)$$

so that M is a parameter dependent only on the unperturbed fields of the cavity. For $\nu^2 << \omega^2$, Eq. (4.7b) shows that a simple relation exists between the plasma frequency ω_p and the shift in resonant frequency of the TM_{010} mode due to the presence of the plasma. This relation is valid whether or not a magnetic field is present. Note that ω_p calculated in this manner is an average over the volume of the plasma with a weighting function of E_z^2.

2. Experiment. A copper cylindrical cavity was used which was 3.690 in. in diameter and 5.115 in. long. The discharge tube was located coaxially with the cavity by passing it through holes .750 in. in diameter in the top and bottom of the cavity. The glass tube was pyrex with an inner diameter of .63 in. and an outer diameter of .74 in. The length of the cavity was large compared to the diameter of these holes in order to reduce the influence of end effects. With the tube in place, the cavity was observed to resonate in the TM_{010} mode at f_a = 2.321 Gc.

The presence of the glass tube will distort the normal mode fields. Thus a calculation of M using Eq. (4.7c) is difficult. Alternately, M may be found experimentally. In order to do this, a rod of lucite was

used which had a diameter of .633 in., about that of the plasma. A pyrex tube like that used in the discharge tube was placed in the cavity with the lucite tube inside it, and the change in the resonant frequency of the cavity was noted when the lucite rod was removed from inside the tube. From Eq. (4.6b),

$$M = - \frac{(f - f_a)/f}{\epsilon_\ell - 1}$$

where ϵ_ℓ is the dielectric constant of lucite. An attempt was made to determine ϵ_ℓ by cavity perturbation techniques. To within the experimental error, the value obtained agreed with that published in the literature,[33] $\epsilon_\ell = 2.58$. The value obtained for M is .051, so that from Eq. (4.7b),

$$f_p = 4.4 \sqrt{f(f - f_a)} \cdot \qquad (4.8)$$

3. Results. Extensive measurements of plasma frequency were made on Tubes Nos. 2 and 3 and are shown in Figs. 16-19.

In Fig. 16, it is seen that the square of the plasma frequency is a linear function of the discharge current over a large range of discharge current, which is in agreement with theory. The approximately linear relationship between the square of the plasma frequency and discharge current has been observed by other workers including Trivelpiece[16] and Osborne, et al.[15] Figures 18 and 19 show that at small magnetic fields the plasma frequency increases rapidly with magnetic field until about 100 gauss is reached. This is probably associated with a rapid decrease of wall currents and recombination at small magnetic fields, and probably indicates that above 100 gauss these processes change only slowly with magnetic field. This effect has been observed by Trivelpiece.[6]

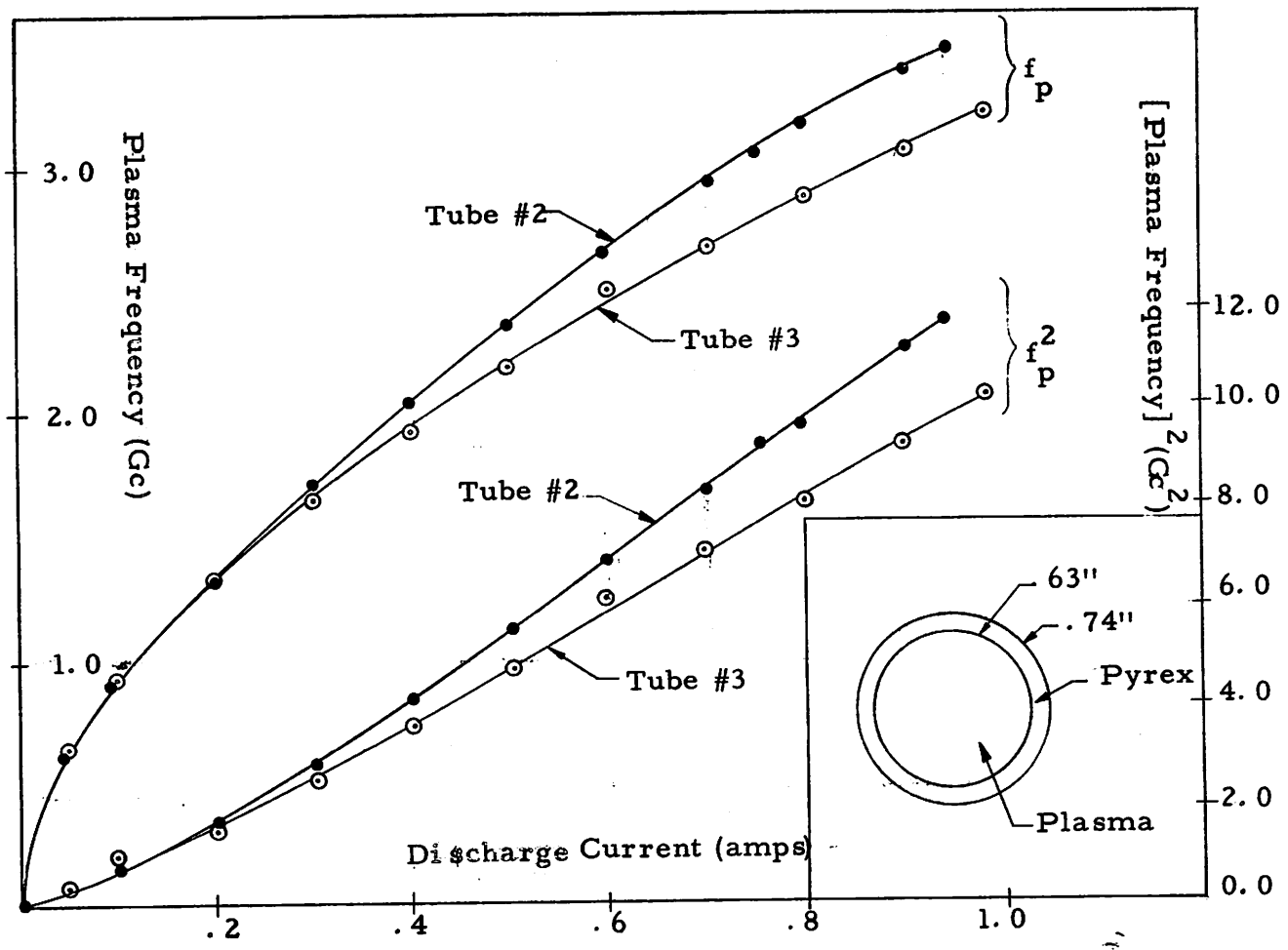

Fig. 16 Plasma Frequency (f_p) vs. Discharge Current for Tubes No. 2 and 3. Error in f_p: Diurnal Variation, $\pm$ 5% $\pm$ 3% $\pm$ 3% at . 3, . 6, and . 9 amps., Respectively; End Effects, 1% Experimental Points Can Be Maximum of 3% Low.

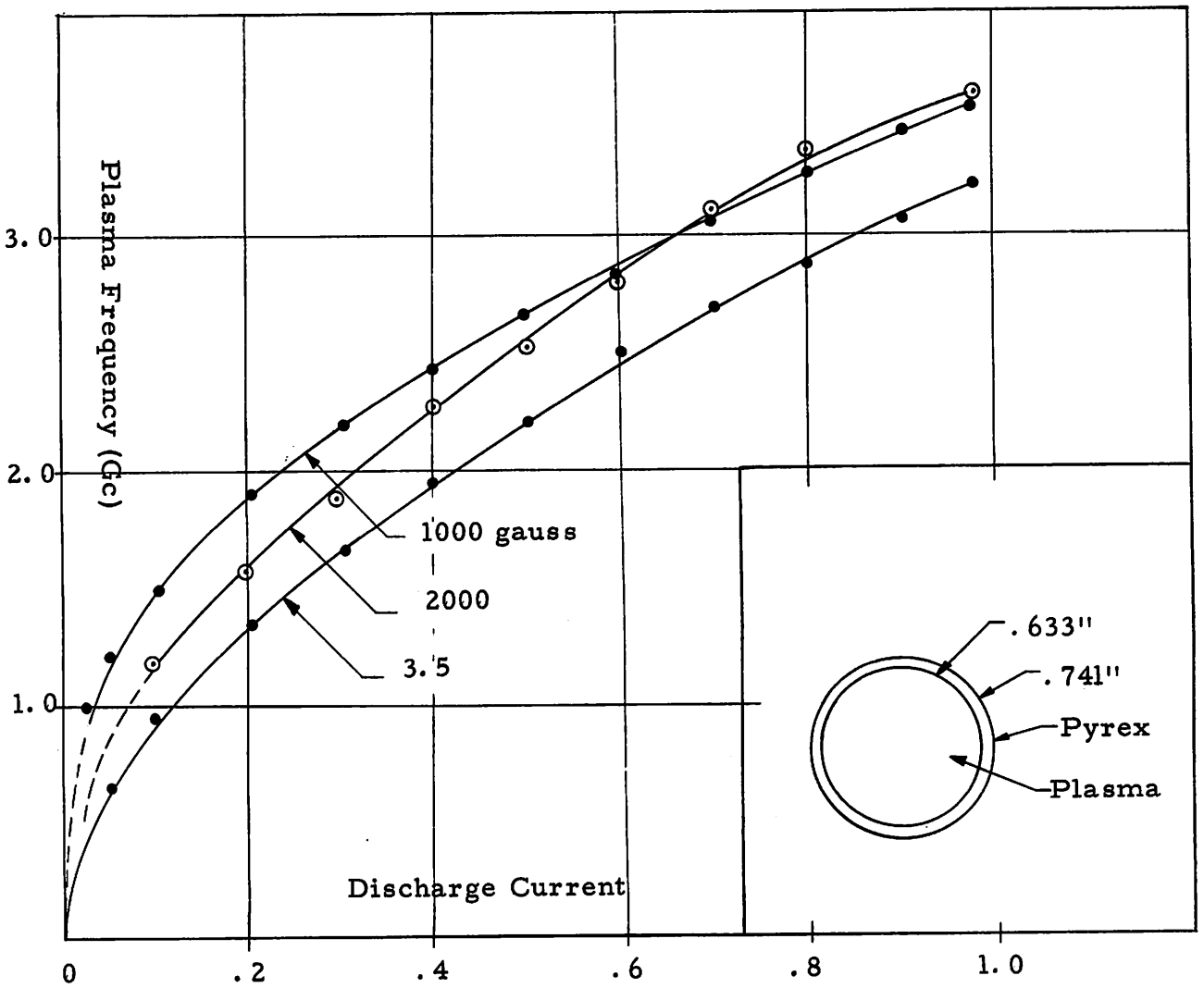

Fig. 17 Plasma Frequency (f_p) vs. Discharge Current for Tube No. 3 with Magnetic Field as the Parameter. Error in f_p: Diurnal Variation, $\pm$ 5% $\pm$ 3% $\pm$ 3% at .3, .6, and .9 amps., Respectively; End Effects, 1% Experimental Points Can Be Maximum of 3% Low.

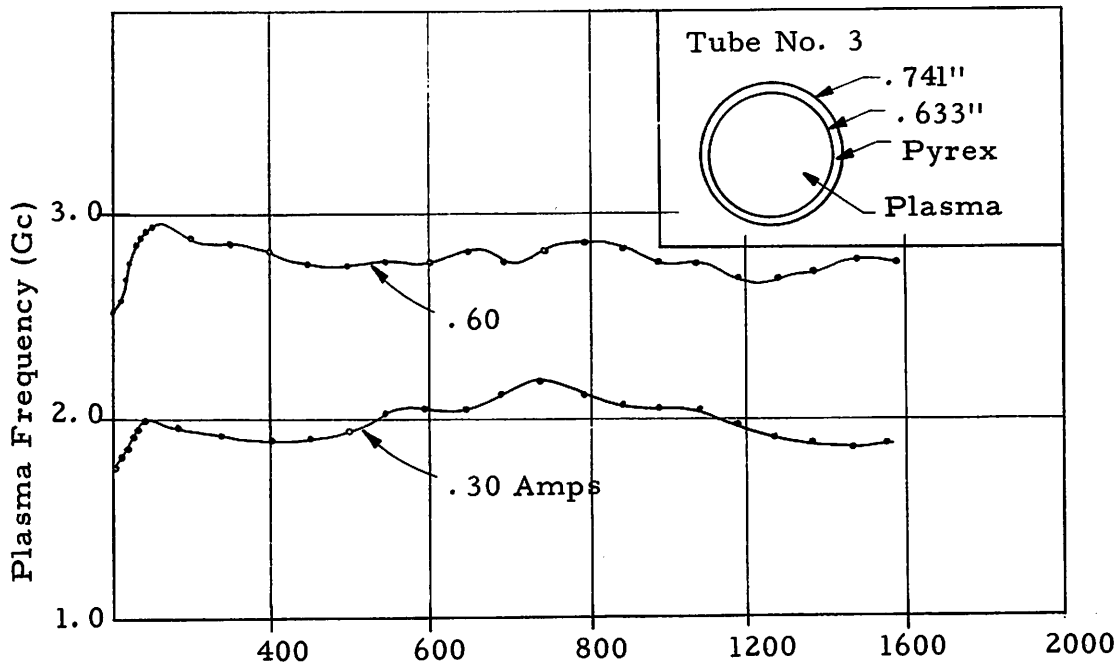

Fig. 18 Plasma Frequency (f_p) vs. Magnetic Field for Tube No. 3 with Discharge Current as the Parameter. Error in f_p: Diurnal Variation, $\pm$ 5%, $\pm$ 3% at .3, .6 amps., Respectively; End Effects, 1%, Experimental Points can be a Maximum of 3% Low.

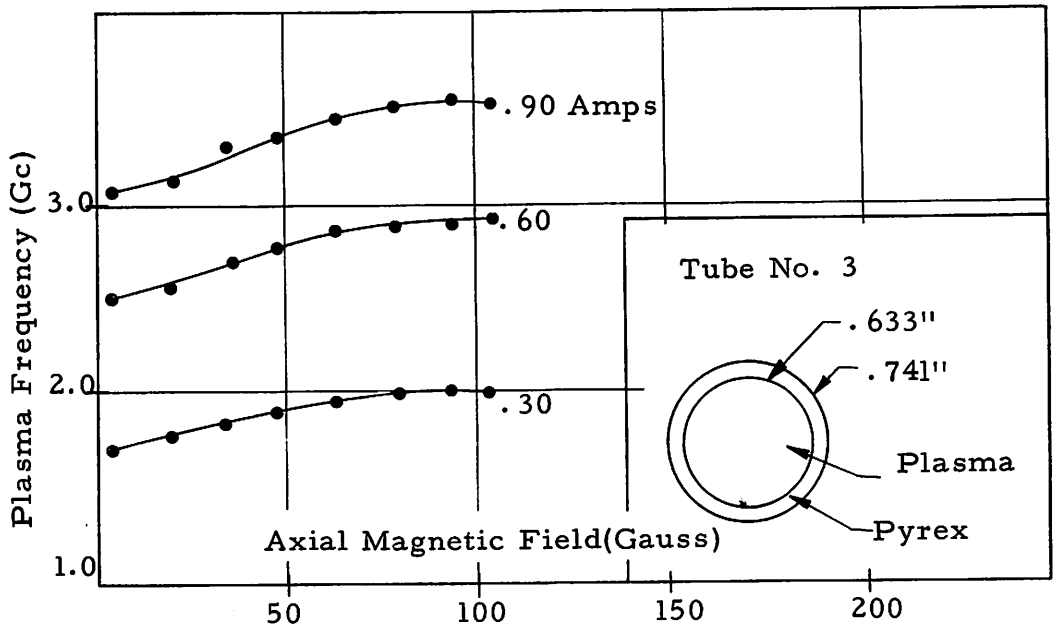

Fig. 19 Plasma Frequency (f_p) vs. Magnetic Field for Tube No. 3 With Discharge Current as the Parameter. Error in f_p: Diurnal Variation, $\pm$ 5%, $\pm$ 3%, $\pm$ 3% at .3, .6, .9 amps., Respectively; End Effects, 1%; experimental Points can be a Maximum of 3% Low.

There was experimental evidence which showed that the values of f_p for Tube No. 2 shown in Fig. 16 were larger than the true values of f_p for some of the measurements in which this tube was used. After this tube had been operated for well over 100 hours, the cathode emission began to deteriorate. This was characterized by a slight increase of voltage drop across the tube and increased sensitivity of voltage drop to current. Increasing the filament power would improve but not entirely cure this condition. Measurements were continued nevertheless, since the positive column of the discharge still retained the characteristic qualities described in Section III and the Appendix. Plasma frequency measurements reported in Fig. 16 were made during the period of reduced cathode emission.

It was possible to estimate that f_p during the period of high emission was lower than for reduced emission by the percentages shown in Table 4.1.

TABLE 4.1 FOR HIGH CATHODE EMISSION, f_p FOR TUBE NO. 2 (SHOWN IN FIG. 16). SHOULD BE REDUCED BY THE INDICATED PERCENTAGES.

discharge current (amps.)	percent	applies to
1.0	7	Fig. 20
.8	7	Fig. 21
.2	~0	----

4. Error. The error in these experiments comes from three sources. First, it should be noted that the perturbation method is inherently an approximation. The approximation was introduced in Eq. (4.6)

where we replaced $\bar{E}$, the exact field in the presence of the plasma, by $\bar{E}_a$, the field in the absence of the plasma. However, Buchsbaum, et al.[22] have indicated that the error introduced by this approximation will be small if $(f_p/f)^2$ is not too large. Incidentally, they show that f_p determined by the perturbation method will be less than the true f_p. Also, the error is greater, the greater is $(f_p/f)^2$.

An estimate of the error for our case can be made by comparing $(f_p/f)^2$ determined by the perturbation method with that obtained by an exact field analysis for the case where the glass tube is absent. By starting with a given $\Delta f/f$, $(f_p/f)^2$ determined by the two methods can be found with relative ease. For $\Delta f/f = .0700$, the perturbation method gives $(f_p/f)^2$ of 1.34 while the field equations give an $(f_p/f)^2$ of 1.42. Assuming that the field analysis yields the exact value of f_p/f, the perturbation method gives in this instance a value of f_p/f that is 2.7 percent low. As predicted by Buchsbaum et al.,[22] the perturbation method results in a conservative value of f_p/f. For the cavity used, an $(f_p/f)^2$ of 1.34 corresponds to an f_p of 2.90 Gc., roughly, the maximum f_p measured. Thus 2.7 percent is about the maximum error expected from this source, which we round off to 3 percent.

The second source of error is due to end effects. The length of the cavity was made large compared to the glass tube diameter in order to minimize this error. A hole was drilled in the end walls of the cavity through which the glass tube passes. Certainly in the region of these holes $\bar{E}$ is markedly different from $\bar{E}_a$ so that the contribution of these regions to the integrals in Eq. (4.6) will cause error. We can minimize this error by making the volume of these regions small compared to the total volume.

An estimate of the error introduced can be found by experimental methods. For the lucite rod, $\epsilon_\ell - 1$ is 1.58 which, it will be noted, has the same significance in the perturbation equation as an $(f_p/f)^2$ of 1.58.

$\Delta f/f$ was measured for the rod and glass tube extending through the wall in the manner in which all the measurements were made. Then $\Delta f/f$ was measured for the case where one of the holes was filled with a metal plug, and the glass tube and rod were thus terminated on a continuous wall. For this latter case, $\bar{E}$ and $\bar{E}_a$ should be about the same. A difference of about 1 percent was found between the two values of $\Delta f/f$, which leads to an error in f_p/f of 1/2 percent. The error in f_p/f due to both ends of the cavity is twice this, or 1 percent.

Finally, we recognize that there will be diurnal variations of the electron concentration and of f_p for a given discharge current probably due to diurnal variations in vapor pressure. We must then ask, if f_p is measured on one day at a given discharge current, how much variation would we expect between this value and another made on another day at the same discharge current?

An approximate answer to this question can be obtained by comparing the results of four different series of measurements of f_p vs. discharge current scattered over a period of three months. This comparison indicates that at nearly zero magnetic field, the mean variation in f_p is less at large values of f_p than at small values. At discharge currents of .3, .6, and .9 amp., the mean variation is $\pm$ 5 percent, $\pm$ 3 percent, and $\pm$ 3 percent, respectively. When a magnetic field is present, this variation is somewhat larger.

V. RESULTS

The measurements were directed toward the investigation of two plasma waveguide modes, a backward mode and a perturbed waveguide mode, the results of which are presented below. In addition, the results of measurements of noise and parameter drift in the plasma are presented.

A. THE BACKWARD-WAVE MODE

In Section II we have seen that at no magnetic field the plasma waveguide theory predicts that in addition to a low-pass forward wave mode at no magnetic field there will be an infinite set of pass-band modes. While the former is symmetric in the azimuthal coordinate ϕ (i.e., $n = 0$), the azimuthal dependence of the latter are described by $n = 1, 2, 3, \ldots$. Since the fields of these modes vary as the modified Bessel functions, their energy tends to be concentrated near the plasma-dielectric interface, and hence these modes are called surface modes. While the $n = 0$ mode is a forward mode, the high permittivity of the dielectric causes the $n = 1$ mode to be a backward mode.

In this section, we describe an investigation of the $n = 1$ mode. The traveling wave system described in Section III was used in which the $n = 1$ mode was excited by a double-ring coupler.

In Figs. 20-23, Brillouin Diagrams of the $n = 0$ and 1 modes are given with plasma frequency as the parameter. The magnetic field in these measurements, and in fact in all measurements reported in this section, except where noted, was the residual magnetic field in the magnet which was measured to be 3.5 gauss. It was not possible to measure the $n = 1$ mode at $f_p = 2.0$ or 1.4 Gc. because of high attenuation. High Attenuation also limited the range over which β could be measured.

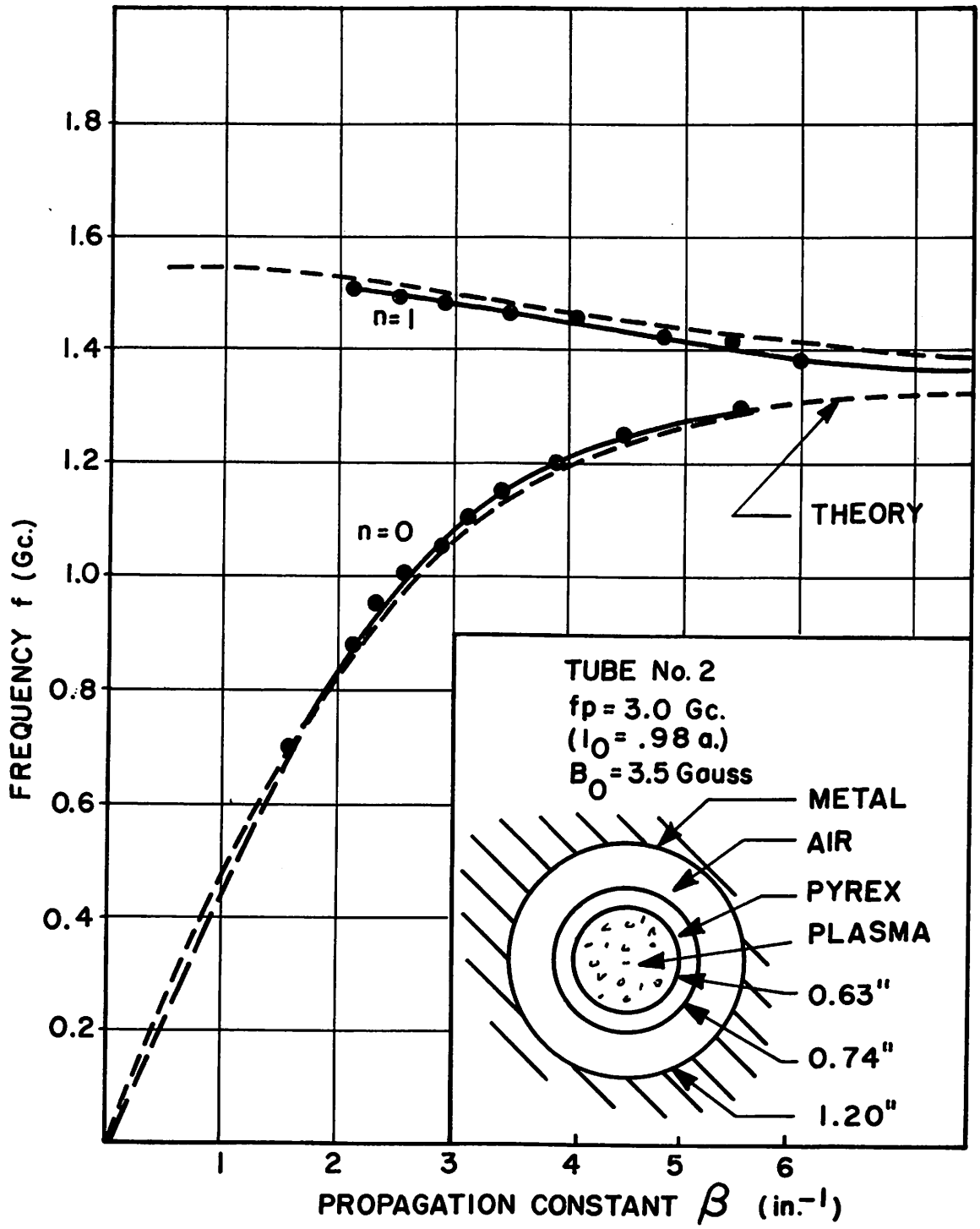

Fig. 20 Brillouin Diagram for n = 0 and n = 1 Modes for f_p = 3.0 Gc. (I_o = .98 amp.). Error in β: Approximately ± 3 Percent.

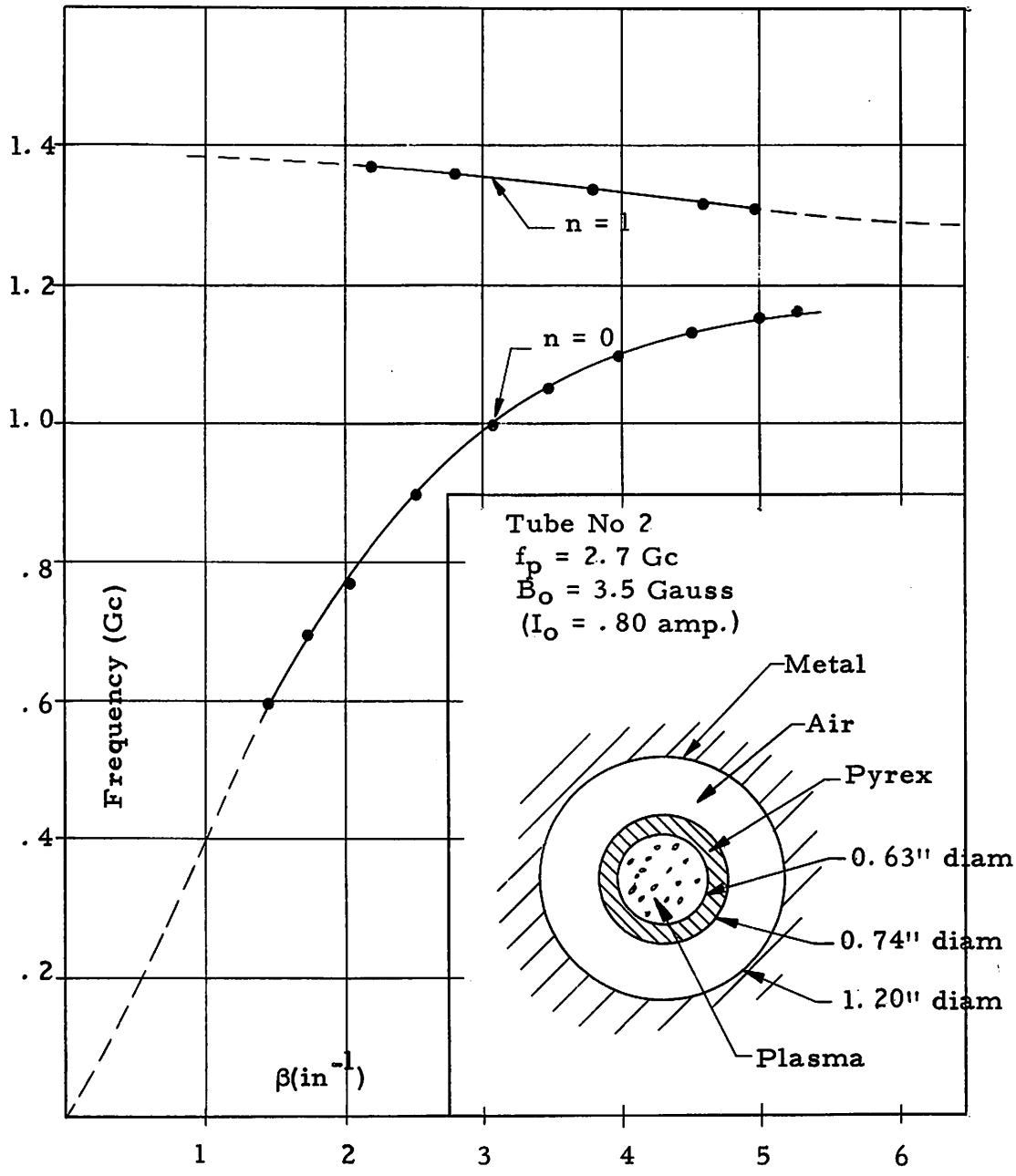

Fig. 21 Brillouin Diagram for n = 0 and n = 1 Modes for f_p = 2.7 Gc. (I_o = .80 amp.). Error in β: Approximately ± 3 Percent.

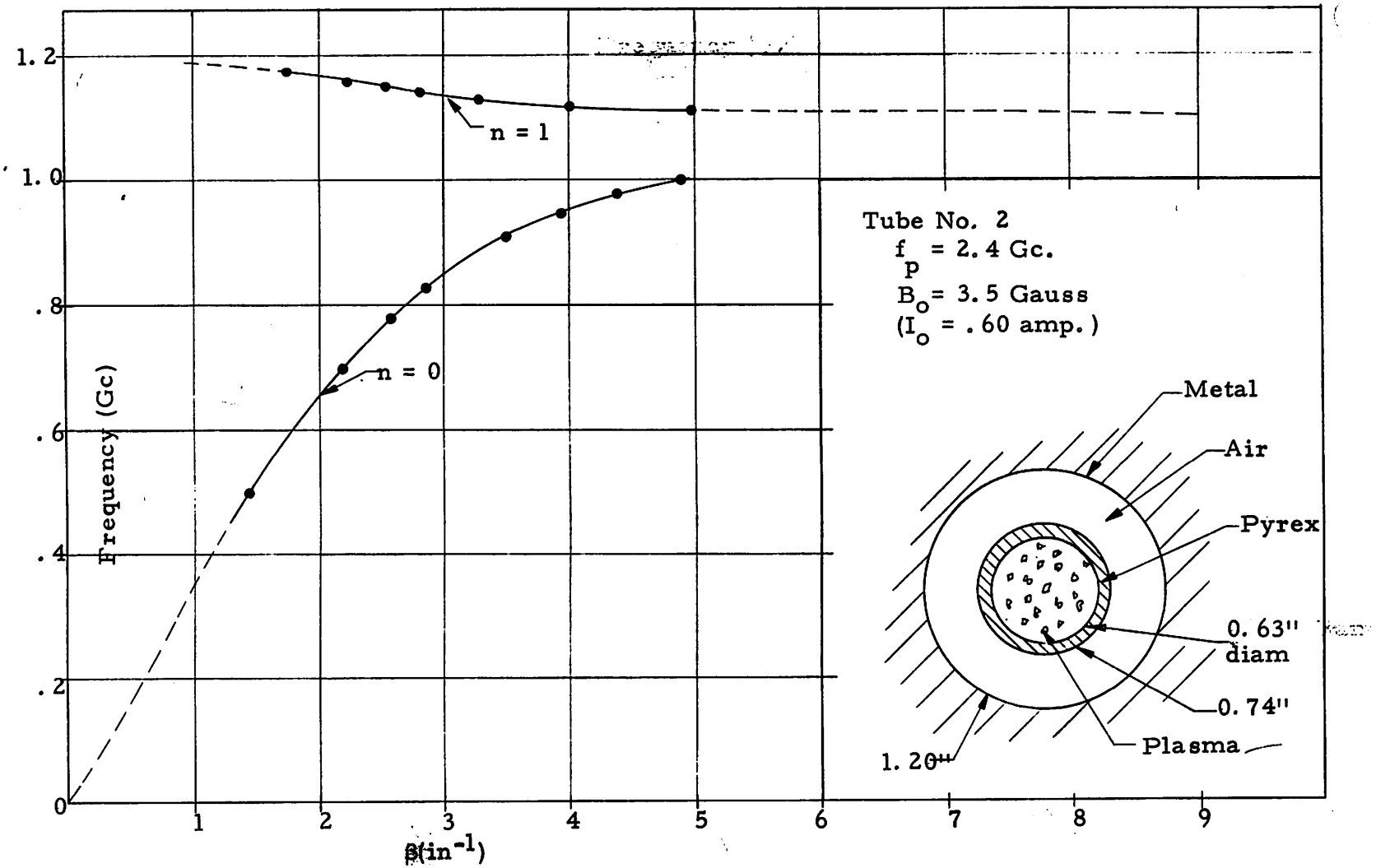

Fig. 22 Brillouin Diagram for n = 0 and n = 1 Modes for f_p = 2.4 Gc. (I_o = .60 amp.). Error in β: Approximately ± 3 Percent.

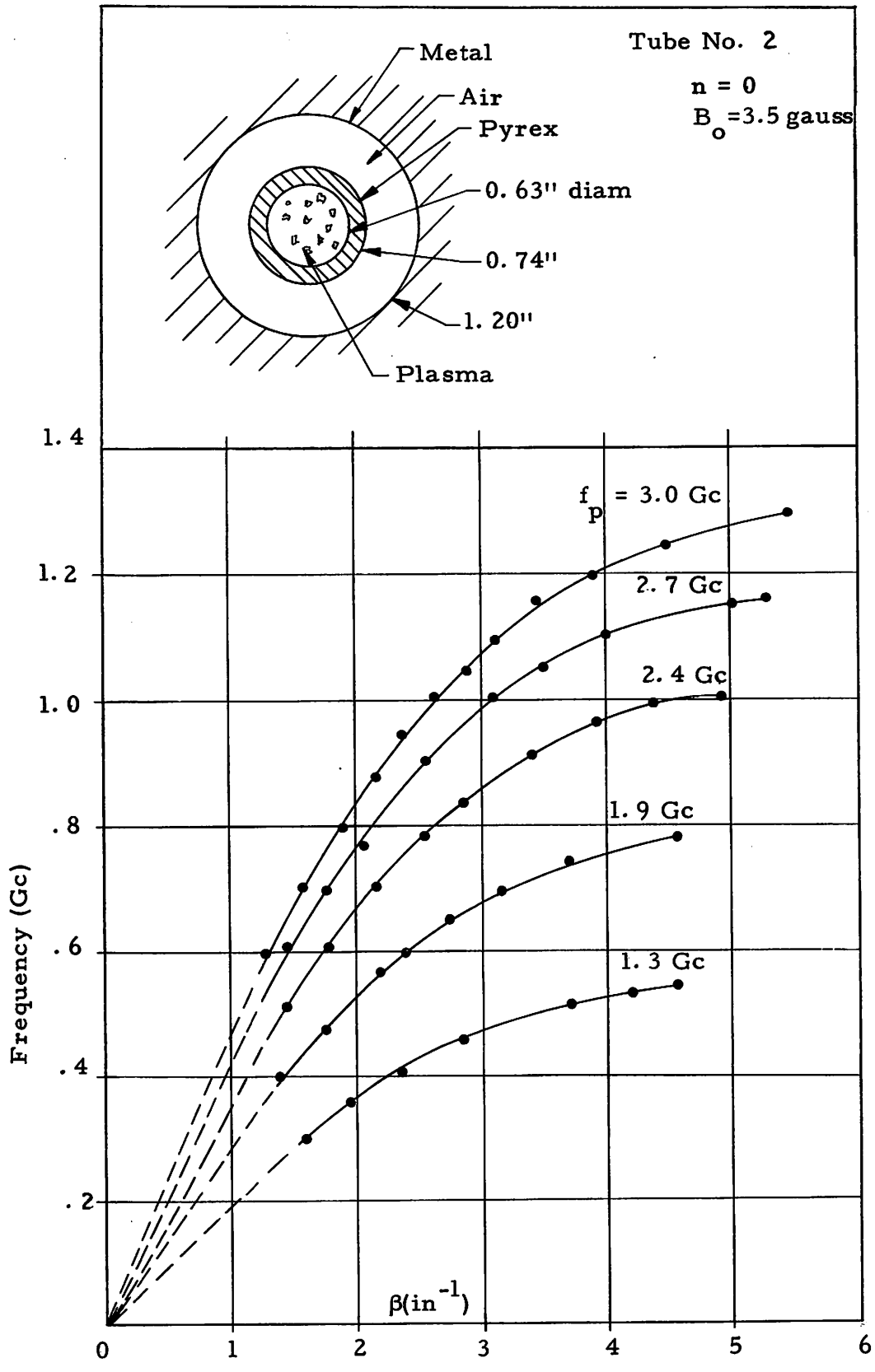

Fig. 23 Brillouin Diagram for n = 0 Modes. Error in β: Approximately ± 3 Percent.

We have pointed out in Section III that the azimuthal dependence of E_z is proportional to cos ϕ for the n = 1 mode. Since E_r (the component to which the detection probe is sensitive) also has this dependence, we test this ϕ-dependence by probing the mode azimuthally. As explained in Section III, this was done by holding the probe fixed and rotating both coupler and discharge tube. A radial plot of a quantity proportional to E_r vs ϕ is shown in Fig. 24 for the n = 1 mode. Although this plot was made for a particular set of parameters, it is nevertheless typical. Figure 25 shows a plot of the same quantities for the n = 0 mode.

Although both plots differ from the mathematically ideal (dashed curves), it is clear that a cos ϕ dependence is predominant in Fig. 24, while Fig. 25 shows that E_r is independent of ϕ. The distortion of these plots probably is due to the glass wall being of non-uniform thickness. The location of the glass discharge tube with respect to the copper waveguide was checked and the length of the air gap between them was invariant to .002 in. On the other hand, the glass wall thickness varied by $\pm$ .002 in. (measured in a similar glass tube). This thickness is critical since it is in the glass that the energy is concentrated.

In addition to measurements of propagation constant, measurements of α, the attenuation constant of the mode, were made. For the n = 1 mode typical plots of α are shown in Fig. 26. Also shown are the corresponding plots of β. It will be noted that the variation of α with frequency is in qualitative agreement with Eq. (2.44), which predicts that for a constant electron-collision frequency, α will be inversely proportional to the group velocity, $d\omega/d\beta$.

In Fig. 2 we have seen that the n = 2 surface mode occupies approximately the same portion of the spectrum as the n = 1 mode. We may demonstrate that in the previous measurements, the system was relatively free

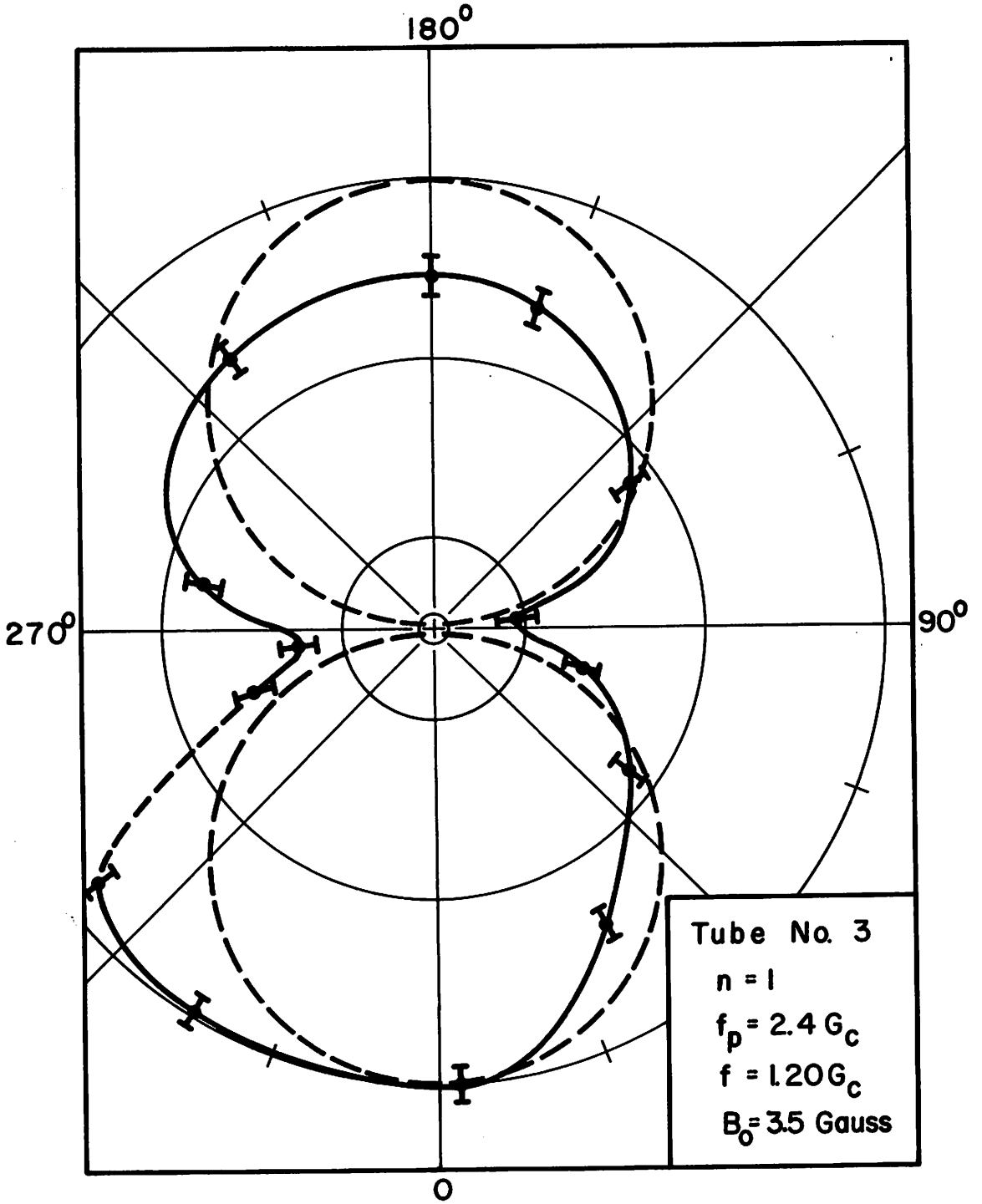

Fig. 24 Field Plot of a Quantity Proportional to E_r vs. the Azimuthal Coordinate ϕ for n = 1 Mode.

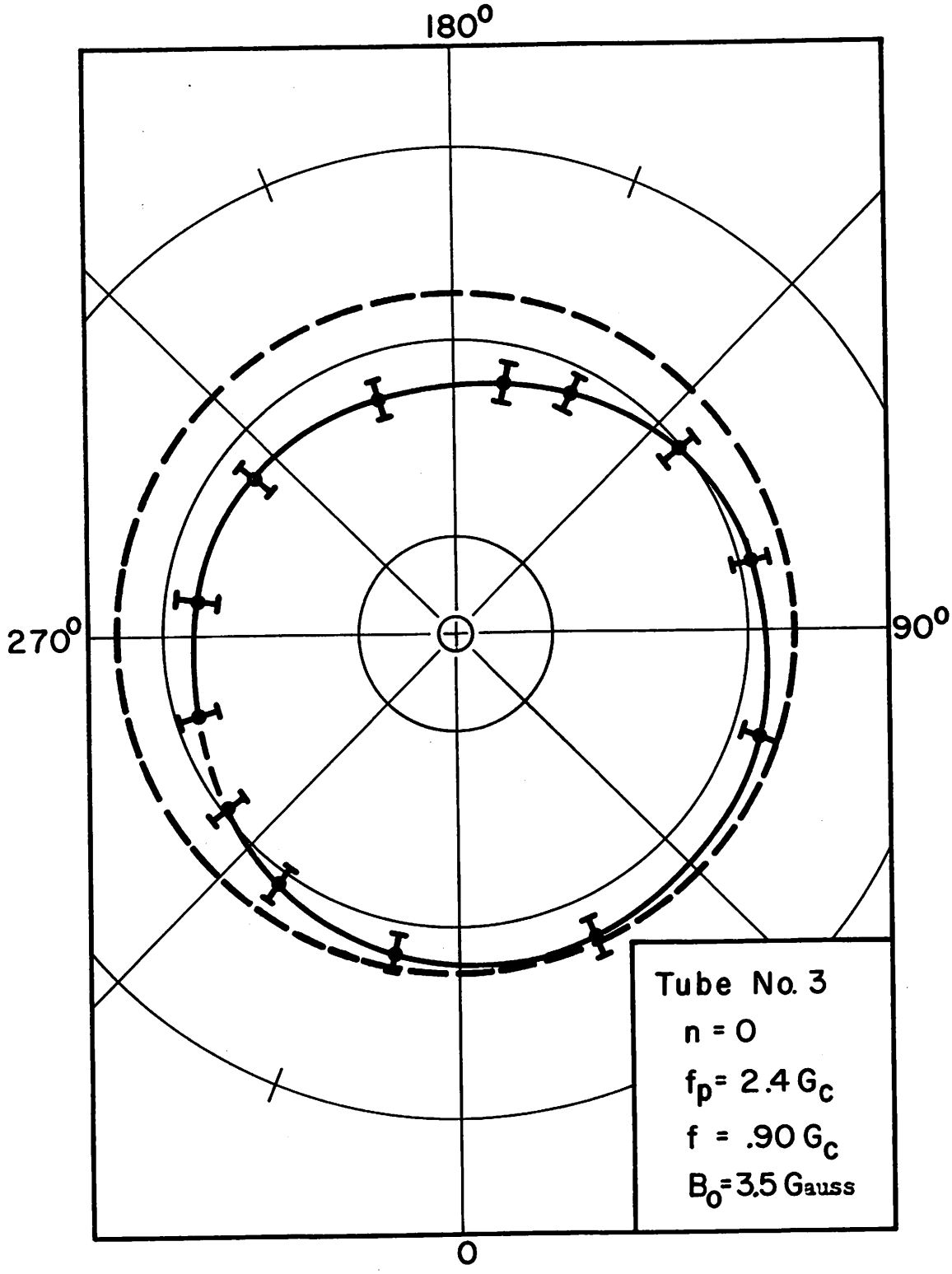

Fig. 25 Field Plot of a Quantity Proportional to E_r vs. the Azimuthal Coordinate ϕ for n = 0 Mode.

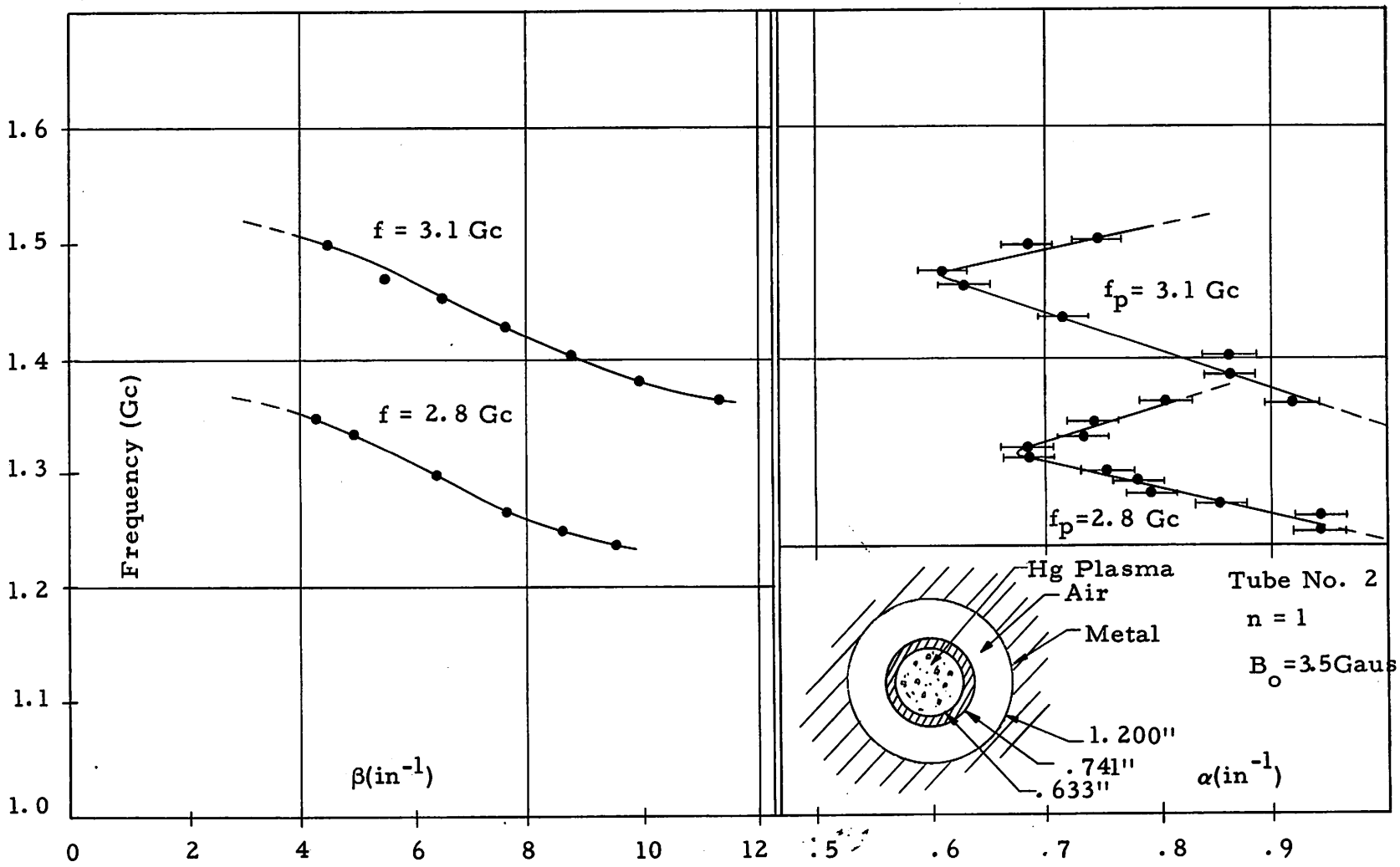

Fig. 26 Complex Propagation Constant $\gamma = \beta = i\alpha$ vs. Frequency for the n = 1 Mode. Error in β: Approx. $\pm$ 3 Percent.

from this and higher order modes by plotting relative amplitude vs. distance at frequencies in the n = 1 frequency band. This has been done in Fig. 27 at one frequency, the variation at that frequency being typical of the variation at other frequencies in the n = 1 band. Here it is seen that the maximum deviation from a purely linear variation of amplitude with distance (the condition for total absence of higher order modes) is very small.

It was of interest to determine the behavior of the n = 0 and n = 1 modes at large values of β where the excitation frequency is in the neighborhood of the theoretical cut-off frequency (for a lossless system),

$$f_{co} = f_p / \sqrt{1 + \epsilon_2} \qquad (5.1)$$

where ϵ_2 is the dielectric constant of the glass. In order to do this, both β and α were measured near the coupler where the amplitude of the mode was a maximum. This made measurements possible where α is large.

The results are shown in Fig. 28. The interesting point to observe here is that there exists a frequency band inside which both the n = 0 and the n = 1 modes will propagate. From Fig. 28 we see that there was propagation of both modes from 1.06 to 1.09 Gc. If attenuation had not limited the measurements, we would have found that this band was more extensive.

This behavior is predicted by the plasma waveguide theory developed in II. B. Referring to Fig. 2, we see that the n = 0 mode has a maximum frequency of propagation which is greater than f_{co}. Thus, there will indeed exist a band of frequencies common to both modes which extends from f_{co} to the maximum frequency on propagation of the n = 0 mode.

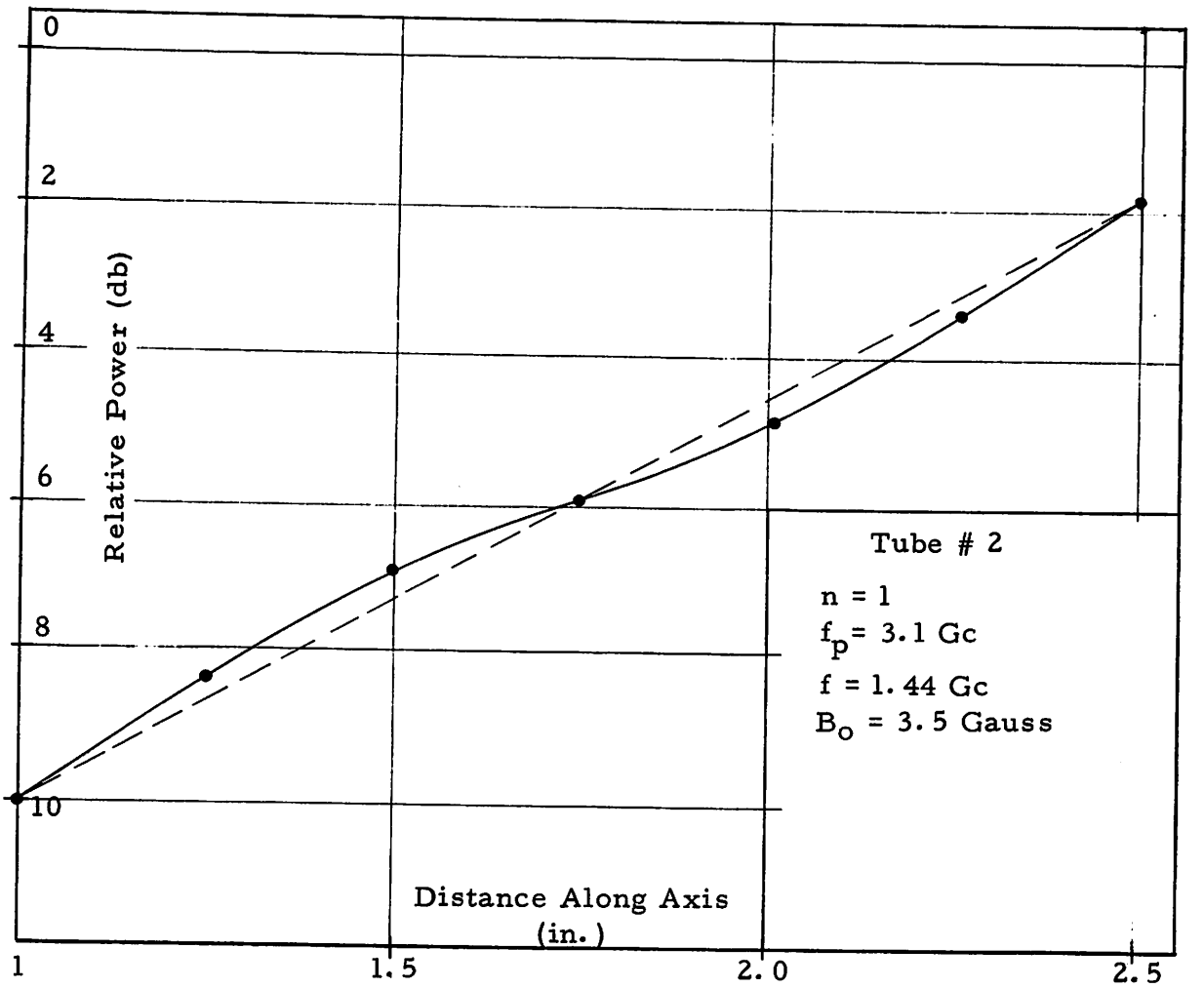

Fig. 27 Variation of Amplitude of n = 1 Mode vs. Distance Along the Waveguide. The Position Indicated by 1.0 on the Abscissa is Near the Termination.

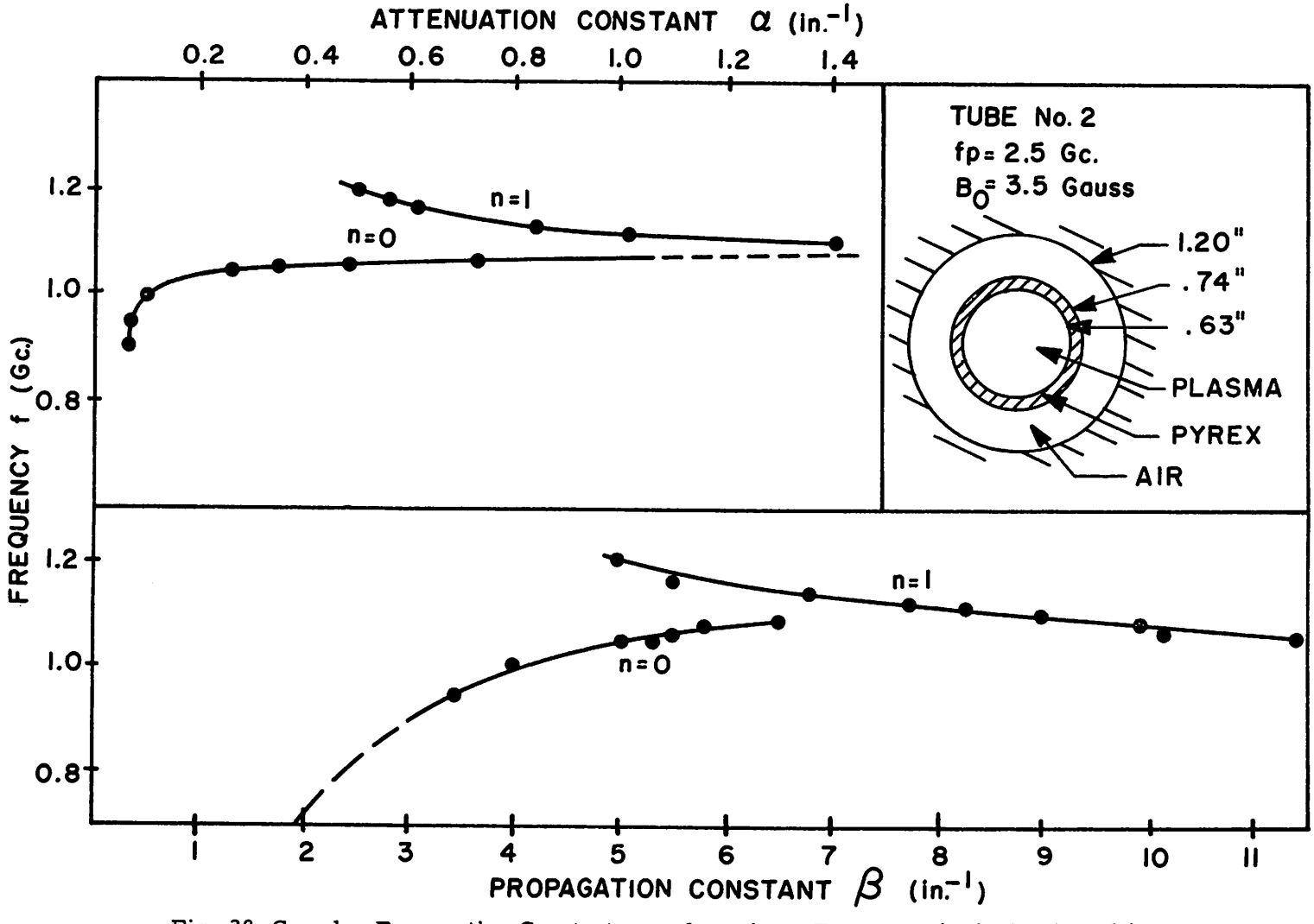

Fig. 28 Complex Propagation Constant $\gamma = \beta = -\alpha i$ vs. Frequency in the Region of f_{co}. Error May Be Large for All Quantities since Measurements were Made in a Region Where f_p was Varying with Axial Position (Region S in Fig. 29a).

As a final note, in measuring the n = 0 mode in Fig. 28, it was not possible to make measurements at values of β greater than 6.5(in.)$^{-1}$ because the loss was too great. This is in accordance with Eq. (2.44), since for large values of β, $d\omega/d\beta$ is very small.

We note that again Eq. (2.44) gives the correct qualitative dependence of α on the group velocity assuming a constant electron-collision frequency. Quantitatively, using Eq. (2.44) both Figs. 26 and 28 predict an electron-collision frequency of approximately 200 Mc., which is in rough agreement with the collision frequency predicted by cavity perturbation techniques and also Table 3.1.

In the measurements that have been discussed above, the backward nature of the n = 1 mode was extremely evident. It was reported in Section III that continuous monitoring of the phase of a mode was possible by means of a calibrated line stretcher in the reference arm of a microwave bridge (see Fig. 14). For the n = 0 mode, as the detection probe was moved away from the coupler the line stretcher had to be extended in order to keep the bridge in balance, thus indicating a wave whose phase was lagging as it proceeded away from the coupler. This is of course the characteristic of a forward wave.

At a frequency in the n = 1 pass-band, as the longitudinal probe moved away from the coupler, the line stretcher had to be shortened, thus indicating a wave whose phase advanced as it proceeded away from the coupler. This is the characteristic of a backward wave in which the phase velocity is toward the coupler while the energy velocity must be away from the coupler (the energy velocity must be away from the coupler for any wave).

We would now like to determine how well the theory developed in II. B predicts the experimental results, in particular, the curves for the n = 0 and n = 1 modes shown in Fig. 20.

The theoretical results presented in Fig. 2 have been obtained for the dimensions of the experimental plasma waveguide. Thus, these results may be directly compared with the experimental results in Fig. 20 if the parameter f_{co}, the cut-off frequency, is available. This cannot be determined directly from Fig. 20 because it was not possible (due to high attenuation) to make measurements at large enough values of β to determine to what frequency the two curves are becoming asymptotic. Therefore, the following procedure was adopted: f_{co} was chosen so that a theoretical curve would coincide exactly with the corresponding experimental curve at $\beta = 4.5\ (\text{in.})^{-1}$.

From Fig. 2, at $\beta = 4.5(\text{in.})^{-1}$ ($\beta a = 1.42$), $f/f_{co} = .99$ for the n = 0 mode and $f/f_{co} = 1.16$ for the n = 1 mode. Now referring to Fig. 20, at $\beta = 4.5\ (\text{in.})^{-1}$, f = 1.24 Gc. for the n = 0 mode and f = 1.44 Gc. for the n = 1 mode. Thus, the theoretical n = 0 curve will coincide with the experimental n = 0 curve at $\beta = 4.5\ (\text{in.})^{-1}$ if $f_{co} = 1.25$ Gc., while the theoretical and experimental n = 1 curves will coincide at $\beta = 4.5(\text{in.})^{-1}$ if $f_{co} = 1.24$ Gc. We split the difference and let

$$f_{co} = 1.245 \text{ Gc.}$$

The resulting theoretical curves for the n = 0 and n = 1 modes are shown as dashed curves in Fig. 20. We note the close agreement nearly everywhere between theory and experiment. In fact, we confirm that the value of β chosen to make a theoretical and experimental curve coincide for the purpose of determining f_{co} is entirely arbitrary. Any value of β could have been chosen yielding nearly the same value of f_{co}, and consequently the same excellent agreement between theory and experiment would be obtained.

Referring to the experimental results shown in Figs. 21 and 22, once again it can be demonstrated that there is close agreement between theory

and experiment.

From Eq. (5.1) we note that there is a definite relationship between f_{co} and the plasma frequency f_p. For $f_{co} = 1.245$ Gc., the corresponding plasma frequency is $f_p = 3.00$ Gc. where we have taken $\epsilon_2 = 4.82$, the permittivity of pyrex.[32] We may obtain an independent check on this value of f_p by using the results of the cavity measurements reported in IV. B. In Fig. 20, the discharge current is .99 amp. Referring to Fig. 16, and taking into account the reduction factor in Table 4.1, we see that the plasma frequency predicted by the cavity perturbation method for this discharge current is $f_p = 3.25$ Gc., which is 8 percent higher than that obtained above from Eq. (5.1).

It is of considerable interest to make a large number of comparisons of f_p determined from Eq. (5.1) with f_p determined by the cavity perturbation technique. From the data that has been taken on Tubes Nos. 2 and 3, it has been possible to make nine comparisons. From a plot of the n = 0 or the n = 1 mode at a certain discharge current, f_{co} was chosen so that the appropriate theoretical curve would coincide with the experimental curve at $\beta = 4.5\ (\text{in.})^{-1}$. Then f_p was found from Eq. (5.1). For the same discharge current, f_p was found from Fig. 16 using Table 4.1.

The nine comparisons showed that the values of f_p found in the two different ways differed on the average by 6.2 percent. The largest deviation was 11 percent and the smallest was 2 percent. In all cases, the cavity-determined f_p was larger than the f_p found from Eq. (5.1). This difference probably exists because the measurements used to obtain the two values of f_p to be compared were made of the order of weeks apart. In terms of the discussion of errors at the end of IV. B, this error can be attributed to diurnal variations.

The cavity-determined f_p is an average of f_p over the cross section of the discharge tube with a weighting function that is nearly unity. f_{co}, however, depends on f_p at the discharge tube wall, since at large values of β this is where the energy of the mode is concentrated. We will point out in the Appendix that at the wall, the electron density, and hence f_p^2, may be of the order of 20 percent less than its value on the discharge tube axis. We may therefore be tempted to attribute the 6.2 difference between the cavity-determined f_p and f_p obtained from f_{co} to the decrease of the electron density at the wall.

This is probably not a valid conclusion. Trivelpiece[6] has analyzed a case in which the electron number density n_e in the plasma has a parabolic radial dependence,

$$n_e = n_{ea} (1 - \mu (\frac{r}{a})^2$$

where n_{ea} is the number density on the axis. The Brillouin diagram has been found for the n = 0 mode. Since the parameters for the case that Trivelpiece analyzes are nearly identical to the parameters of the experimental system used in this project (i.e., nearly the same ratio of inner to outer diameter of the discharge tube, nearly the same ratio of discharge tube inner diameter to waveguide diameter, nearly the same permittivity of glass), the results he finds should be applicable. He finds that for $\mu = .2$, or a 20 percent decrease in number density at the plasma-glass tube interface, at $\beta = 5\ (\text{in.})^{-1}$ (about the largest β for the n = 0 mode that was measured), the corresponding angular frequency ω is less than 1 percent lower than ω for $\mu = 0$, or constant number density across the cross section of the tube. Therefore, in the range of β in which the measurements reported here were made, the Brillouin diagram for the n = 0 mode does not appear to be a sensitive function of μ.

In Fig. 26 it will be noted that the range of β in the n = 1 pass-band extends from 4.5 $(in.)^{-1}$ to 11 $(in.)^{-1}$ while in Figs. 21 through 23, the range of β extends from $2(in.)^{-1}$ to about 7 $(in.)^{-1}$. By monitoring phase with distance it was possible to discern that in the former case f_p was decreasing in the region of the coupler, as shown qualitatively in Fig. 29a, while in the latter case it remained fairly constant along the tube, as shown in Fig. 29b. In the former case the emission was reduced due to deterioration of cathode emission, while in the latter case the emission was high. In the former case the anode was probably quite hot.

Since for the case of varying f_p, both the upper and lower cut-off frequencies of the n = 1 mode will vary in proportion to f_p, then excitation of the n = 1 mode at the position of the coupler will result in propagation within a restricted frequency range f_{co}' to f_u' down the length of the system. The measurements shown in Fig. 26 were made at the terminated end of the system and so would be subject to this restricted range.

A wave at frequency f_{co}' propagates over the region S at a propagation constant away from cut-off and so experiences relatively little attenuation over this distance. Only as the wave front travels beyond this range does it experience heavy attenuation. Thus, at the measuring position a wave at f_{co}' in Fig. 29 a will have experienced the same attenuation as f_{co}' in Fig. 26b where the former wave is nearer cut-off at the position of measurement and so will have a larger β than the latter wave. We assume that at frequencies lower than f_{co}' in the two cases the attenuation is so great at the measuring position that β cannot be measured. A similar argument would show that if f_u' are the frequencies in the two cases above which the attenuation is so great at the measuring position that β cannot be measured, that at f_u', β for the case in Fig. 29a is larger than the β for Fig. 29b.

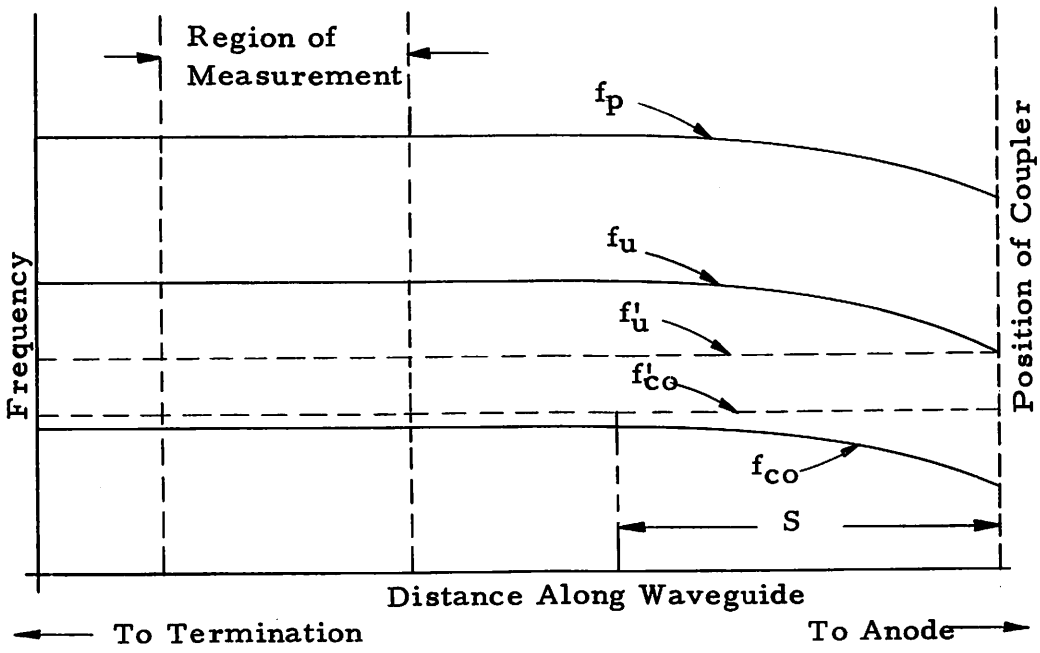

Fig. 29a Variation of n = 1 Cut-off Frequencies for a Case in Which f_p Varies with Axial Position.

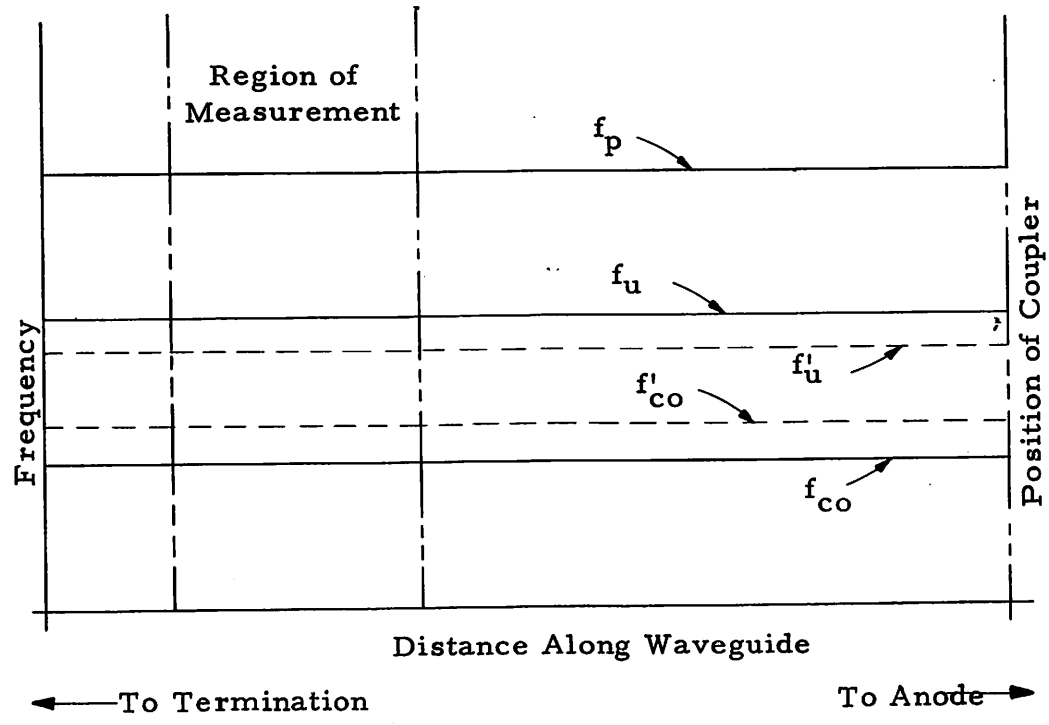

Fig. 29b The Case where f_p is a Constant with Respect to Axial Position.

Finally, the effect of magnetic field on the n = 1 mode was investigated. Here, a 60^{o} coupler was used to excite the system. It was found that the only modes present to any extent up to about 8 gauss were the n = 1 and the n = 0 modes. No variation of propagation constant or attenuation constant could be measured over this range of magnetic field. Above 8 gauss additional modes were excited in the pass-band of the n = 1 mode. Drift in the system did not allow measurement of these modes by the techniques of IV. A. The attenuation of all modes except the n = 0 mode increased rapidly with magnetic field so that at 60 gauss the total power detected by the detection probe at a fixed longitudinal position had dropped by 30 db and continued to drop at larger magnetic fields. There was no indication that the frequency band of the n = 1 mode had shifted. It was observed that the VSWR (about 6. 5) of the coupler did not change while the magnetic field was being varied so that the power being coupled into the modes remained constant.

B. PERTURBED TE_{11} WAVEGUIDE MODE

The resonant system technique described in III was used to determine the variation of propagation constant β with frequency for the perturbed TE_{11} waveguide mode. The application of a dc magnetic field causes the plasma column to become anisotropic so that according to the discussion of II. C we may expect that the TE_{11}^{+} circularly polarized mode will have a different propagation constant from the TE_{11}^{-} mode. In the resonant system there will be resonances associated with each of these modes which we have labeled TE_{11m}^{+} and TE_{11m}^{-}. Here, m has the usual significance of being the number of maxima of E_r on the axis. If ℓ is the separation of adjacent minima, then

$$\beta = \pi/\ell \qquad (5.3)$$

This method of measuring β has proved to be useful and has allowed the desired variation of β with frequency to be found for the TE_{11}^{+} and TE_{11}^{-} modes. It is shown in Fig. 30.

Generally, the Q of the resonant system was low, of the order of 50. Nevertheless, the power ratio between successive maxima and minima as measured by the detection probe was large, typically, 20 to 30 db so that precise measurements of ℓ, the distance between minima, was always possible. In all determinations of β, ℓ was the distance from the anode-end wall to the first minimum. Here it was assumed that the anode-end wall acts like a continuous shorting plane across the system. The validity of this assumption was confirmed by noting that ℓ determined in this way was indistinguishable from the distance from the first minimum to the second.

It was found that sufficient points to determine the desired curves could be obtained by varying the length of the resonant system from a maximum of 6.56 in. to about 4 in. with m taking on the values 2, 3, 4, 5. In Fig. 30, each point is labeled with the appropriate m. The points for which m is circled were obtained with the resonant system at its maximum length. It will be noted that the circled-m points which have the same m do not have exactly the same β. The explanation for this is two-fold. Firstly, since the "shorting-plane" at the cathode-end of the system is merely a metal ring filling the gap between the glass tube and the copper waveguide, the effective position of the reflecting plane at this end may vary slightly with frequency. Secondly, the resonance Q was low enough so that it was difficult to adjust the system to exactly the condition of resonance. Indeed, in many (if not all) of the measurements, the resonant frequency was never exactly attained. This variance from the resonant condition would account for the aforementioned points not occurring at the same β. It should be pointed out here, that the

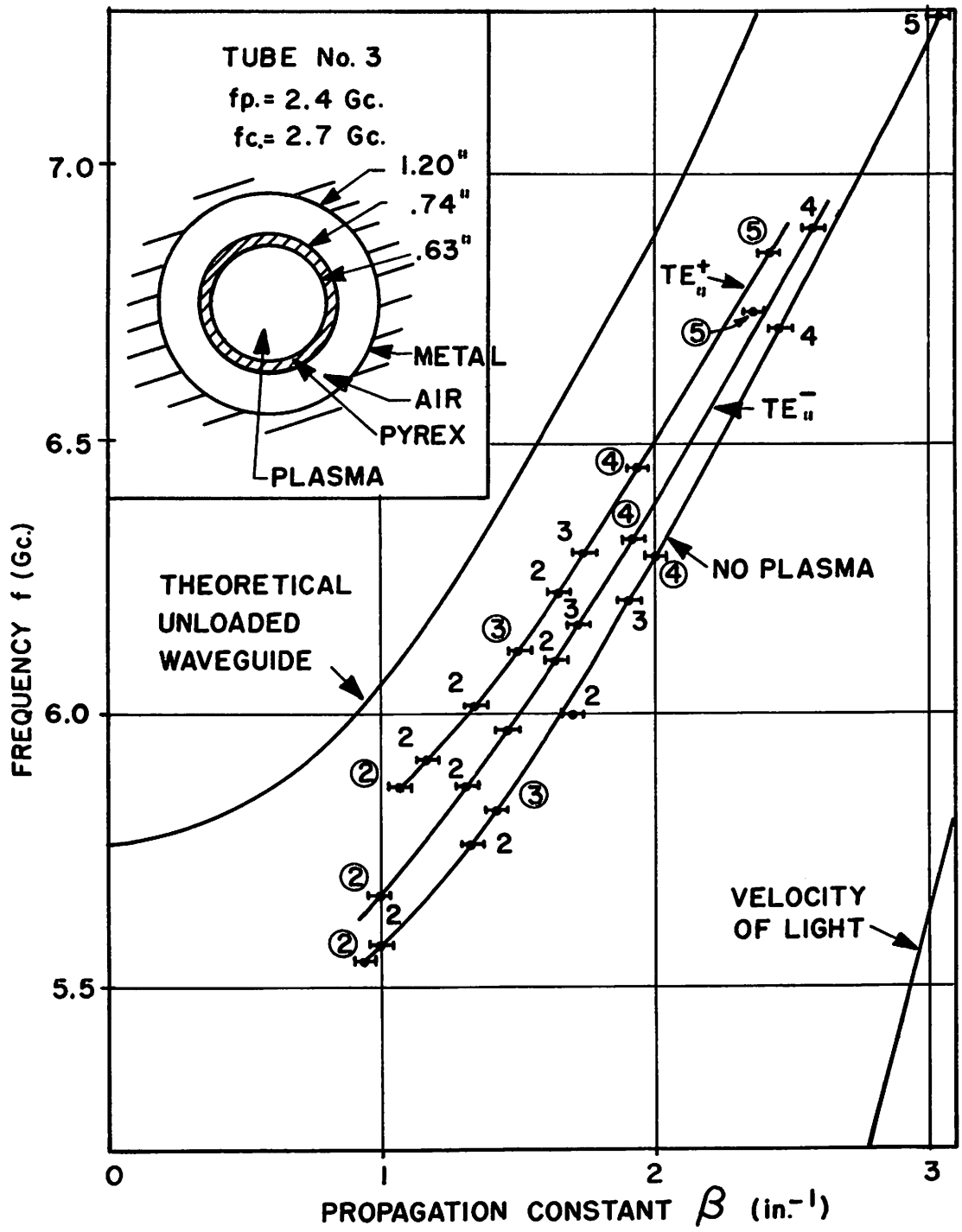

Fig. 30 TE_{11}^{+} and TE_{11}^{-} Perturbed Waveguide Mode Brillouin Diagrams. The Number Indicates the Type of Resonance Used to Obtain the Point, i.e., 2 means TE_{112} Resonance. A Circle Indicates that the Cavity was at its Maximum Length.

exact condition of resonance is not at all essential in these measurements. The condition of resonance is significant only in that it affords mode discrimination and allows effective coupling between a rather simple coupler (a simple probe coupling to E_r) and the resonant mode. The condition for accuracy of the measurements is that the ratio of a field maximum to a minimum be large, indicating that only one mode is present, and allowing a half-wavelength of the corresponding waveguide mode to be accurately measured.

The variation of β with frequency shown in Fig. 30 is in agreement with the qualitative discussion given in II. The curve labeled "no plasma" was obtained with the waveguide loaded with the glass tube. The dielectric loading will cause the stored energy per unit length to increase. Slater[26] shows that for constant β, this condition will cause the frequency to decrease. Thus, the "no plasma" curve lies below the unloaded waveguide curve in Fig. 30.

The introduction of plasma into the glass tube reduces the stored energy per unit length by virtue of the negative dielectric constant of the plasma. Thus, the TE_{11}^- curve which is little affected by the magnetic field (Fig. 31) will lie above the "no plasma" curve. Finally, we have seen in II that the TE_{11}^+ curve will lie above the TE_{11}^- curve by approximately 130 Mc. for f_c = 2.73 Gc. This is roughly in agreement with Fig. 30.

Figure 31 shows the dependence of the TE_{11}^+ and TE_{11}^- modes on the magnetic field. Specifically, the TE_{112}^+ and TE_{112}^- resonances with the resonant system at its maximum length are shown. Careful checking shows that any TE_{11m}^+ resonance will have the same dependence as does the T_{112}^+ shown in Fig. 31. Any TE_{11m}^- resonance will have the same dependence as the TE_{112}^- resonance.

It is seen that the TE_{112}^- resonance is insensitive to magnetic field except at low fields while the TE_{112}^+ resonants is quite sensitive to magnetic field. Below 500 guass it was not possible to detect the latter resonance

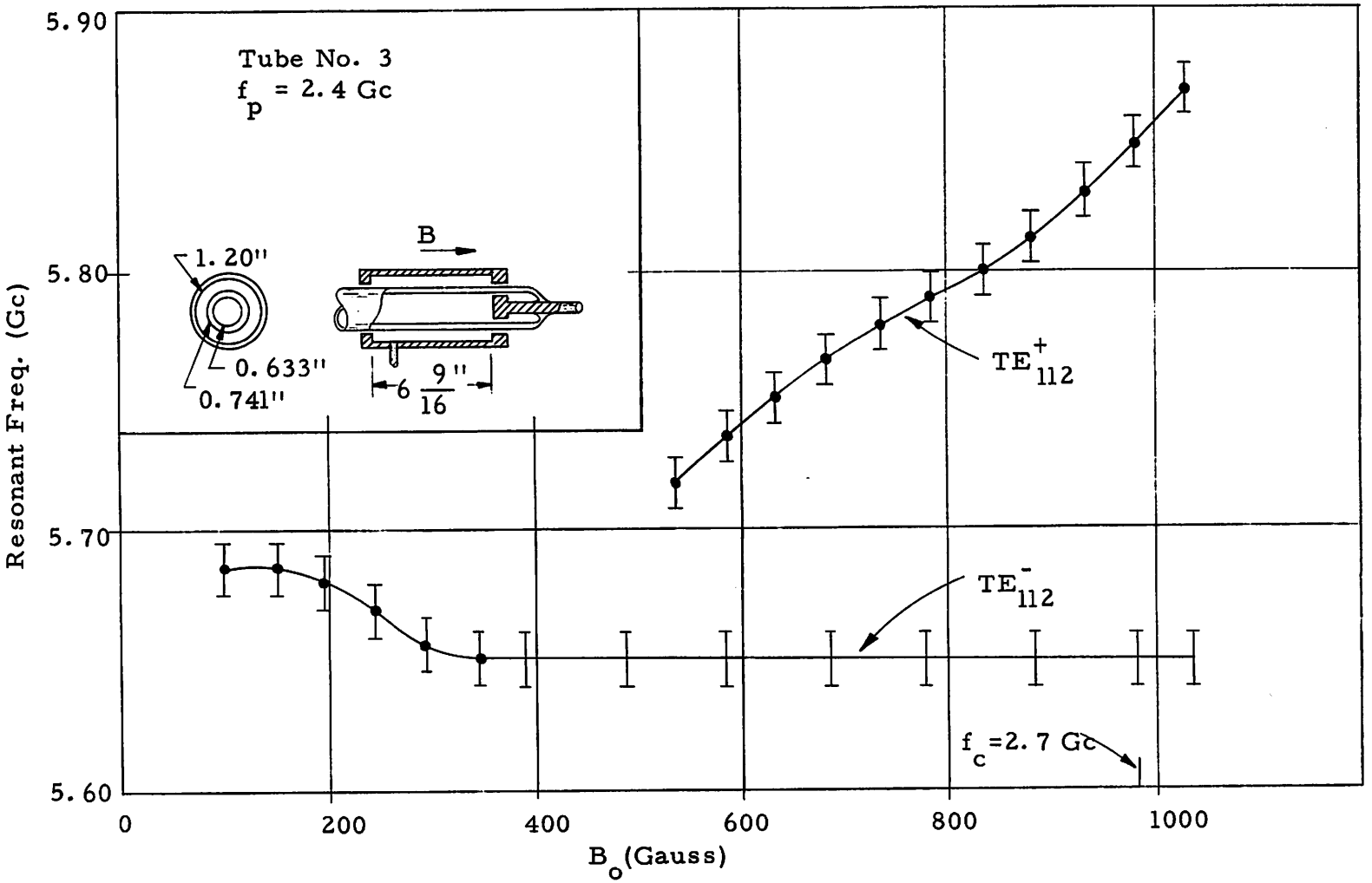

Fig. 31 Variation of Resonant Frequency of TE^+_{112} and TE^-_{112} Resonances with Magnetic Field. f_p = 2.4 Gc.

because it was masked by the TE_{112}- , a stronger resonance. Above 1050 gauss it was again not possible to measure it because here it was masked by the TE_{113}- resonance.

C. NOISE AND DRIFT

Although noise fluctuations of the parameters of the mercury-vapor discharge positive column did not limit the measurements reported in this report, they are of interest to the development engineer who may be contemplating the use of this discharge in some application. Slow-time drift of the parameters, probably due to small changes in the vapor pressure, were troublesome and constituted the chief source of error in the propagation constant measurements. Both of these detractors are discussed below.

For a mode propagating in the plasma waveguide, the total power P that flows across a cross-section of the system may be represented as the sum of two terms,

$$P = P_s + P_n \qquad (5.4)$$

where P_s is the power at the transmitter or signal frequency, and P_n is the unwanted power at all other frequencies which we call the noise power. We have found experimentally that the noise power output of the transmitter (signal source) is very small compared to P_n, so that P_n is nearly all generated in the plasma waveguide. If we probe the mode with the detection probe, we shall assume that the signal power and the noise power absorbed by the probe and which travel down the coaxial transmission line to the measuring apparatus, will have the same ratio as P_s and P_n at the position of the probe.

It has been possible to measure 10 log (P_s/ P_n) for the n = 0 and n = 1 modes described in V.A. Here, we use the microwave bridge shown

in Fig. 14, where the detector was a high-sensitivity receiver capable of accurate measurement of relative power levels. Disconnecting the reference bridge arm which contains the calibrated line-stretcher and attenuator, the power level of the signal arriving from the detection probe is noted. This power is proportional to the total power $P = P_s + P_n$. We now connect the reference arm of the bridge and balance out the transmitter frequency component of the signal. Thus, the only power which can now reach the receiver is proportional to P_n so that we are able to measure $10 \log (P/P_n)$. From this, $10 \log (P_s/P_n)$ is easily obtained.

Measurements of this type have been made on both the $n = 0$ and $n = 1$ modes. We find that $10 \log (P_s/P_n)$ is independent of the input power level to the plasma waveguide. Here, the input power was varied from about 1 milliwatt to .1 milliwatt.

In Fig. 32 we show the variation of $10 \log (P_s/P_n)$ as a function of frequency for the detection probe far from the double-ring coupler. The noise power increases relative to the signal power for the $n = 0$ mode as ω_{co} is approached. For the $n = 1$ mode, $10 \log (P_s/P_n)$ is nearly constant across its band. In Fig. 33, $10 \log (P_s/P_n)$ is shown as a function of probe position at discreet frequencies. In all cases, the noise power <u>decreases</u> relative to the signal power as the input coupler is approached.

We have examined the signal emerging from the detection probe with a spectrum analyzer which has a 1000 cps sweep rate. This means that the spectrum analyzer will display the spectrum of the signal on the cathode-ray tube screen at millisecond intervals. From this it was possible to determine that if E_{r1} is the radial field component which excites the detection probe at time t_1, then a millisecond later at t_2, the radial field component E_{r2} will be slightly different in amplitude and phase from E_{r1}. A millisecond later at t_3, E_{r3} will be slightly different from E_{r2}, etc. E_{r1}, E_{r2}, E_{r3}, ... are shown in Fig. 34. Thus, there appears to be a small

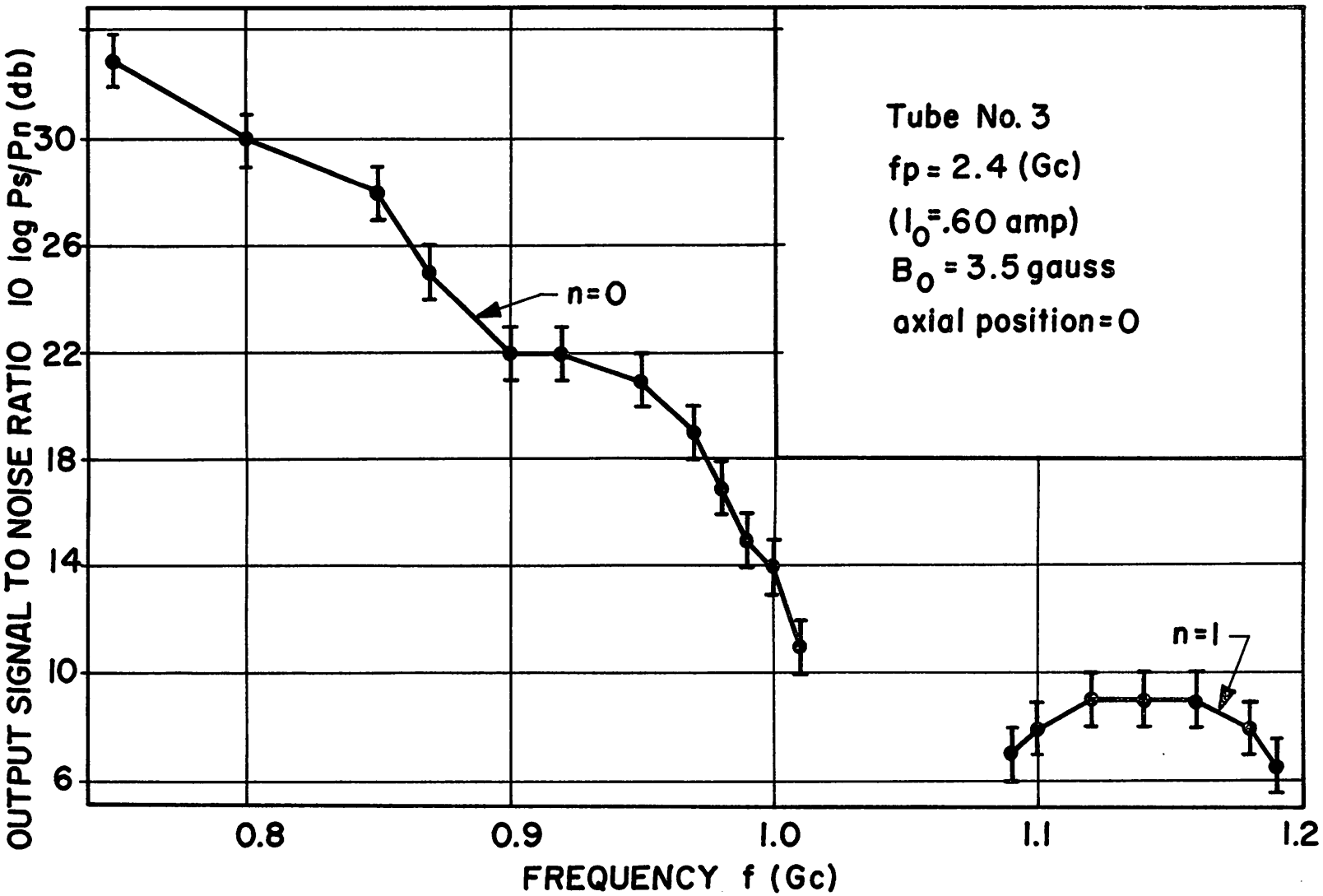

Fig. 32 Signal to Noise Ratio for n = 0,1 Modes vs. Frequency; f_p = 2.4 Gc.

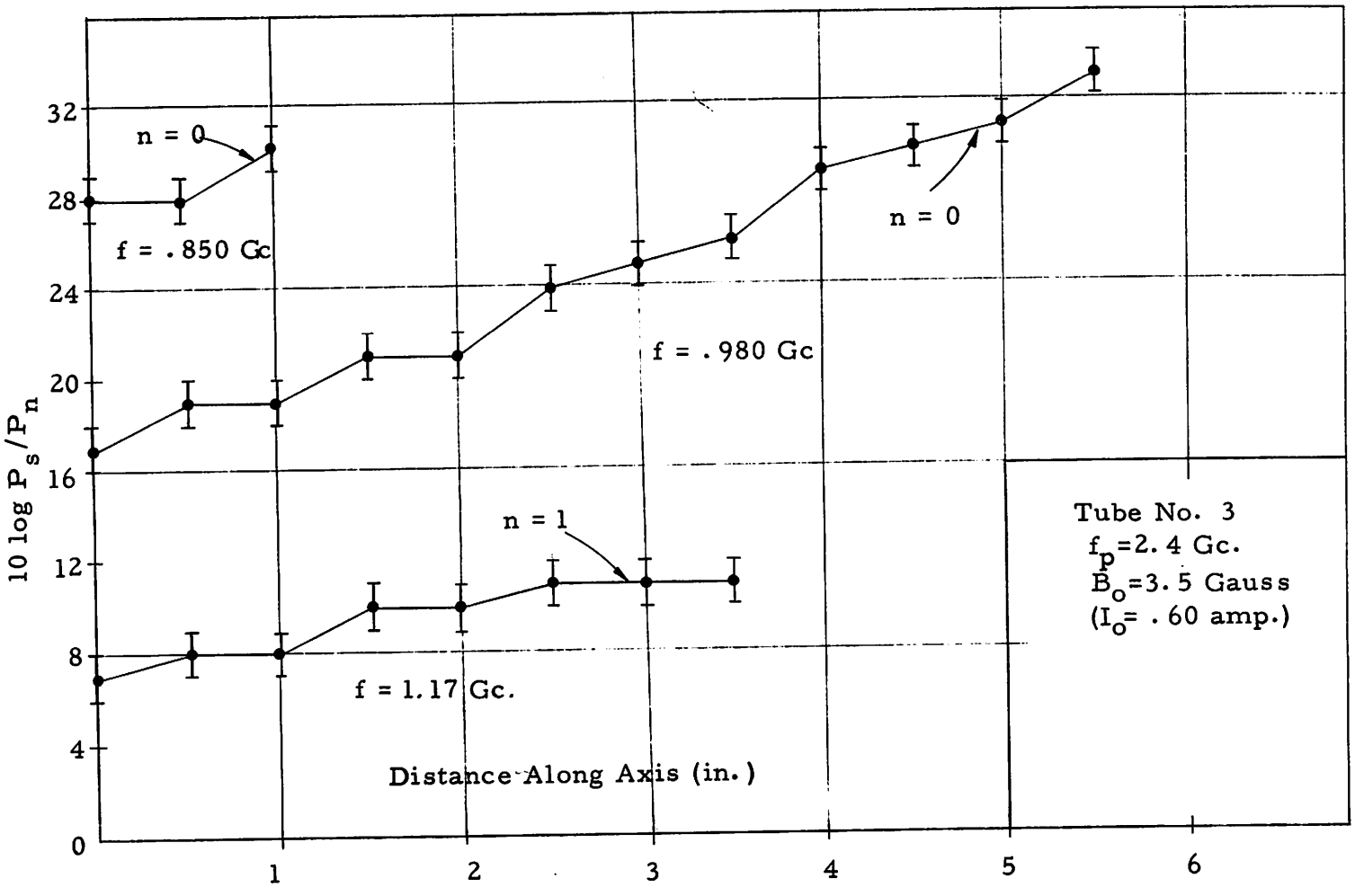

Fig. 33 Signal to Noise Ratio vs. Distance Along Plasma Waveguide. The Position Indicated by 0 is Near the Termination.

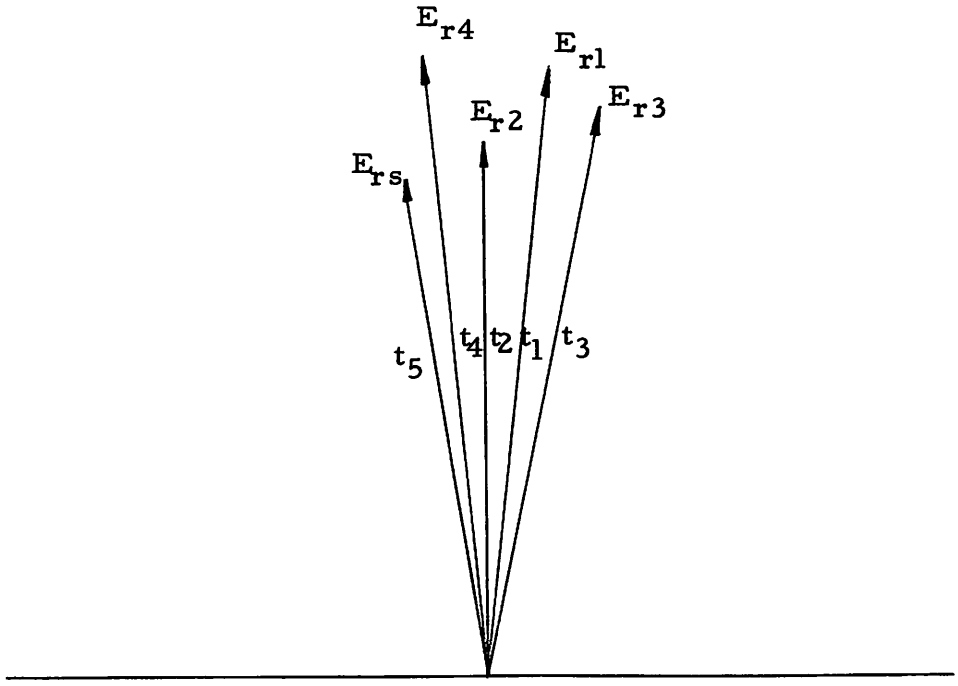

Fig. 34 Phasor Diagram of E_r at Five Observation Times.

phase and amplitude modulation of the signal, and therefore, P_n is the power in the side-bands which exist by virtue of this modulation. It was also possible to determine from observations with the spectrum analyzer that the amplitude and phase modulation frequencies were less than 1 Mc.

We now propose a simple model of the plasma which will explain all the observations described above. Assume that the electron number density n_e consists of a part which is independent of time, n_{eo}, and a small time-varying part, $\Delta n_e(t)$, so that

$$n_e = n_{eo} + \Delta n_e(t) \qquad (5.5)$$

n_{eo} may be regarded as a time-average of n_e while $\Delta n_e(t)$ is a noise fluctuation of n_e whose frequency components are less than 1 Mc. Assume that $\Delta n_e(t)$ is independent of position so that the electron density everywhere in the positive column is fluctuating coherently.

Equation (5.5) for n_e will lead to a plasma angular frequency

$$\omega_p = \omega_{po} + \Delta\omega_p(t) \tag{5.6}$$

and a cut-off angular frequency

$$\omega_{co} = (\omega_{co})_o + \Delta\omega_{co}(t) \quad . \tag{5.7}$$

If the n = 0 mode or the n = 1 mode is propagating in the system with a propagation constant β and an attenuation constant α, then

$$\beta = \beta_o + \Delta\beta(t) \quad , \tag{5.8}$$

and

$$\alpha = \alpha_o + \Delta\alpha(t) \quad . \tag{5.9}$$

In the above expressions a quantity with a subscript "o" is a time average quantity while a quantity preceded by Δ is a noise fluctuation of the quantity due to $\Delta n_e(t)$.

If the probe is a distance L from the coupler, then E_r, the component of electric field to which the probe is sensitive, will be related to E_r at the coupler by the factor

$$\exp(-\alpha L - i\beta L) = \exp(-\alpha_o L - i\beta_o L) \exp[-\Delta\alpha(t)L] \exp[-i\Delta\beta(t)L] . \tag{5.10}$$

The factors

$$\exp[-\Delta\alpha(t)L] \text{ and } \exp[-i\Delta\beta(t)L]$$

will account for the amplitude and phase modulation, respectively, of the wave and P_n will be the resulting power in the side-bands.

It is clear now that $10 \log P_s/P_n$ will be independent of the input power supplied by the transmitter because the system is linear.

To explain qualitatively the variation of $10 \log P_s/P_n$ shown in Figs. 32 and 33, consider a particular angular frequency ω_k in the noise frequency spectrum. Suppose that the component of $\Delta n_e(t)$ at this frequency is $\Delta n_{ek} \sin \omega_k t$, so that the factors producing amplitude and phase modulation at ω_k in Eq. (5.10) are,

$$\exp [-\Delta\alpha_k L \sin (\omega t + \theta')] \quad \text{and} \quad \exp [-i\Delta\beta_k L \sin (\omega t + \theta'')]$$

respectively. The greater the $\Delta\alpha_k L$ and $\Delta\beta_k L$, the more power there will be in the side-bands associated with ω_k and the greater will be the contribution to P_n at ω_k. The same is true at all other noise frequencies.

Referring to the Brillouin diagrams for the $n = 0$ and $n = 1$ modes shown in Fig. 28, it can be seen that a fluctuation of ω_{co} at the noise frequency ω_k of amplitude $\Delta (\omega_{co})_k$ will cause both $\Delta\beta_k$ and $\Delta\alpha_k$ to increase as the transmitter frequency approaches $(\omega_{co})_o$. Thus, for constant P_s and L, P_n will increase as the transmitter frequency approaches $(\omega_{co})_o$. This is in agreement with the variation of $10 \log P_s/P_n$ shown in Fig. 32. At a constant transmitter frequency, if the detection probe is moved toward the coupler so that L decreases, then $\Delta\alpha_k L$ and $\Delta \beta_k L$ will decrease and therefore P_n will decrease, which is in agreement with the variation of $10 \log P_s/P_n$ shown in Fig. 33.

The model of the plasma which we have made use of above, and which is summarized by Eq. (5.5), has been predicted approximately by Crawford and Lawson.[34] They find that in a mercury-vapor discharge, except for a region extending 8 in. beyond the cathode, there is a noise fluctuation of the electron number density which is coherent from point to

point. The diameter of their discharge was 2 cm. and they operated at a discharge current of approximately .1 amp. All measurements reported in this section were made near the anode, where presumably the fluctuations of n_e were coherent.

Crawford and Lawson postulate that there is a source of noise voltages in the region near the cathode and that waves of noise voltage propagate down the positive column with phase velocities greater than 10^9 cm/sec. The spectrum of the noise voltage frequencies shows predominate components at 60 Kc. and 105 Kc. at .1 amp. discharge current. They have measured relative fluctuations in n_e and find that they become somewhat greater as the cathode is approached.

We conclude the discussion of noise by noting that for measurements in which a d. c. magnetic field was present, for example, in measurements on the $TE_{11}+$ and $TE_{11}-$ modes, $10 \log P_s/P_n \sim 0$; i. e., the noise power is very large and implies that the presence of a magnetic field introduces a new source of noise into the system.

Slow drift of the phase shift of a mode from the coupler to the detection probe was the chief cause of error in the propagation constant measurements. This is probably due to a drift in the vapor pressure which causes the electron number density n_e to vary. We have been able to estimate that drift in phase shift causes a $\pm$ 3 percent error in the measurement of β. The amplitude of a mode at the position of the detection probe was quite constant, varying less than .1 db over a 7 minute observation time.

VI. SUMMARY AND CONCLUSIONS

In this report we have examined experimentally the properties of certain modes in a plasma waveguide of circular symmetry. When the magnetic field is essentially zero, a backward-wave pass-band mode has been found which is a n = 1 surface wave. Using the expression for the permittivity tensor which neglects the effects of thermal motion of the electrons and ions of the plasma and also collisions between plasma components, it has been possible to predict the propagation constant β of the n = 1 mode and also the low-pass n = 0 mode with considerable precision.

This result was predicted in II. There it was indicated that the electron temperatures typically found in a mercury-vapor discharge positive column should have little effect on the values of the elements of the permittivity tensor. In that section we further pointed out that for the n = 0 mode, the collision frequency ν has negligible effect on the propagation constant β except where the attenuation constant is very large. Specifically, for the n = 0 mode propagating in a two region system, if

$$2\alpha s < \frac{\pi}{2} \tag{2.37}$$

the neglect of collisions and of the thermal velocities of the plasma components will <u>not</u> lead to appreciable error in the calculation of the propagation constant. We would not be surprised to find that the same criterion could be applied to a three-region system and to other modes besides the n = 0. The measurements reported above are experimental evidence that this criterion is applicable to the n = 0 and n = 1 modes in a three-region system.

Both the n = 0 and n = 1 modes were excited by a novel coupler, called a double-ring coupler, which is geometrically symmetric. It was presumed that the non-symmetric n = 1 mode was excited by virtue of the electric field between its two rings being non-symmetric; i.e., the field varies as a function of the azimuthal coordinate. At the point where the two rings are attached to the exciting coaxial transmission line, the electric field probably is greatest and is a minimum on the opposite side of the rings. That is, if ϕ, the azimuthal coordinate, is zero at the position where the rings are excited, then the field between the rings is a maximum at $\phi = 0$ and a minimum at $\phi = 180^{o}$. It is suggested that if it is desired to make the electric field independent of ϕ so that it will not excite the non-symmetric n = 1 mode, then the rings could be squeezed together at $\phi = 180^{o}$ so as to boost the electric field there. A better way of saying this is that instead of the planes of the two rings being parallel, they should be set at an angle such that the rings will be closer together at $\phi = 180^{o}$ than at $\phi = 0$. Conversely, the field may be made more non-iniform so that the n = 1 mode will be excited more effectively by setting the planes of the rings at such an angle that the rings are farther apart at $\phi = 180^{o}$ than at $\phi = 0$.

Noise measurements have been made on both the n = 0 and the n = 1 modes. We have found that the signal-to-noise ratio, 10 log P_s/P_n, is better than 30 db for the n = 0 mode if we are in the region of constant phase velocity. It will drop to about 12 db as the cut-off angular frequency ω_{co} is approached. For the n = 1 mode, 10 log P_s/P_n is low, of the order of 7 db. This ratio is independent of input transmitter power. The results of the noise measurements can be explained by a simple model of the plasma, and independent verification of the validity of this model may be found in the work of Crawford and Lawson.[35]

For the case of an anisotropic plasma, the propagation constants for the $TE_{11}+$ and the $TE_{11}-$ modes have been found and the results are in qualitative agreement with the theory. These measurements were made in a resonant system. It was found that each waveguide mode would give rise to a series of resonances, $TE_{11m}+$ and $TE_{11m}-$. These resonances were easily excited by a simple probe, like the detection probe, which coupled to E_r of a mode.

It has been pointed out in Section II that the glass tube which confines the plasma has a significant effect on the propagation constants of both the n = 0 and the n = 1 modes. In fact, it is due to the presence of the glass tube that the n = 1 mode is a backward-wave mode. We might expect, then, that by the proper choice of the ratios of a/b and a/c, and ϵ_2 (see Fig. 1), we can make the n = 1 mode not only a backward-wave as was the case investigated in this report, but also a forward-wave as Trivelpiece shows,[6] and finally a forward-wave over part of the range of β and a backward-wave over the rest of the range of β. The latter variation of β would be accomplished by using a rather high permittivity ϵ_2 and making the wall of the tube very thin.

It is not difficult to conceive of practical devices based on the modes that have been investigated in this paper. For example, it is known that the interaction of an electron beam with the n = 0 mode will result in forward-wave amplification of an applied signal,[35] while it is possible that interaction of an electron beam with the n = 1 mode might result in backward-wave oscillation (Boyd[35] shows that the beam can be focused without the use of a magnetic field). Various passive devices are also possible such as a phase shifter or switch.

The chief difficulty in constructing these devices is the unavailability of a suitable plasma medium. It should be clear that the mercury-vapor discharge is unsuitable because of three detracting characteristics:

drift of parameters, significant noise modulation of the signal, end loss, particularly for the n = 1 mode. It is conceivable that the first two could be reduced, but it is doubtful if they could be entirely eliminated. For example, drift could be reduced by careful temperature control of the discharge tube. Since noise voltages evidentally propagate as waves,[34] it might be possible to interrupt this propagation by placing a reflecting screen across the discharge. It was found early in this project that a course floating screen of four fine tungsten wires placed across the discharge did not appear to alter its characteristics. No noise measurements were made at that time.

To the best knowledge of the author, the most superior plasma for practical devices that exists at the present time is a cesium thermal plasma constructed by G. S. Kino and his co-workers at Stanford University.[1] Through temperature control of the enclosing glass envelope, drift has been effectively eliminated. By ensuring that an electron sheath exists around the plasma-producing tungsten buttons or spirals, and taking certain other precautions, a plasma has been created which is oscillation free. Because the percent ionization of the cesium is nearly 100 percent and because the temperature of the plasma components is about 1000°C, the collision frequency ν is of the order of a few megacycles.

This plasma also has its detracting aspects. The equipment needed to provide temperature control is cumbersome. Also, the only way that the electron density can be altered is to change the temperature of the cesium vapor, the time necessary to accomplish this being of the order of minutes. Also, a high magnetic field is needed to confine the plasma. From a manufacturer's point of view, this is not appealing.

Thus, the chief problem in device work at the present time-- the problem that stands in the way of the modes described here and elsewhere

being put to practical use--is the unavailability of a good plasma. Until this is developed, traveling-wave tubes will always be more appealing than the plasma amplifier and ferrite phase shifters will be preferable to plasma phase shifters.

VII. APPENDIX - ELECTRICAL CHARACTERISTICS OF A LOW PRESSURE DISCHARGE IN THE ABSENCE OF A MAGNETIC FIELD

In a hot-cathode arc discharge which is contained in a long dielectric tube, nearly all of the volume of the discharge has characteristics which allow it to be classified as the positive column. Near the cathode, anode, and dielectric tube, however, there are boundary regions with properties quite unlike the positive column. The characteristics of these regions have been described in the literature and have recently been summarized by Crawford and Kino.[36]

Directly in front of the cathode is a narrow region of less than 1 mm. thickness. The portion of this region nearest the cathode is an electron sheath. The potential drop across this region is about that of the ionization potential (10.4 volts for mercury). The motion of the electrons in this region is similar to that in a diode with the result that the electrons emerge from this region with highly directed velocities, very little velocity spread, and energies of about the ionization potential. These electrons are known as primary electrons.

Next, there is a region where so-called ultimate electrons exist which have approximately an isotropic Maxwellian velocity distribution. These are much more numerous than the primary electrons emerging from the "diode" region. Beyond this region the primary electrons become scattered and transformed into ultimate electrons. The mechanism of scattering appears to be associated with a high frequency plasma oscillation.[37] Workers have reported observing a bright meniscus-shaped area in this region, although it was not apparent in the discharge tubes used in the experiments reported here. Beyond this region only ultimate electrons exist and this is the region that occupies almost all of the discharge

volume, the positive column.

Near the anode there is a sheath, again of the order of a millimeter in length, the polarity of which depends on the thermal current density in the positive column, the size of the anode, and the total current that is being passed through the tube.[29]

Finally, along the dielectric tube, a narrow, negative sheath exists which is due to equal electron and ion current flow to the wall. This will be discussed in more detail below.

The properties of the positive column do not depend on its length. We assume that it is homogeneous except near its boundaries. The concentration of electrons is nearly equal to that of ions so that the positive column is essentially electrically neutral and fits our definition of a plasma.

The average temperature of the electrons in the positive column is of the order of 20,000°K. This temperature is essentially independent of radial position of the electon.[29] The temperature of the ions is slightly greater than the wall temperature, while the temperature of the neutral atoms is that of the wall. The degree of ionization of the mercury vapor is always small (of the order of a few tenths of a percent for mercury vapor). Consequently, because the thermal velocity of the electrons is much larger than that of the ions, the primary collisional process is either electron-neutral collisions or electron-wall collisions. These will be typically of the order of tens or hundreds of megacycles. One of the interesting features of the electron behavior is that their velocity distribution is approximately Maxwellian, as can be demonstrated by probe measurements. Druyvesteyn and Penning[29] suggest that high frequency oscillations in the plasma may be essential for the establishment of a Maxwellian distribution.

A Maxwellian velocity distribution is in a sense paradoxical ("Langmuir's Paradox") because at low pressures electrons in the high-velocity tail of the Maxwellian curve should escape through the sheath at the wall to recombine with ions at the wall. High-frequency oscillations in the sheath have been postulated as the mechanism which prevents this from happening.[38]

Recombination of ions and electrons occurs primarily at the dielectric wall. It is unlikely that recombination will occur in the body of the discharge because the laws of energy and momentum conservation cannot be simultaneously met in a simple two-body recombining collision. Thus a three-body collision or a two-body collision with the emission of a photon[39] is necessary for recombination, both occurrences being improbable in the discharge body. The wall, however, constitutes a convenient third body.

Equilibrium requires that for each electron and ion lost through recombination another pair must be created. This occurs in the body of the positive column through ionization of neutral atoms by an axial electric field. This field also causes electrons and ions to have drift velocities which are superimposed on their thermal velocities.

The production of electron-ion pairs in the body of the positive column and the loss of electron-ion pairs at the wall implies that a current of both electrons and ions must flow radially outward to the wall. In order to regulate the flow to just the right amount, a radial electric field exists in the direction of the wall. This tends to speed up the low-velocity ions and slow down the high-velocity electrons so that the radial current densities of these two particles are exactly equal and of just the right amount to supply the loss through recombination. This radial electric field originates on net positive charge in the body of the positive column, implying that the positive column is not precisely electrically neutral, but is slightly positive. In fact,

the positive column is neutral at the center and becomes increasingly positive toward the wall. Since there is no field outside the dielectric discharge tube, we must postulate a layer of negative charge (electrons) on the wall on which the electric field lines terminate. This layer of charge occurs, in fact, when the tube is first turned on, at which time electrons quickly diffuse to the wall.

Note that the potential drop, in going from the relatively neutral body of the positive column to the wall, is negative. According to the Boltzmann distribution, a potential which decreases toward the wall requires that the electron density must also decrease toward the wall. Indeed, Killian[40] has found using probe techniques that the electron density in a mercury-vapor discharge at the wall will have decreased of the order of 20 percent from its value on the axis.

The effect of increasing the discharge current chiefly increases the charge density only and has little effect on the electric field in the positive column or on the temperature of the charged particles. Thus the drift velocity is also independent of current. This means that the charge density is proportional to the discharge current. Since the plasma frequency is proportional to the square-root of the charge density, the plasma frequency should be proportional to the square-root of the discharge current.

REFERENCES

1. Radiation and Waves in Plasmas (ed. by M. Mitchner), Stanford University Press, 1961, see contribution by G. S. Kino.

2. Wada, J. Y., and R. C. Knechtli, "Generation and Application of Highly Ionized Quiescent Cesium Plasma in Steady State," Proc. I. R. E., 49, pp. 1926-1931, (December) 1961.

3. D'Angelo, N., N. Rynn, "Diffusion of a Cold Cesium Plasma Across a Magnetic Field," Phys. Fluids, 4, pp. 275-276, (February) 1961.

4. Hahn, W. C., "Small-Signal Theory of Velocity-Modulated Electron Beams," Gen. Elec. Rev., 33, pp. 591-596, (June) 1939.

5. Ramo, S., "Space Charge Waves and Field Waves in an Electron Beam," Phys. Rev., 56, pp. 276-283, (August) 1939.

6. Trivelpiece, A. W., "Slow Wave Propagation in Plasma Waveguides," California Inst. of Tech., Pasadena, Tech. Report No. 7, (May) 1958. Also, Trivelpiece, A. W. and R. W. Gould, "Space Charge Waves in Cylindrical Plasma Columns," J. Appl. Phys., 30, pp. 1784-1793, (November) 1959.

7. Bevc, V., and T. E. Everhart, "Fast Waves in Plasma-Filled Waveguides," University of California, Berkeley, California, Inst. of Engineering Res. Tech. Report Series No. 60, Issue No. 362, (July 11) 1961.

8. Rosen, P. "The Propagation of Electromagnetic Waves in a Tube Containing a Coaxial D. C. Discharge," J. Appl. Phys., 20, p. 868, (September) 1949.

9. Johnson, T. W., "Theory of Electromagnetic Wave Propagation in Plasma Loaded Structures," RCA Victor, Montreal, Canada, Research Report, Project No. 4335, (October) 1962.

10. Allis, W. P., S. J. Buchsbaum, and A. Bers, Waves in Anisotropic Plasmas, M. I. T. Press, Cambridge, Mass., 1963.

11. Chorney, P., "Electron-Stimulated Ion Oscillations," Mass. Institute of Tech., Cambridge, Mass., Tech. Report No. 277, (May 26) 1958.

12. Riedel, H. and J. Thelen, "Wave Propagation in a Cold Cable with an Impressed Longitudinal Magnetic Field," Electrophysikalisches Institut der Technischen Hochschule, München, Germany, Technical Final Report, April 1, 1959 to March 31, 1960.

13. Goldstein, L., and N. L. Cohen, "Radiofrequency Conductivity of Gas-Discharge Plasmas in the Microwave Region," Phys. Rev., 73, p. 83, (January) 1948.

14. Goldstein, L,. and N. L. Cohen, "Behavior of Gas Discharge Plasmas in High-Frequency Electromagnetic Fields," Elect. Commun., 28, p. 305, (December) 1951.

15. Osborne, F.J. F., J. V. Gore, T. W. Johnson, and M. P. Bachynski, "Characteristics of Isotropic Plasma Loaded Waveguides," RCA Victor, Montreal, Canada, Research Report, Project No. 4335, (October) 1962.

16. Agdur, B., and B. Enander, "Resonance of a Microwave Cavity Partially Filled with a Plasma," J. Appl.Phys, 33, pp. 575-581, (February) 1962.

17. Golant, V.E., A.P. Zhilinskii, M.V. Krivosheev, and G. P. Nekrutkin, "Propagation of Microwaves through Waveguides Filled with Plasma," Soviet Physics Tech. Physics, 6, pp. 38-50, (July) 1961.

18. Narasinga Rao, K.V., J.T. Verdeyen, and L. Goldstein, "Interaction of Microwaves in Gaseous Plasmas Immersed in Magnetic Fields," Proc. I.R.E., 49, pp. 1877-1889, (December) 1961.

19. Goldstein, L., "Nonreciprocal Electromagnetic Wave Propagation in Ionized Gaseous Media," Trans. I.R.E., MTT-6, pp. 19-28, (January) 1958.

20. Advances in Electronics and Electron Physics, Vol. VII (Ed. by L. Marton), Academic Press, Inc., 1955, see section by L. Goldstein.

21. Pringle, D.H., and E.M. Bradley, "Some New Microwave Control Valves Employing the Negative Glow Discharge," J. Electronics, 1, p. 389, (January) 1956.

22. Buchsbaum, S.J., L. Mower, and S. C. Brown, "Interaction between Cold Plasmas and Guided Electromagnetic Waves," Phys. Fluids, 3, pp. 1-14, (Sept.-Oct.) 1960.

23. Delcroix, J.-L., Introduction to the Theory of Ionized Gases, Interscience Publishers, Inc., New York, 1960.

24. Bayet, P.M., J.L. Delcroix, J.F. Denisse, "Theorie Cinetique des Plasmas Homogenes Faiblement Ionises, II.," Le Journal de Physique et Radium, 15, pp. 795-803, (December) 1954.

25. Bayet, P. M., J.L. Celcroix, J.F. Denisse, "Theorie Cinetique des Plasmas Homogenes Faiblement Ionises, II.," Le Journal de Physique et Radium, 16, pp. 274-280, (April) 1955.

26. Slater, J.C., "Microwave Electronics," Rev. Mod. Phys., 18, pp. 441-512, (October) 1946.

27. Ramo, S. and J. R. Whinnery, Fields and Waves in Modern Radio, J. Wiley and Sons, New York, 1953.

28. Tonning, A., "Energy Density in Continuous Electromagnetic Media," I.R.E. Trans. on Antennas and Propagation, 8, pp. 428-435, 1960.

29. Druyvesteyn, M.J. and F.M. Penning, "The Mechanism of Electrical Discharges in Gases at Low Pressure," Rev. Mod. Phys., 12, pp. 87-174, (April) 1940.

30. von Engel, Ionized Gases, Oxford University Press, 1955, p. 224.

31. Armstrong, E. B., K. G. Emeleus, J. R. Neill, "Low-Frequency Disturbances in Gaseous Conductors," Proc. Roy. Irish Acad., A 54, pp. 291-310, (December) 1951.

32. Carlile, R.N., "Experimental Investigation of Microwave Propagation in a Plasma Waveguide," Doctoral Dissertation, University of California, Berkeley, 1963. (See Appendix B)

33. Dielectric Materials and Applications, (A.R. von Hippel, ed.), Technology Press of M.I.T. and John Wiley and Sons, New York, 1954.

34. Crawford, F.W., and J.D. Lawson, "Some Measurements on Fluctuations in a Plasma," Plasma Physics-Accelerators-Thermonuclear Research, 3, pp. 179-185, (July) 1961.

35. Boyd, G. D., "Experiments on the Interaction of a Modulated Electron Beam with a Plasma," California Institute of Technology, Pasadena, Calif., Tech. Report No. 11, (May) 1959.

36. Crawford, F. and G. S. Kino, "Oscillations and Noise in Low-Pressure DC Discharges," ML Report No. 817, Stanford University, Stanford, California, June 1961.

37. Penning, F. M., "Scattering of Electrons in Ionized Gases," Nature 118, p. 301, (August) 1926.

38. Langmuir, I., "Oscillations in Ionized Gases," Proc. Natl. Acad. Sci. U.S., 14, pp. 627-637, (August) 1928.

39. Compton, K. T., and I. Langmuir, Revs. Modern Phys., 2, p. 123, 1930.

40. Killian, R. J., Phys. Rev., 35, p. 1238, 1930.